NEBULIZED FLAME IONIZATION DETECTION IN HIGH PERFORMANCE LIQUID CHROMATOGRAPHY

By

Erepamowei Young

A Doctoral Thesis submitted in partial fulfilment of the requirements for the award of

Doctor of Philosophy

Loughborough University

2008

Supervisor: Professor R.M. Smith
Department of Chemistry

Acknowledgements

I wish to express thanks to Prof R.M. Smith for guiding the research to completion. In addition, thanks to Dr B.L. Sharp for his input especially in the instrumentation.

My special thanks to my sponsor, the Bayelsa State Government (Nigeria).

Dedication

To my father, Mr Young Okodoko.

Contents

Abstract

A nebulized flame ionization detector interfaced with LC was examined and found to be more versatile in applications than common LC detectors, such as UV, RID, ELSD and CAD. The technique can be used for both volatile and non-volatile analytes. It is compatible with gradient elution and can be used for the analysis of non chromophore-possessing analytes. The calibration plots of non-volatile analytes were linear in contrast to other aerosol-based detectors, such as ELSD and CAD.

The technique was examined in three consecutive stages; optimization of the FID, testing the response patterns of analytes (volatile and non-volatile) and applications to the analysis of compounds of diverse functional groups.

The optimum conditions for the operation of the FID were: hydrogen, 157 mL/min; nitrogen, 250 mL/min; air, 654 mL/min; spray chamber internal diameter, 40 mm, collector internal diameter, 4mm and eluent (water), 1 mL/min.

The calibration plots of all volatile analytes were linear while those of the non-volatile analytes were linear only when anions (in the form of sulfuric acid, nitric acid, hydrochloric acid, orthophosphoric acid, sodium sulphate and ammonium sulphate) were added to the eluent.

The separations of diverse analytes (alcohols, aldehydes, ketones, amines, amino acids, carboxylic acids and sugars) gave detection limits in the low μg range.

List of acronyms

AEC-PAD	Anion exchange chromatography-pulsed amperometric detector
AFID	Alkali flame ionization detector
CAD	Charged aerosol detector
CNLSD	Condensation nucleation light scattering detector
ELSD	Evaporative light scattering detector
FIA	Flow injection analysis
FIA-FID	Flow injection analysis-flame ionization detector
FID	Flame ionization detector
GC	Gas chromatography
GC-FID	Gas chromatography-flame ionization detector
HPLC	High performance liquid chromatography
LC	Liquid chromatography
LC-FID	Liquid chromatography-flame ionization detector
LC-MS	Liquid chromatography-mass spectrometry
LOD	Limit of detection
LC-RID	Liquid chromatography-refractive index detector
LC-UV	Liquid chromatography-ultraviolet detector
MS	Mass spectrometry
PS-DVB	Polystyrene divinylbenzene
RID	Refractive index detector
RSD	Relative standard deviation
SD	Standard deviation
UV	Ultraviolet detection

CHAPTER ONE

Introduction

The equipment for the chromatographic separation of a mixture comprises two major components; the column and the detector. The constituents of a mixture are separated in the column and are subsequently monitored by a detector when they exit the column. Detectors can be broadly divided into two groups, viz., selective and universal. The ultraviolet [UV (direct and indirect)], fluorescence (direct and indirect) and electrochemical detectors are examples of selective detectors. As the name implies, they are limited in their applications. Universality, as a characteristic of detectors, can be defined in terms of qualitative and quantitative analysis. The former is a measure of the widespread identification of analytes; the more diverse analytes that a detector can monitor, the more it is considered universal. If a detector is quantitatively universal, one calibration standard can be used to quantify compounds of diverse functional groups. It can also be used to quantify compounds whose identities are not known (e.g, impurities, degradants etc) or if there is no pure standard.

Many universal detectors have been developed in order to widen the applications of liquid-phase separation. Examples of universal detectors include refractive index detectors (RID), evaporative light scattering detector (ELSD), charged aerosol detector (CAD) and flame ionization detector (FID). Alternative coupled detectors, such as LC-MS and LC-ICP-MS, are sophisticated analytical instruments in their own right but have limitations and fall outside the scope of the current project. Although they can provide more information about an analyte, they represent a significant higher cost [1, 2]. Although, they are more versatile compared to the selective detectors, they have also been identified as having limitations which have kept analytical chemists on the search for more versatile

detectors. This current work on liquid chromatography-flame ionization detection (LC-FID) was born out of this search for a universal detector.

A brief discussion of selected detectors and their limitations is presented in the following sections.

1.1 Selective HPLC detectors

These are generally well described in most HPLC texts and only the main points are discussed here.

1.1.1 UV detector (direct)

An absorption detector (UV) measures the loss in intensity of ultraviolet or visible light when an optically dense analyte interacts with it. It is the most commonly used detector owing to its analytical capabilities; it is sensitive (limits of detection, 0.1 - 1 ng) [3] and has a wide linear range. It is also suitable for gradient elution because of its insensitivity to environmental factors (temperature and pressure) and to changes in the mobile phase composition, although it places some limitation on eluents (eluent must have a suitable wavelength-cut-off) or buffer being used [4].

Absorption takes place at wavelengths above 200 nm, provided the molecule has at least a chromophore. Some examples of chromophores are given below [5].

1. a double bond adjacent to an atom with a lone electron pair;
2. bromine, iodine or sulphur;
3. two or more conjugated double or triple bonds;
4. an aromatic ring; and
5. inorganic ions; Br^-, I^-, etc.

1.1.2 UV detector (indirect)

The UV detector is limited, in that it cannot detect compounds such as carbohydrates, lipids or most amino acids because they do not possess a chromophore [4]. Detection of such compounds can be made possible either by derivatization or indirect detection. Derivatization involves the tagging of the compound being studied with a chromophore. Common derivatization reagents for amino acids and carboxylic acids are 1-fluoro-2,4-dinitrobenzene and phenacyl bromide, respectively [6]. These derivatization procedures may require from 4 to 24 hours, involving many tedious chemical reactions with potential for incomplete reaction and analyte losses at each transfer step [7].

The indirect detection involves measuring a strong signal from the background electrolyte, and which is displaced by a weak signal from an analyte as it passes the detector. The principle can be applied to any type of detection. An absorbing ion with the same sign of charge as the analyte is added to the background electrolyte to provide a steady background signal. When the analyte ion emerges, the concentration of background ion necessarily decreases, because electro-neutrality must be preserved. If the analyte ion is not absorbing, the absorbance level decreases when the analyte emerges and a negative signal is observed; for example, the indirect ultraviolet detection of chloride anion in the presence of the ultraviolet absorbing chromate anion. In the absence of the analyte, the chromate ion gives a steady absorbance at 254 nm. When the chloride ion reaches the detector, there is less chromate ion present and chloride ion does not absorb; therefore the detector signal decreases [8]. The indirect detection, which could be very sensitive, has some inherent limitations; the dynamic range is much less than when using absorbance in the conventional mode and it can only be applied to ionizable analytes. Another disadvantage of the indirect mode is that, the chromatographic system must be thoroughly flushed after use to remove the background chromophore [4].

1.1.3 Fluorescence detector (direct)

The fluorescence detector responds to the emission of light from a molecule in an excited state [8]. In order to detect an analyte by this detector, the analyte must possess a fluorophore and the detector must be set to the correct excitation and emission wavelengths. Examples of fluorophore include:

- Aromatic functional groups, especially if held co-planar with ring;
- Compounds containing aliphatic and alicyclic carbonyl structures or highly conjugated double-bond structures;
- Fusion of benzene rings to simple heterocylic nucleus (pyridine, furan, thiophene, pyrrole); isolated heterocyclic nucleus do not fluoresce. Fusion increases the molar absorptivity and decreases the lifetime of their excited states.

Advantages of fluorescence over UV detection

The fluorescence detector is typically about 1000 times more sensitive than the UV detector for compounds with a chromophore [5]. This can be explained in terms of low background signal; it is an emission technique in which the background signal in the absence of a fluorophore is zero [9]. Another factor which enhances sensitivity in fluorescence is the dependence of the fluorescence intensity on the source intensity, that is, the fluorescence power and hence the sensitivity, can be increased by increasing the intensity of the light source. This is in contrast with UV because absorbance is essentially independent of the source intensity.

Fluorescence detector also exhibits higher selectivity than UV because the detection is based on two wavelengths (excitation and emission) instead of one (absorbance) in the UV. The selectivity is enhanced because very few analytes posses the same fluorophore [9].

Limitations

The fluorescence detector is very limited in respect of the range of analytes it can monitor. There are several factors which affect the fluorescence ability of analytes [10]. The fluorescence detector is further limited by these factors; effect of substitution, structural rigidity, temperature and solvents, pH and dissolved oxygen [10].

Effect of substitution

- Halogen-substitution decreases the fluorescence; the decrease is more significant with an increase in the atomic number of the halogen;
- Substitution of a carboxylic acid or carbonyl group on an aromatic ring generally inhibits fluorescence.

Effect of structural rigidity

The quantum efficiency, which is a measure of fluorescence intensity, for fluorene and biphenyl are nearly 1.0 and 0.2 respectively under similar conditions of measurement. The difference in fluorescence behaviour appears to be largely due to the increase in rigidity furnished by the bridging methylene group in fluorene [10].

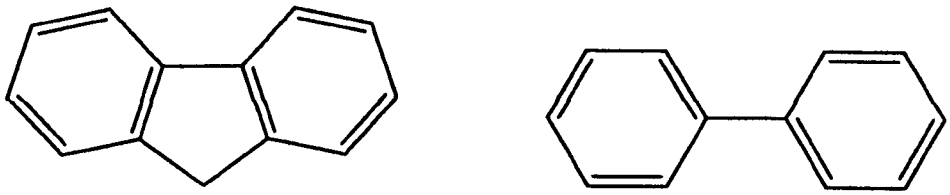

Fluorene Biphenyl

Figure 1.1. Structures of fluorene and biphenyl [10].

Temperature and solvent effects

The fluorescence response of most compounds decreases with an increasing temperatures because the increased frequency of collisions at elevated temperature improves the probability of deactivation by external conversion. The fluorescence of a molecule is decreased by solvents containing heavy atoms or the presence of other solutes with such atoms in their structure; carbon tetrachloride and ethyl iodide are examples [10].

Effect of pH on fluorescence

The fluorescence of an aromatic compound with acidic or basic ring substituent is usually pH-dependent. This could be explained in terms of a change in the degree of ionization with pH [10].

Effect of dissolved oxygen

The presence of dissolved oxygen in the solution often reduces the intensity of fluorescence in a solution. This effect may be the result of the photochemically-induced oxidation of the fluorescing species [10].

1.1.4 Fluorescence detector (indirect)

As in UV detection, derivatization is an option for non-fluorescing analytes. Common derivatization reagents for amino acids and carboxylic acids are o-phthalaldehyde and 9-anthryldiazomethane, respectively [6].

Another option for non-fluorescing analytes is indirect detection. The principles and limitations of the indirect UV detection are applicable to the indirect fluorescence detection. However, only one difference exists; the mobile phase additive is a fluorescing ion while that of the UV is an absorbing ion [10].

1.1.5 Electrochemical detector

Oxidizable and reducible compounds can be detected by electrochemical detectors [5]. Oxidizable compounds include phenols (phenol, chlorinated phenols, hydroquinone, catecholamines, estrogens, morphine), aromatic amines (aniline, benzidines, hydrazines), heterocyclic compounds (indoles, tryptophan) etc. The nitro aromatics, diazo compounds and anthraquinones are examples of reducible compounds [9], but their determination is hindered by the ready-reduction of atmospheric oxygen. These detectors are limited to compounds that exhibit electrochemical properties; compounds that do not have electrochemical properties cannot be detected.

1.2 Universal detectors

Compounds that cannot be detected by the selective detectors (UV, fluorescence and electrochemical) can be monitored by RID, ELSD, CAD and FID.

1.2.1 Refractive index detector (RID)

The refractive index detector (RID) is the most popular and least expensive of the universal detectors. Besides, it is more compatible with miniaturization than the UV detector [11]. This is because RID is an intensive property of the medium and does not decrease on miniaturization whereas absorbance is an extensive property of the optical medium, that is, the absorbance decreases linearly with the optical path length according to Lambert-Beer law.

a Principles of operation

A schematic of a refractive index detector is shown in Figure 1.2 [12]. It works by comparing the refractive index of the mobile phase (in the reference cell) and sample (in the sample cell). If the separated components of a sample reach the refractometer flow cell, the composition of the flow

cell changes with a consequent change in the RI of the solution. The change in the RI of the medium will cause a change in the direction of light (refraction of light). By keeping wavelength, temperature and pressure constant, a change in the RI, measured by the refractometer, is due only to a changing sample concentration; a high concentration of a solute refracts a beam of light more than a dilute solution. Therefore, high concentrations of sample yield large peaks.

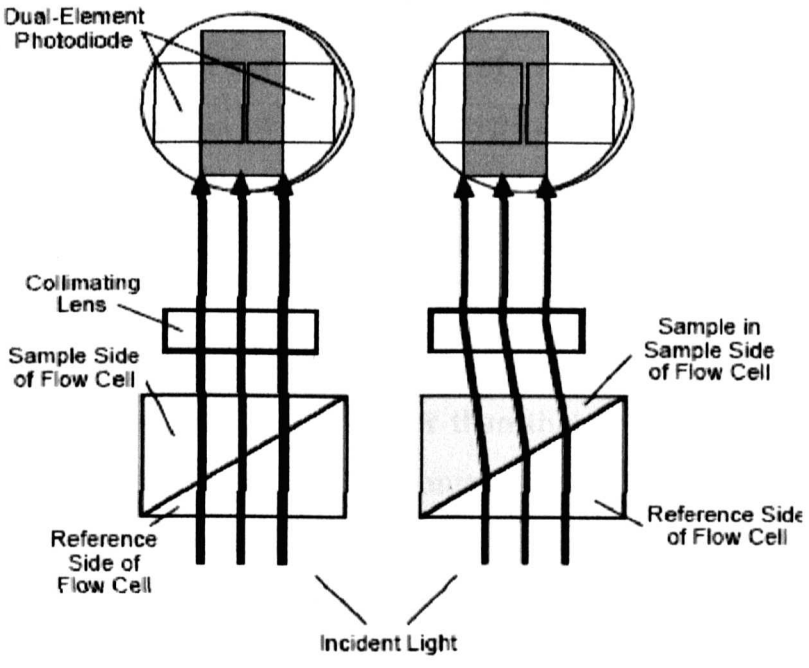

Figure 1.2. A schematic of the RI detector [12].

b Applications

The analysis of carbohydrates, lipids, proteins, amino acids etc, is difficult with UV because they do not possess sufficiently strong chromophore. The RID is an option for the analysis of these compounds because their refractive indices are sufficiently different from the common HPLC mobile phases [4].

c *Limitations of the RID*

Although it is a universal detector, the RI detector exhibits limited sensitivity, poor selectivity, non-compatibility with gradient elution and it is extremely sensitive to temperature and pressure fluctuations [13 - 16]. The non-compatibility with gradient elution precludes the analysis of complex mixtures.

Sensitivity: The sensitivity of the RI detector is limited by two factors. The first is the small difference in RI between the mobile phase and the analyte. A comparison of the refractive index values of a typical eluent and analytes confirms that the addition of traces of a typical organic compound to a water-methanol eluent will have only a small effect on the overall refractive index [9]. The second factor is noise. The sensitivity of the RI detector, just like any other detector, is governed by the signal-to-noise ratio, that is, the sensitivity decreases as the baseline noise increases. The RI detector exhibits poor sensitivity (about 1000 times higher than that of the UV detector) [5] due to a high baseline noise. The major contributors to the baseline noise are vibrations of the optical system [11] and thermal fluctuations in the flow cell [17]. The most sensitive refractometers, which are commercially available (differential diffractometers) for HPLC, offer a short-term RI noise of approximately 2.5 nRIU (RIU = refractive index unit). Since the temperature dependence of RI of water is approximately 100 μRIU/°C at 25 °C, and as much as 600 μRIU/°C for organic solvents, it is obvious that such a high sensitivity RI measurement require extensive thermal equilibration, and in practice, it is difficult to obtain very high sensitivity.

Selectivity: The RI of most solutes differs only in the second or third decimal place resulting in poor selectivity [17].

Incompatibility with gradient elution: Since the measurement of response in this detector is based on the RI of the mobile phase and the analyte, the

former must be kept constant. The mobile phase composition changes in gradient elution making it impossible to effect measurements as the baseline shifts [5].

Temperature and pressure: Temperature fluctuations affect the density of the mobile phase and hence the RI. Back-pressure pulsations from a dripping waste tube can cause short-term noise cycling and hence the working of the detector [12].

1.2.2 Evaporative light scattering detector (ELSD)

The ELSD was developed in the late 1970s and 1980s and it is another universal detector [14]. Unlike the RID, which is an optical detector, the ELSD is based on the scattering of light. One advantage of the ELSD is that, it is relatively an inexpensive alternative method compared to mass spectrometry (MS) for the detection of non-volatile compounds that do not absorb UV light. It has an advantage over the refractive index detector in that, its chromatographic baseline is not affected by changes in environmental factors (temperature and pressure) or mobile phase composition during gradient elution. For this reason, it can be used for the analysis of complex mixtures, which requires gradient elution for good separation [13].

a Principles of operation

The principle of operation involves the pneumatic nebulization of the column effluent to form an aerosol, followed by solvent evaporation in a heated drift tube. The droplet cloud emerging from the evaporator is subsequently passed through a light beam and the amount of light scattered by the non-volatile droplets is detected by a photomultiplier. Figure 1.3 shows the schematic of the ELSD [18].

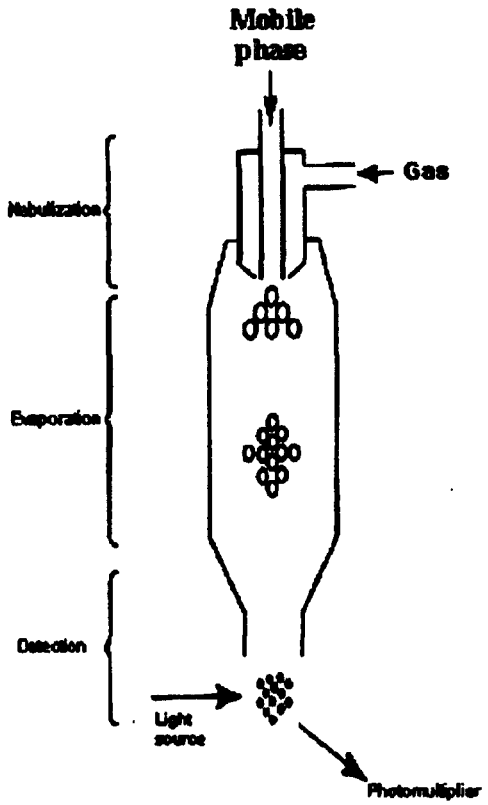

Figure 1.3. Schematic of the ELSD [18].

b Applications

It is used for the analysis of compounds that lack a chromophore, such as many underivatized amino acids, carbohydrates, lipids, polymers, surfactants, drug substances and natural products [15]. Table 1.1 shows some practical situations where the ELSD was applied.

Table 1.1. Selected application areas of ELSD

Analyte	Matrix	LOD	Reference
Phospholipids	main wheat flour		[19]
Triacylglycerols	human milk		[20]
Lipids			[21]
Free acids and mono-, and di- triglycerides			[22]
Carbohydrates	drinks	0.2 - 1.2 µg	[23]
Fatty acids		0.0001 - 0.0110 mg/mL	[24]
Alkoxyglycerols and other non-polar lipids			[25]
Hydrophobic surfactant proteins			[26]
Triglycerides	oils and fats	0.2 µg	[27]
Determination of 1-deoxynojirimycin	mulberry leaves	100 ng	[28]
Sulforaphane	broccoli samples	0.5 µg	[29]
Inorganic anions	porous graphitic carbon	50 ppm	[30]
Polyethylene glycol and polyethylene oxide		µg/mL levels	[31]

c ELSD as a tool for qualitative analysis

The ELSD is a universal detector, that is, it responds to virtually all compounds provided the volatilities of the compounds are lower than that

of the mobile phase [32]. Analytes that are too volatile will be lost during the process of evaporation.

d ELSD as a tool for quantitative analysis

Linearity: One disadvantage of the ELSD is that, the response is non-linear which renders quantification difficult over a wide range of concentration without an extensive calibration [20, 21, 29, 33 – 36].

This non-linearity could be explained in terms of the particle size heterogeneity at different concentration levels. As with many aerosol-forming processes, light scattering depends on the size of the aerosol particles compared to the wavelength of the incident light. Charlesworth [37] examined the particle size heterogeneity and detection mechanism of the evaporative light scattering detector (ELSD) and found that a plot of peak area versus concentration gave a sigmoid curve; the calibration curves were approximately linear for concentrations of solutes in the range of 7.5 x 10^{-5} to 3.0 x 10^{-3} g cm^{-3} but above and below this range, the response was non-linear with an accompanying reduction in sensitivity [37].

The non-linear response was attributed to the interplay of different mechanisms (Raleigh scattering, Mie scattering, reflection and refraction) of light scattering at the different concentration levels. The predominant scattering mechanism at concentration range of 7.5 x 10^{-5} to 3.0 x 10^{-3} g cm^{-3} is reflection and refraction. Below and above this concentration range, the predominant mechanisms are Raleigh and Mie scatterings, respectively [37].

The importance of each process is governed by the radius of the particles compared to the wavelength of the incident light. Raleigh scattering is most predominant when the particles are very much smaller than the wavelength of the incident light. In this case the incident light quanta induce oscillating dipoles in each particle they strike, and these in turn radiate comparatively

low intensity light in all directions which interferes with the incident light resulting in reduced response and non-linearity [37].

When the dimensions of the particles are greater than the wavelength of light, they no longer behave as point sources and Mie scattering becomes the predominant mechanism. In this process, different points on the same particle are exposed to the incident light with a variety of amplitudes and phases and the induced oscillating dipoles produce waves which interfere with each other. Because of this, the scattered light can have a greater or lesser intensity than comparable Raleigh scattering, depending on the angles at which observations are carried out [37].

As the particle sizes approach the wavelength of the incident light, then reflection and refraction begin to prevail. These two always occur together and are due simply to the deviations of the light quanta as they encounter the boundaries between phases. The sum of the intensities of the light reflected and refracted is equal to the total intensity of the incident light. A linear plot was observed at this concentration range [37].

In order to address the particle size limitation when the particles are not sufficiently large to scatter light effectively, an additional step of condensation nucleation was introduced [31, 38]. In the condensation process, particles were grown to sizes more effective at scattering light by first saturating the gas surrounding the particles with the vapours of condensable fluid and then passing the mixture through a condenser. This technique is called condensation nucleation light scattering detection (CNLSD). An improved linearity and lower detection limits were found with CNLSD compared to the ELSD [31, 38]. The detection limit of CNLSD was less than 1 ng/mL, which is over two orders of magnitude lower than a commercial ELSD. An overview of the experimental set up of CNLSD is shown in Figure 1.4 [38].

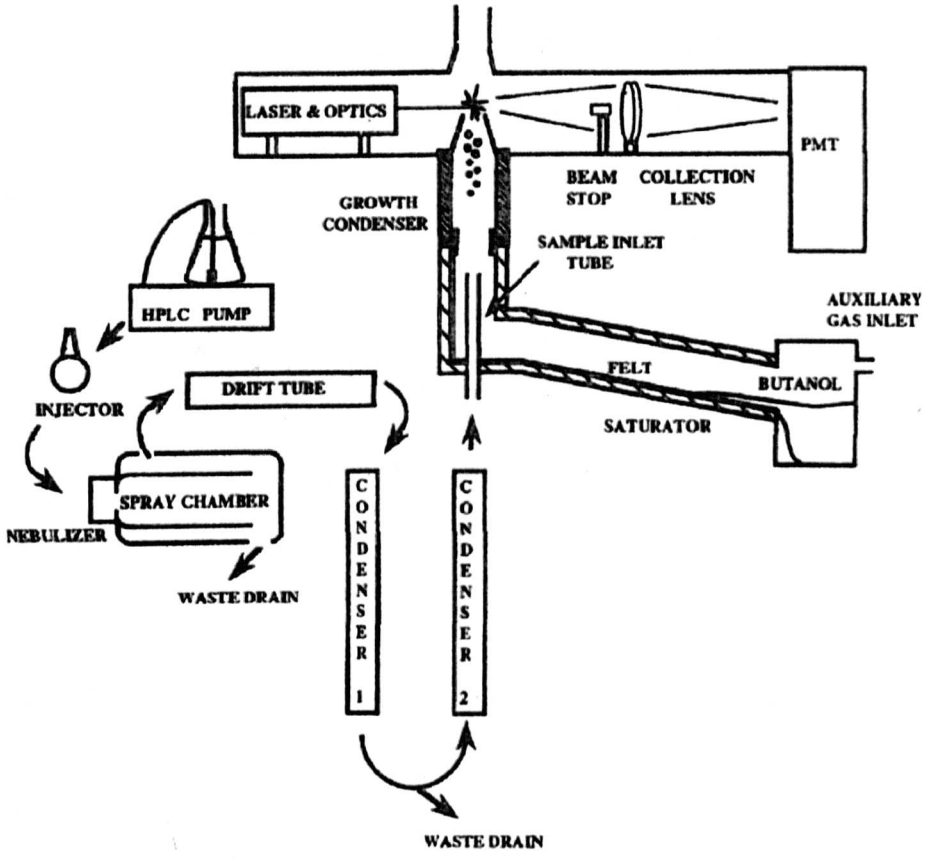

Figure 1.4. An overview of the experimental set of CNLSD [38].

Another effect of particle size limitation was seen in the analysis of volatile analytes. Volatile analytes give particle sizes that are not effective in scattering light. In order to improve the particle size for effective light scattering, non-volatile mobile phase additives could be used. But these additives could produce a constant background signal resulting in loss of sensitivity. Because of the undesirable loss of sensitivity associated with the use of non-volatile additives, ELSD cannot be used to measure volatile analytes [16].

Precision and limits of detection: Gamache *et al.* [15] determined the precision (variability of measurement values) and limits of detection of glucose, caffeine, propranolol and chlorpromazine. The variability (percent

relative standard deviation) was measured for 10 replicate injections. The variabilities obtained were 3.52, 3.61, 2.95, 2.41 for glucose, caffeine, propranolol and chlorpromazine respectively. The detection limits ranged from 100 to 150 ng.

Universality: Universality in terms of quantitative analysis means an empirical consistency in response for compounds of diverse functional groups irrespective of the analysis conditions [15].

Unfortunately, ELSD often generates very different responses for compounds of the same molecular weight [39]. This limitation in universality is due to its high sensitivity to many operating parameters, including composition and flow rate of the mobile phase, flow rate of the nebulizing gas and the temperature of the vaporizing tube [40 & 41].

Gamache *et al.* [15] explained the dependence of the ELSD response on mobile phase composition in terms of nebulization. They found that the response was directly proportional to the percentage of organic content in the eluent; the nebulization efficiency increased with the percentage organic content. The mobile phase flow rate also influences the nebulization process [42].

The relationship among detector response, nebulizing gas flow rate and temperature was studied [42]. They found that the response was found to be directly proportional to the temperature of the evaporation tube and inversely proportional to the flow rate of the nebulizing gas.

1.2.3 Corona charged aerosol detector (CAD)

The CAD, just like the ELSD, is an aerosol-based detector but it is a more sensitive version of the latter. It is also compatible with gradient elution chromatography.

a Principles of operation

In the CAD, the aerosol particles are not detected by light scattering but instead, are given an electrical charge by mixing them with a stream of charged nitrogen (Fig 1.5) [43]. The principle of detection involves the following steps: pneumatic nebulization of the column effluent into an aerosol. The coarse particles of the aerosol collide with the impactor and are drained away and the fine aerosol passes through a drying tube where the solvent is dried, much as in ELSD. The dried particles are given a positive charge by mixing them with a stream of a positively charged secondary gas (nitrogen). Any high-mobility particles are removed by a negatively charged ion trap and the rest of the charged solute particles are collected and measured. It generates a signal in direct proportion to the quantity of each particle [44 - 46].

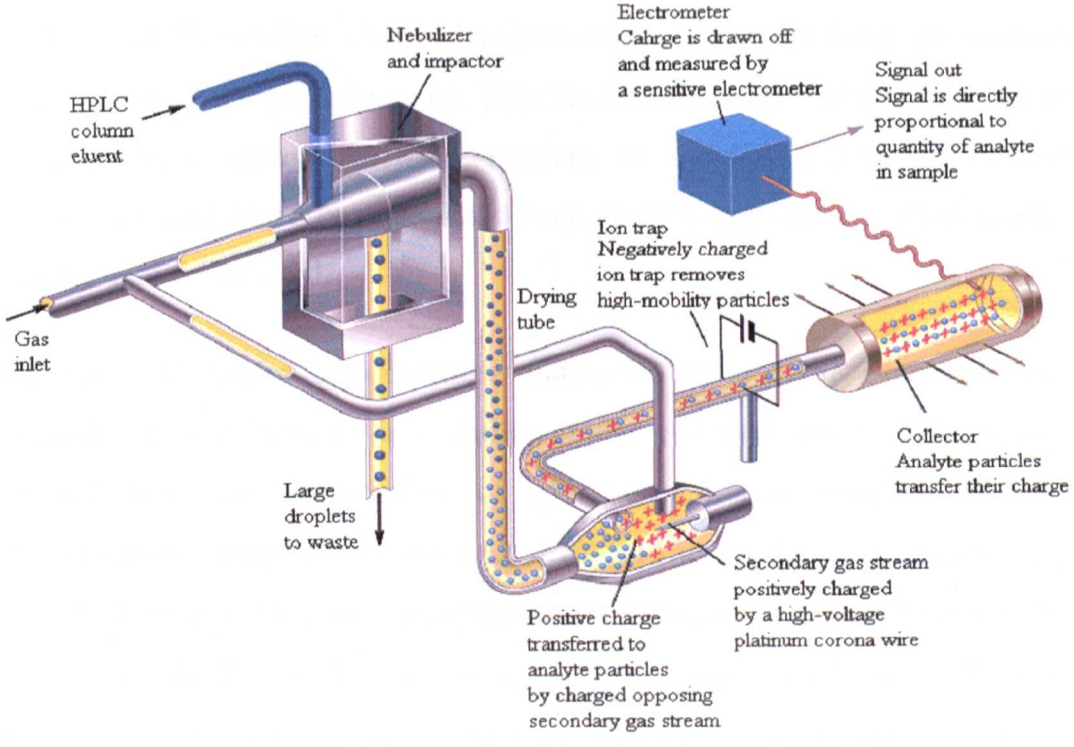

Figure 1.5. Schematic of a CAD [43].

b Applications

It has the same application capability as ELSD in respect of the scope of analytes, that is, it can be used in the analysis of many underivatized amino acids, carbohydrates, lipids, polymers, surfactants, drug substances and natural products.

c CAD as a tool for qualitative analysis

Just like the ELSD, it responds to all analytes provided they are sufficiently non-volatile.

d CAD as a tool for quantitative analysis

Linearity: The response of the CAD is non-linear which can be explained in terms of Raleigh charge limit and it is valid for liquid particles and loosely-held agglomerates of solid particles [47, 48]. The Raleigh limit defines the maximum number of charges a particle can hold before the mutual repulsion of the excess charge overcomes the cohesive force of surface tension, tearing the particle apart. This limit also means that the number of charges, which determines the sensitivity of the CAD, depends on the particle size and since particle sizes vary at different concentration levels, linearity will be affected.

Precision and limits of detection: Gamache *et al.* [15] examined the variability of the detector and limits of detection of some analytes and reported that the variabilities of glucose, caffeine, propranolol and chlorpromazine responses were 1.62, 1.75, 1.14 and 1.48, respectively. The limits of detection for these compounds were found to range from 5 to 20 ng. The variabilities and limits of detection of these analytes with ELSD were also reported [15]. An improvement in the limit of detection and a two-fold improvement in response-variabilities were found in favour of the CAD. These improvements were attributable to the differences in particle-

detection technology since the aerosol-formation stage is similar for both detectors. Light scattering efficiency is dependent upon particle diameter and involves exponential changes between regimes (Raleigh, Mie, refraction and reflection). This may have been responsible for the limited sensitivity and high variability of the ELSD. On the other hand, the response obtained with electrical aerosol detection technology used with CAD may exhibit unimodal efficiency over a wider range of particle diameters.

Universality: In contrast to ELSD, the response of the CAD is independent of chemical structure, in that different compounds of the same molecular weight generate similar responses provided the analytes are sufficiently non-volatile and the mobile phase composition is kept constant [44]. A factor that limits the universality of CAD is the dependence of response on mobile phase composition, as is known with ELSD. An increase in the organic content of the mobile phase can improve the transport efficiency of the nebulizer; this in turn, can result in a greater number of particles reaching the detector chamber and hence in a higher signal [49].

One way of eliminating the mobile phase composition effect on the detector response is to make sure that the mobile-phase composition reaching the detector always remains constant by adding a compensation mixer so that the overall composition is constant. For example, if the separation starts with 10% acetonitrile (ACN) in the mobile phase, and ACN concentration increases to 90% between 2 and 15 minutes, the mobile phase used for corona CAD signal compensation should contain 90% ACN for the first 2 minutes, and the ACN concentration should decrease from 90 to 10% between 2 and 15 minutes [49].

Another limitation of the CAD is that, it does not respond to volatile compounds as they are lost with the eluent during the drying stage, and the response to compounds of intermediate volatility can be inconsistent. For example, in preliminary flow injection experiments, butyl paraben showed

inconsistent responses that were generally lower than expected and varied from experiment to experiment [49].

1.2.4 Standard flame ionization detector (FID)

The FID is the most commonly used GC detector but rarely used in LC. It offers so many advantages, viz., its response is not affected by modest changes in flow, pressure or temperature and does not respond to common carrier gas impurities, such as carbon dioxide and water under normal operation [50].

a Principles of operations

A schematic of a typical GC-FID is shown in Figure 1.6 [50]. The carrier gas from the bottom of the detector is mixed with hydrogen combustion gas plus an optional make-up gas in the area below the flame jet. This mixture is then burned just above the jet tip in an air flow to produce ions. An electric field induced by a negative polarizing voltage (applied between the jet tip and a collector electrode) accelerates ions to the collector and signals are sent to the electrometer. Depending on the FID design, either the collector or the jet tip is kept at ground potential. Air, carbon dioxide and water exhaust gases are vented from the top of the detector body [51].

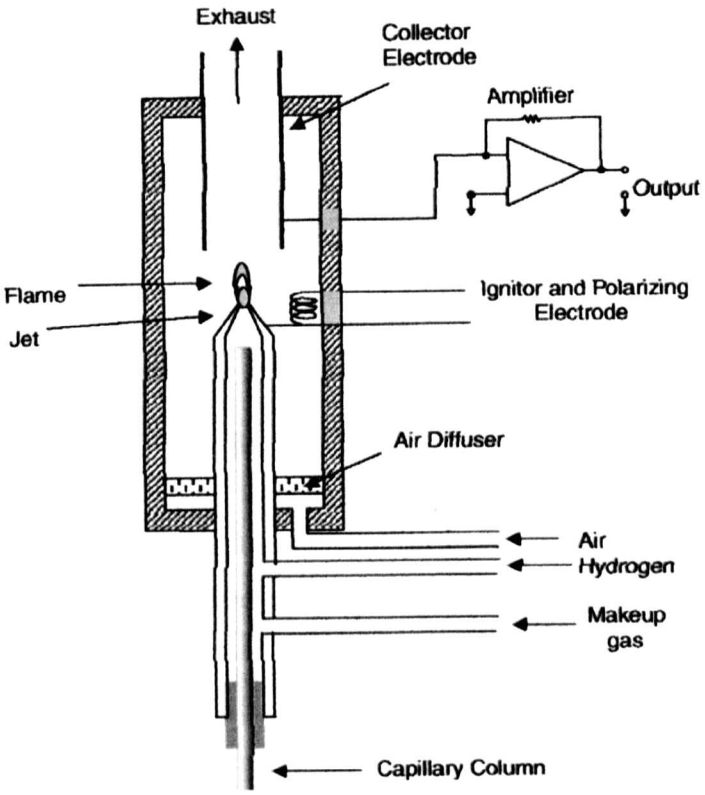

Figure 1.6. Schematic of the FID [50].

Mechanism of detection

The processes involved in the ionization mechanism in the FID are shown below [52 – 55].

$$\text{carbon-compound} \xrightarrow[\text{flame}]{\text{FID}} CHO^{+} \xrightarrow{H_2O} \left[H_3O(H_2O)_n\right]^{+} + CO$$

(a) (b)

In the flame, organic compounds eluting from the column undergo degradation reactions in the hydrogen-rich region, forming a group of single carbon species. The single species subsequently react with air to produce (a) which then reacts with the water produced in the hydrogen flame to generate hydronium ions which eventually polymerize to produce (b) and CO. The ion current produced is proportional to the amount of

carbon compound present. The details of the FID mechanism have been reviewed [53 - 55].

b *Applications*

In gas liquid chromatography, the FID is used for the analysis of gaseous, liquid and volatile solid samples [50].

c *FID as a tool for qualitative analysis*

It is a very versatile detector that responds to all compounds possessing C – H bond (s) [50].

d *FID as a tool for quantitative analysis*

It has a linear range of approximately 10^{-7}. It also exhibits limits of detection as low as 10^{-13} g.C/s [50].

1.2.5 FID as a liquid chromatography detector

The working mechanism of the FID is the same for both modes; gas chromatography (GC) and liquid chromatography (LC) modes. However, two differences exist between GC-FID and LC-FID; the column and the sampling systems. In the LC-FID equipment, the LC columns, which are more versatile, replace the GC columns. In the GC-FID, the sample is introduced into an inlet system before the column where it is converted to a vapour for more sensitive detection. There is no inlet system in the configuration of LC-FID equipment; it is replaced with interfaces such as the transfer detectors, thermospray, eluent-jet etc. These interfaces are discussed in the subsequent sections.

1.3 Liquid chromatography-flame ionization detection (LC-FID) interfaces

This section is basically concern with a review of the evolution of the LC-FID interfaces. These include those used with hydro-organic mobile phases (methanol-water, acetonitrile-water etc) and those used with 100% water as a mobile phase.

1.3.1 Interfaces used with hydro-organic mobile phases

An obvious disadvantage of coupling LC to FID is the high detector response of the organic modifiers commonly used in reversed or normal phase LC. Since the FID responds to the organic components of mobile phases, there should be a way of removing the organic components from the effluent before the detector, otherwise the analyte signal will be obscured by the organic modifier signal [56]. Interfaces such as the transport detectors and thermospray, have been identified with this capability.

a Transport detectors

These detectors were the earliest interfaces developed to interface liquid chromatography to flame ionization detector. A transport detector consists of a carrier, which can be a metal chain, wire, disc, or similar device which is continuously moving between the effluent introduction point and the detector [57]. They work by drying the mobile phase from the carrier medium before detecting the residue directly or as pyrolysis products [58]. A comprehensive review of these detectors has been reported [59]. In addition to the capability of removing the organic components of the mobile phase, they give a similar response for a rather wide range of compounds [60].

Since the moving object with its speed is an integral part of the detector, it is important to recall their empirical values. Typical operating conditions for the wire-transport detector are: wire diameter, 0.4 mm; speed, 5 to 15

cm/min; eluent flow-rate, 10 to 70 µL/min; carrier gas flow-rate, about 35 mL/min; FID temperature, 200 to 400 °C; air flow-rate, 590 mL/min; hydrogen, 32 mL/min [61 - 64].

In general, the transport detectors are designed to analyze non-volatile compounds, such as carbohydrates, fatty acids, glyceride esters, steroids, and phospholipids [61 - 64]. Veening *et al.* [63] reported detection limits that ranged from 100 to 400 ng for the carbohydrates.

Since the eluent is dried before detection, their applications are limited to the analysis of non-volatile analytes. However, the analysis of semi-volatiles were made possible by the introduction of the Tracor Model 945 LC-FID system; a modified transport detector.

There are two modes of detection in the transport detectors; detection of analyte residue and the detection of pyrolysis products.

i *Detection of analyte residue*

A typical transport detector for use with a flame ionization detector (in this case, the related alkali flame ionization detector) is shown in Figure 1.7. The transport mechanism operates as follows. The wire is reeled off from a storage coil (1), passes via rollers (2, 3) through an activation oven (4) which is heated to 750 °C to remove impurities and led through a coating block (5). Here, it receives part of the effluent from the column (12). The amount of liquid carried depends on the speed of the wire feed and mobile phase flow rate; a typical amount is 0.5%. The wire then passes through a combustion oven (7) heated to 700 °C. Air is led into the combustion oven through the sides and carries the combustion products into the detector (8). The flow-rates of the gas can be adjusted by needle valves (10) and controlled by manometers (9) [62].

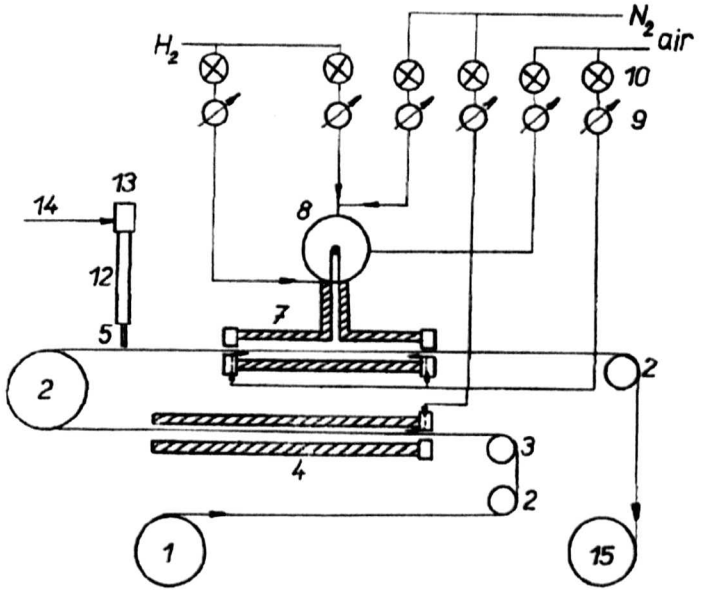

Figure 1.7. Schematic of the alkali flame ionization detector with residue detection. (1) wire storage coil, (2, 3) rollers, (4) activated oven, (5) coating block, (7) combustion oven (8) AFID (9) manometer (10) needle valves (12) column (13) membrane sampler (14) effluent [62].

ii Detection of pyrolysis products

Veening *et al.* [63] examined the Pye Unicam LCM moving wire flame ionization detector. In this technique, pyrolysis products were detected instead of the residue. The working principle involved the following: the moving wire was supplied from a rotating spool and initially passed through a cleaner oven operated at 850 °C where impurities were removed by oxidation in a stream of air. The wire then moved past the coating block where the effluent was deposited. After deposition, the wire moved through an evaporator, set at 180 °C - 200 °C, which selectively removed the solvent in a stream of air. Finally, the wire passed through the oxidizer tube where sample components were oxidized at 850 °C to carbon dioxide and steam in a stream of air. The resultant carbon dioxide was mixed with a stream of nitrogen and hydrogen and was reduced to methane in a reactor (350 °C) in the presence of a nickel catalyst, which was finally detected by FID. In this detection mode, the signal was directly proportional to the amount of

carbon deposited on the wire hence it could be used for quantitative analysis [56].

Tracor Model 945 LC-FID system

Transport detectors are normally limited to the analysis of non-volatile analytes [53]. But semi-volatile analytes could be analyzed with the Tracor Model 945 LC-FID system, which was developed [65] and introduced at the 1983 Pittsburgh Conference. The detector consisted of a fibrous quartz belt at the periphery of a rotating disc enclosed in a heated-air-swept housing. The total LC effluent was applied as a fine stream onto the rotating porous quartz belt. As the disc rotated, the solvent was vaporized while the non-volatile analytes were carried to the FID. A second much hotter flame was used to clean the belt.

Pearson [66, 67] modified the Tracor system to accommodate a reduction of the evaporation block temperature from 150 °C to 68 °C. The modified system was able to extend the use of the system to the lower molecular weight alkanes, that is, from C_{32} to C_{24}.

Problems of the transport detectors

Although transport detectors are capable of removing the eluent before detection [68], some shortcomings have been identified. Generally, they have only been given limited attention in analytical chemistry because at the relatively high flow rates used in conventional HPLC columns, only a small fraction of the column effluent is coated on the moving surface, thus seriously impairing the limits of detection [63].

Inherently, they are complex designs and loss of volatile analytes is common during the solvent removal process [57, 58, 69]. A schematic of a typical moving-wire transport detector, illustrating the complexity of the design, is shown in Figure 1.7 [62]. Features, such as the wire storage coil,

rollers, activated oven, coating block manometers which may otherwise cause analytical problems, are not needed in the recent interfaces such as thermospray, eluent-jet, nebulizer etc, which will be discussed latter.

Memory effects and poor desorption are also observed with transport detectors. Marquet *et al.* [57], Brewer *et al.* [70] and Combs *et al.* [71] observed 'memory effects' commonly seen as ghost peaks in the use of these detectors. These detectors were also identified with poor sensitivities, probably due to poor desorption of non-volatile and polar analytes from the moving object [71].

These detectors also undergo dimensional changes when heated, contamination of one part of the wire by structural components, and the general lack of reliability of the mechanism [68].

Dijk [64] found the tendency of solute to creep during the period of drying, thus causing the occurrence of irregular intervals of places of extremely high concentration along the moving chain [64].

Malcolme-Lawes *et al.* [68] found the limitations of the moving chain in quantitative analysis. This was attributed to the loss of components from the chain and the electrical noise generated by the chain mesh. Another observation made by them was the melting and spreading of non-volatile analytes over the chain [68].

b Thermospray

In the application of this interface (Fig 1.8) [33], the effluent from the LC column is thermally nebulized and/or vaporized by an electrically heated probe in the presence of a warm carrier gas. The volatile molecules of the solvent if present and low boiling-point sample molecules in the aerosol are vaporized and then removed in a counter-current membrane diffusion cell. The higher boiling-point sample molecules in the form of particles are not

removed in the membrane and are detected by a downstream flame ionization detector (FID) [33]. Disanzo *et al.* [33] used this interface to study the n-paraffins and found that only samples with an initial boiling point greater than 375 °C could be detected. The condensate pump could only remove about 75% of the solvent (hexane), the remainder of the solvent was removed by the membrane [33]. Disanzo *et al.* determined aromatics and found detection limits of approximately 0.5 µg under the following conditions: nebulization temperature, 80 - 85 °C; spray chamber temperature, 60 - 65 °C; membrane temperature, 60 - 65 °C and FID temperature, 130 - 150 °C.

This interface is used for non-volatile analytes [33, 56]. Combs *et al.* [71] identified the possibility of thermal degradation of analytes due to the heated nebulizer.

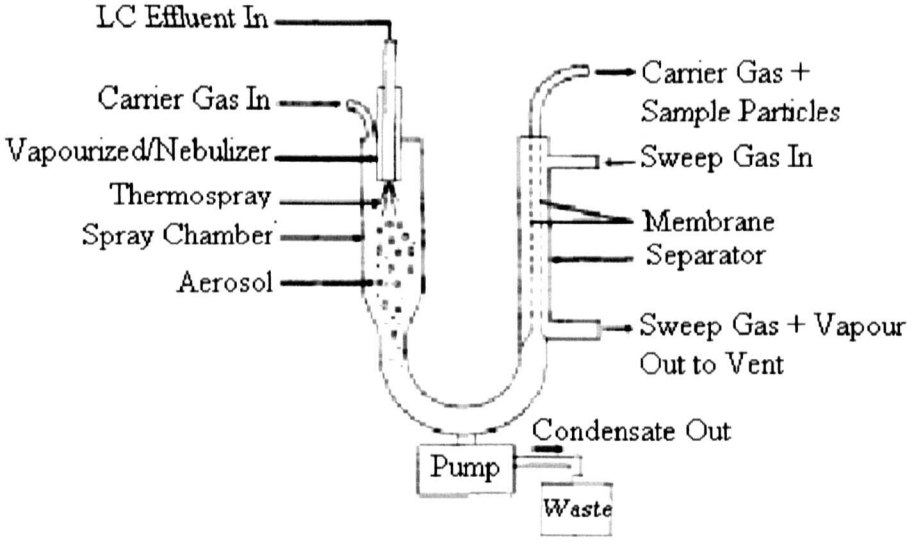

Figure 1.8. Schematic of thermospray interface for solvent removal [33].

1.3.2 Interfaces used with 100% water as mobile phase

In order to reduce the eluent signal, one approach is to use 100% water as the eluent. This allows the direct coupling of the LC to the FID because the

problems of removing the organic components of the mobile phase before detection are not issues; the aqueous eluent generates no response in the FID [58, 72, 73].

Beside its transparency to the FID, 100% water as eluent offers several advantages; it is not toxic, not flammable and relatively less expensive compared to common HPLC eluents (methanol, acetonitrile, etc) [74].

Although water at ambient temperature is a weak solvent in reversed-phase chromatography, it exhibits comparable eluent properties with the usual reversed-phase eluents (methanol-water, acetonitrile-water etc) when heated to high temperatures. Water above its normal boiling point up to its supercritical temperature exhibits reduced viscocity, an increased ability to dissolve non-polar compounds, and decreased polarity. All of these properties result in the liquid having properties comparable to an organic solvent [75].

Several advantages are associated with the use of water (heated to high temperatures) as an eluent. At these temperatures, it becomes a useful parameter to enhance chromatographic parameters such as resolution, efficiency and speed [74, 76 – 83].

a Drop headspace interface

Bruckner *et al.* [56] developed a drop headspace interface for FID used with superheated water chromatography. In this interface, drops of eluent formed at the tip of silica tubing, fall unobstructed. A controlled-flow of helium entered the cell via a hole below the level of the growing drop. A portion of the helium stream flowed upward past the drop, picking up any organic components evaporating from the drop (Figure 1.9). The analyte-rich helium then flowed to the detector. Typical eluent and helium flow rates used in this interface are 0.67 mL/min and 35 mL/min respectively.

The interface was used for the analysis of 1-butanol, 1,1,2-trichloromethane, butanone, chlorobenzene, toluene, ethylbenzene and o-xylene at flow-rates of 300 mL/min and 30 mL/min respectively, for air and hydrogen and the limits of detections ranged from 0.5 to 9 ppb. A linear dynamic range of 5 orders of magnitude was also reported for 1-butanol; this was comparable to GC-FID.

Its use is limited to the analysis of volatile analytes. Quigley *et al.* [84] demonstrated this by using this interface to selectively determine the volatile alcohols in a mixture of alcohols and phenols. A disadvantage of this interface was a reduction of column efficiency due to the large volume of the cell [56].

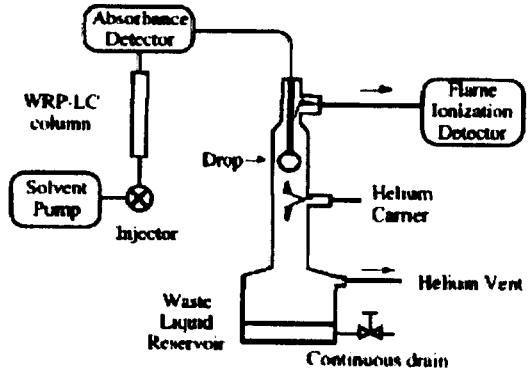

Figure 1.9. Schematic of LC with UV absorbance and flame ionization detections, highlighting the drop headspace interface that transports volatile analytes from the LC eluent to the FID [56].

b Eluent-jet interface

The eluent-jet [58] is not based on evaporation or nebulization of the eluent, but on the formation of an eluent-jet, which consists of a stream of small droplets. Although, it was originally used in liquid chromatography-mass spectrometry (LC-MS), the principle of operation is similar for both applications; LC-FID and LC-MS.

The liquid introduction process is based on a sharp temperature gradient at the tip of the fused silica liquid introduction capillary (A) (Figure 1.10) [85].

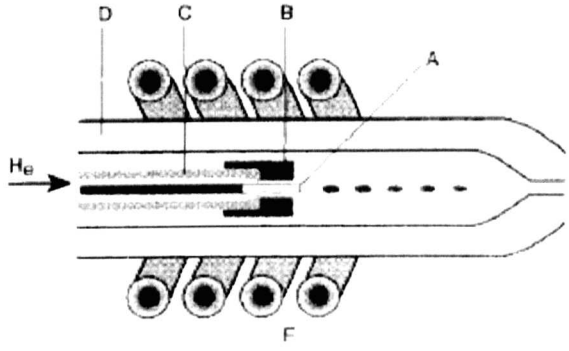

Figure 1.10. An eluent-jet interface. A, fused-silica liquid introduction capillary; B, metal ring; C, quartz tube; D, desolvation tube and E, induction coil [85].

The sharp temperature gradient is induced by heating a small metal ring (B) mounted on the top of a small quartz tube providing helium cooling (C). These parts are inserted in (D), a wider quartz tube. The metal ring is heated by means of high-frequency induction, which is a non-contact method of heating electrically conducting materials. The induction heater produces a radio frequency (900 -1100 kHz) current in the induction coil (E) placed on the outside of the desolvation tube. This generates an alternating magnetic field in the desolvation tube, which induces an electrical current in the small metal ring, developing sufficient heating power [85].

The potential of an eluent-jet interface with μLC-FID was examined with test compounds ranging from highly polar, thermolabile, semi-volatile and non-volatile compounds like amino acids, organic acids, alkylphosphonic acids, and carbohydrates. The results showed a linear dynamic range of four orders of magnitude [58]; an order of magnitude better than a nebulization interface for less volatile compounds. Probably, this can be explained by the divergence of the nebulization interface which is much larger than that of the eluent-jet that produces essentially a straight jet of droplets [85].

Hooijschuur *et al.* [58] also reported detection limits that ranged from 0.2 – 5 ng.

c Direct liquid introduction (DLI) interface

Miller *et al.* [40] examined a direct liquid introduction interface in which the liquid chromatography was connected to the flame ionization detector via a heated capillary tube (usually 10 – 50 μm i.d) with a transfer restrictor. This set up was used in the determination of alcohols and caffeine and a detection limit of 1 ng was reported at eluent flow rates of 20 - 50 μL/min and 5 ng at flow rates of 100 to 200 μL/min.

They reported instability of the FID at flow rates greater than 0.2 mL/minutes. This was explained in terms of a volume expansion of the eluent when it becomes vapour in the FID resulting in the instability of the analytical flame and sometimes, flame-out.

Besides flame instability, there were some other interesting issues associated with the direct liquid introduction via a crimped or narrow restrictor capillary. It was easily clogged because of the crimped part of the restrictor [86, 87]. The clogging problem may be due to the fact that fused silica reacts with water in the FID at elevated temperatures [87].

Another issue is the distance of the capillary from the tip of the jet. The best FID stability was obtained when the connecting tube was 3 – 3.5 cm below the jet tip. When the tube was placed too close to the jet tip, spikes were produced and when the tube was placed too far from the tip of the jet, the peak efficiency was reduced [87].

The internal diameter of the jet was yet another issue of concern. Carrier water flow rates of 100 μL/min or higher were compatible with the use of wide bore FID jet resulting in an improved stability of the FID signal. However, the FID sensitivity was decreased. Hence, the water flow rates of

50 µL/min or lower was used with the standard FID jet instead of the wide-bore jet [88].

The instability of the FID resulting from the splitless design can be remedied either by using a micro-bore column that is compatible with low flow rates or splitting the effluent. Both measures work by preventing too much eluent from reaching the FID.

i Micro-bore column

Yang *et al.* [89] developed a direct introduction interface with a micro-bore column (0.5 mm internal diameter) at flow rates of 20 - 30 µL/min. They made a number of observations. The FID was stable and faster thermal equilibration of the column was observed compared to the traditional HPLC columns with a typical internal diameter of 4.6 mm. The linear dynamic range for leucine and tryptophan was 6 to 6000 ng. They analysed carbohydrates, amino acids and organic acids and found low limits of detection ranging from 0.3 to 3 ng for the amino acids. The detection limits were low because the total effluent was introduced into the FID without a split.

ii Effluent split

One of the alternative solutions to the FID flame instability is to split the effluent before the FID. Marquet *et al.* [57] and Conte *et al.* [90] identified the need to reduce the effluent flow because the FID flame has little tolerance for large volumes of effluent. However, the effluent split resulted in loss of sensitivity.

Yarita *et al.* [91] also developed a direct liquid introduction with effluent split (Figure 1.11). In the experimental set up, a portion of the effluent from the separation column was split using a T-piece. The split effluent was introduced into the FID system via a capillary tube (270 mm x 40 µm i.d)

heated at 150 °C in order to maintain a stable vaporization of the water in the FID system. This set up was used in the determination of ethanol in alcoholic beverages at a flow rate of 7 µL/min and detector temperature of 350 °C. The mean values of ethanol in their samples were comparable with those obtained by GC-FID at the same detector temperature.

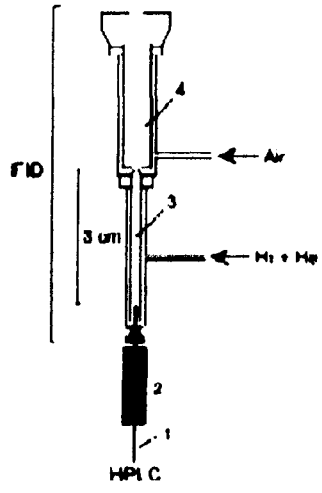

Figure 1.11. Schematic of direct liquid introduction interface with effluent split: 1, fused-silica capillary tube; 2, heater; 3, FID jet; 4, ion collector [91].

An effluent split interface (capillary tube) was employed in the analysis of carbohydrates, amino acids and carboxylic acids. The interface was examined under the following conditions: eluent flow-rate, 0.13 mL/min with a split ratio of 1:10 (FID:waste bottle); the distance between the restrictor outlet and the tip of the FID jet was 5 cm; air flow, 350 mL/min; hydrogen, 135 mL/min; detector temperature, 350 °C. Under these conditions, the limits of detection of these compounds ranged from 38 to 111 ng; a much higher detection limits compared to micro-bore column analysis. A linear dynamic range of three orders of magnitude was also reported [92].

d Pneumatic nebulization interface

This interface, which works by breaking up the liquid stream into an aerosol by the use of a high velocity gas jet, is one of the most commonly used liquid sampling methods in inductively coupled plasma mass spectrometry (ICP-MS) [93] due to its simplicity of design, stability and reliability. In addition, it is more versatile than the transport detectors, drop headspace, and thermospray because it can be used for the analysis of both volatile and non-volatile analytes; transport detectors and thermospray interface are limited to non-volatile and the drop headspace is limited to volatile analytes [85].

Despite these advantages, the nebulization interface needs additional care; the connecting lines and pumping systems should be able to withstand the high pressures needed for such a pneumatic process and consequently, the additional cost of using it [94].

Although it is a sampling method commonly employed in ICP-MS, it is relatively new in interfacing liquid phase separation techniques (HPLC, CE) to detectors, such as FID, MS etc. For such coupling, the concern is that, the interface should not lead to band broadening and hence reduce peak resolution. In order to achieve the goal of good peak resolution, the interface (usually a nebulizer-spray chamber unit) should have a low dead volume. The micro-nebulizers (capable of producing stable aerosol at flow rates in the order of μL/min) and miniaturized spray chambers have been identified with low dead volumes [95 - 103].

The use of the micro-concentric nebulizer (MCN) in separation science was first reported in 1995 by Olesik *et al.* [104] when they used a nebulizer-spray chamber assembly in capillary electrophoresis-inductively coupled plasma mass spectrometry. Since then, many designs of nebulizer and spray

chambers have been used by different groups of workers and these have been reviewed by Taylor *et al.* [105].

Recently, Taylor *et al.* [105], designed and examined a micro-concentric nebulizer (MCN)-spray chamber interface for capillary electrophoresis-inductively coupled mass spectrometry. The spray chamber was made of glass, designed with features (the dimple and flow spoiler) such that the aerosol was under a centrifugal force which served to remove coarse particles. The interaction of the larger particles with the walls of the chamber was increased by the dimple resulting in an enhancement of the removal process. The purpose of the flow spoiler was to stop recirculation of the aerosol which could cause dispersion, increase sample wash-out times and band broadening [105].

The MCN-spray chamber interface was recently used for the examination of a liquid chromatography-flame ionization detection method [106]. They examined the interface and reported the following findings: The optimum FID conditions using carbohydrates as test analytes were: hydrogen, 100 - 110 mL/min; air, 320 mL/min; nitrogen, 420 mL/min; detector temperature, 230 °C; eluent flow rate, 0.7 mL/min. In addition, detection limits of 5.5 ng, 12 ng, 3.5 ng were reported for D-glucose, amino acids and toluene respectively. They also examined and compared the thermospray and MCN interfaces and found that the latter was better. The former was set up as follows: the effluent from the column was linked to the detector by a capillary tubing (30 μm i.d., 17.5 cm). Aerosol formation was effected by heating the transport capillary, which was in the oven, to high temperatures (150 °C - 400 °C). Unfortunately, the method did not yield results as expected due to problems of frequent capillary blockage, instability of the flame at carrier water flow rate of about 0.18 mL/min. Besides, the method was found to be irreproducible and non-robust.

1.4 An overview

Selective detectors

The UV detector is the most commonly used detector because it is sensitive (limit of detection, 0.1 – 1 ng) and easy to use. It is insensitive to environmental factors such as temperature and pressure. However, it is limited to UV-absorbing analytes.

The fluorescence detector is more sensitive (0.001 – 0.01 ng) and selective than the UV detector. Its application is limited in that, fluorescence is limited by structural (substitution, rigidity) and environmental (temperature, type of solvent, pH and dissolved oxygen) factors.

The electrochemical detector has limit of detection of 0.01 – 1 ng. It is limited to the analysis of oxidizable and reducible compounds.

Universal detectors

The refractive index detector exhibits limited sensitivity (LOD, 100 – 1000 ng), poor selectivity, non-compatibility with gradient elution, and it is extremely sensitive to temperature and pressure fluctuations.

The evaporative light scattering and charged-aerosol detectors are aerosol-based. Their chromatographic baselines are not affected by environmental factors such as temperature and pressure fluctuations. Both detectors are limited to the analysis of non-volatile analytes and exhibits non-linear response patterns. The limits of detection of the ELSD ranged from 100 – 150 ng while that of the CAD ranged from 5 – 20 ng.

Comparison of LC-FID interfaces

The nebulization and eluent interfaces are compatible with eluent flow rates of about 1 mL/min, typical of a conventional HPLC whereas the transport detectors, the thermospray and direct liquid introduction interfaces are compatible with flow rates of the order of 10 to 200 μL/min; flow rates higher than this will cause flame instability. From the discussion, it is obvious that only nebulization and eluent interfaces can be used for analyses that inevitably need flow rates of about 1 mL/min.

The transport detectors are the most complex interfaces both in design and operation.

The nebulization and the eluent jet interfaces are the most versatile because they can be used for the analysis of both volatile and non-volatile analytes; the transport detectors and the thermospray are limited to the analysis of non-volatile analytes and the drop headspace is limited to the analysis of volatile analytes.

1.5 Aims and objectives of the present study

This current work, which examines a-nebulized flame ionization detection in liquid chromatography, is a continuation of the work of Bone *et al.* [106]. It is compatible with gradient elution and capable of analyzing non UV-absorbing and non-volatile analytes without derivatization. Its design will also examine the linearity and sensitivity.

The development of the method was carried out in two stages; flow injection analysis (FIA) mode and liquid chromatography (LC) mode. The former mode is aimed at optimizing the FID to ensure that the eluent (100% water) flow, the interface (nebulizer-spray chamber unit) and detector integrate. The latter mode will be concerned with applying the optimized

parameters to separate non-volatile and non UV-absorbing analytes representing different functional groups such as alcohols, amines, amino acids, organic acids and sugars in order to determine the relative responses of different analyte types.

CHAPTER TWO

Experimental

2.1 Materials

Acetophenone, anisole, benzoic acid, methyl benzoate, phenylethylamine, 3-phenylpropanol, 4-phenylbutanol, benzylamine, hexylamine, pentylamine, cyclohexylamine, 1,3-diaminopropane, diethanolamine, ethanolamine, ethylene diamine, maltose, citric acid, malic acid, succinic acid, acetic acid, sorbitol, glucose, D(+)-galactose, arabinose and mannitol, valine, isoleucine, phenylalanine, serine, decyl alcohol, poly (ethylene glycol), glycerol, 4-hydroxybenzamide, 4-hydroxybenzoic acid, benzaldehyde, methanol, propanol, pyridine, resorcinol, o-methyl-acetophenone, hexanone, 2-phenylethanol and heptanone were from Aldrich Chemical Company Inc., Milwaukee, USA.

Dichloromethane, hexane, ammonium sulphate, sodium sulphate and the acids (sulphuric, hydrochloric, orthophosphoric, nitric) were from Fisher Scientific, Loughborough, England.

Propiophenone was acquired from Hopkins & Williams Ltd, Essex, England. Butyl phenyl ketone and butyrophenone were bought from Koch-Light Laboratories Ltd, Colnbrook, England. Lancaster, Morecambe, England supplied benzyl alcohol and diethylamine. Triethylamine and benzoic acid were supplied by Fisons Chemicals, Loughborough, England. Cyclohexanol and m-cresol were supplied by Avocado (Morecambe, England) and Agros Organic (USA) respectively. Aniline was from Alfa Aesar, Heysham, UK. BOC gases (air, hydrogen and nitrogen) Worsley, Manchester. De-ionized water was prepared in the laboratory with an ELGA water purification system, High Wycombe, England.

2.2 Sample solutions

2.2.1 FIA mode

All samples were prepared individually in water.

Optimization of the FID set-up

Valine, 1.26 mg/mL

Volatile Analytes

Methanol, 0.925 mg/mL; propanol, 1.07 mg/mL; hexane, 4 mg/mL and dichloromethane, 2.34 mg/mL.

Non-Volatile Liquid Analytes

Maltose, 1 mg/mL; valine, 1 mg/mL; ethylene glycol, 1.11 mg/mL; poly (ethylene glycol), 0.815 mg/mL; resorcinol, 0.9 mg/mL; 4-hydroxybenzoic acid, 0.66 mg/mL and 4-hydroxybenzamide, 0.65 mg/mL.

Glycerol, 4.25 mg/mL and decyl alcohol, 1.8 mg/mL.

2.2.2 LC mode

Samples were prepared in water as mixtures.

Alcohols

A mixture of alcohols (methanol, 2.93 mg/mL; ethanol, 3.30 mg/mL; propanol, 2.95 mg/mL; butanol, 3.44 mg/mL; cyclohexanol, 2.00 mg/mL; benzyl alcohol, 3.82 mg/mL and m-cresol, 3.19 mg/mL).

Aromatic Alcohols/phenol

A mixture with the following composition was prepared: benzyl alcohol, 2.14 mg/mL and m-cresol, 2.94 mg/mL.

Benzyl alcohol and substituted aryl alcohols

Sample composition: benzyl alcohol, 0.535 mg/mL; 2-phenylethanol, 0.738 mg/mL; 3-phenylpropanol, 0.663 mg/mL and 4-phenylbutanol, 0.400 mg/mL. 100 µl of neat methanol was added to enhance the solubility of the mixture in water.

Aldehydes

Sample composition: formaldehyde (37%) 1.112 mg/mL; acetaldehyde (40%) 1.07 mg/mL and propionaldehyde (97%) 0.428 mg/mL.

Ketones

A mixture of ketones: 2-hexanone, 0427 mg/mL; o-methyl-acetophenone, 0.527 mg/mL; propiophenone, 0.537 mg/mL; 2-heptanone, 0.422 mg/mL and butyrophenone, 4.16 mg/mL.

Organic acids, amides and an aldehyde

Sample contained 4-hydroxybenzamide (2 mg/mL), 4-hydroxybenzoic acid (2 mg/mL), benzoic acid (2 mg/mL) and benzaldehyde (0.144 mg/mL).

Sample contained citric acid, 4.14 mg/mL; malic acid, 5.08 mg/mL; succinic acid, 9.83 mg/mL and acetic acid, 7.98 mg/mL. This mixture was used for the flame ionization detection. A different mixture was prepared for the refractive index detection: citric acid, 0.207 mg/mL; malic acid, 0.254 mg/mL; succinic acid, 0.492 mg/mL and acetic acid, 0.399 mg/mL.

Aromatic amines

A mixture of amines containing pyridine, 0.37 mg/mL; aniline, 1.40 mg/mL and benzylamine, 0.7 mg/mL.

Aliphatic amines

Sample contained benzylamine, 3 mg/mL; pentylamine, 3 mg/mL; phenylethylamine, 4.17 mg/mL and hexylamine, 3.05 mg/mL.

Amino Acids

Sample contained phenylalanine, 0.5 mg/mL; isoleucine, 0.53 mg/mL; valine, 0.55 mg/mL and serine, 0.5 mg/mL. A mixture containing lower concentrations was prepared for the liquid chromatography refractive index detection; 0.15 mg/mL each of valine, isoleucine and phenylalanine.

Sugars

Sample composition for the LC-FID: sorbitol, 2.55 mg/mL; maltose, 5 mg/mL; D(+)-galactose, 2.6 mg/mL; arabinose, 3.6 mg/mL; glucose, 3.8 mg/mL; mannitol, 2.4 mg/mL. For the LC-RID mode, the mixture composed of sorbitol, 0.255 mg/mL; maltose, 0.5 mg/mL; D(+)-galactose, 0.26 mg/mL, arabinose, 0.36 mg/mL; glucose, 0.38 mg/mL and mannitol, 0.24 mg/mL.

2.3 Equipment

2.3.1 Columns

PL HiPlex H 8 μm (300 x 7.7 mm) and PS-DVB (150 x 4.6 mm) were from Polymer Laboratories, Amherst USA. Xterra RP 8 (3.5 μm, 4.6 x 150 mm), Xterra RP 18 (3.5 μm, 4.6 x 150 mm), Xterra MS C18 (5 μm, 2.1 x 150 mm), were supplied by Waters, Ireland. Hewlett Packard HP-5 (Crosslinked 5% Ph Me Siloxane) 30 m x 0.32 mm x 0.25 μm film thickness, Texas, USA, was used for the GC-FID.

The LC-(FID,UV, RID) was constructed using a Varian 3300 flame ionization detector (Walnut, California); Applied Biosystems 757 Absorbance detector

(Crewe, UK); Waters 2410 Differential Refractometer (Milford, USA); Hewlett Packard 1050 quaternary pump (Texas, USA); Gilson M313 peristaltic pump (Villiers. Le. Bel. France); Rheodyne injector (Cotati, California) and Cetac micro-concentric nebulizer (MCN-100), (Omaha, NE, USA).

Viglen computer and HP LaserJet 1022 printer. Operations and data acquisitions were enabled with DataApex Clarity software.

2.3.2 Instrumentation of the LC-FID

The configuration of the LC-FID equipment and its schematic are shown in Figures 2.1 and 2.2 respectively. Essentially, this set up is different from the conventional HPLC equipment in two components; the FID (Figure 2.3), which was mounted on the separate spray chamber oven, but used the GLC electronics and the nebulizer/spray chamber assembly (Figure 2.4).

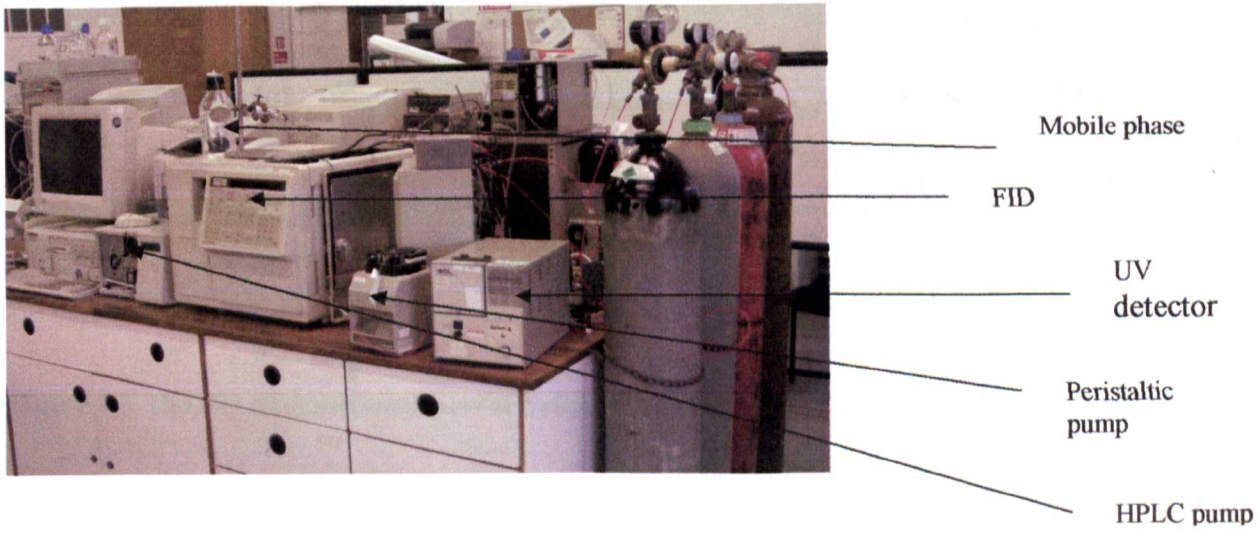

Figure 2.1. The LC-FID equipment.

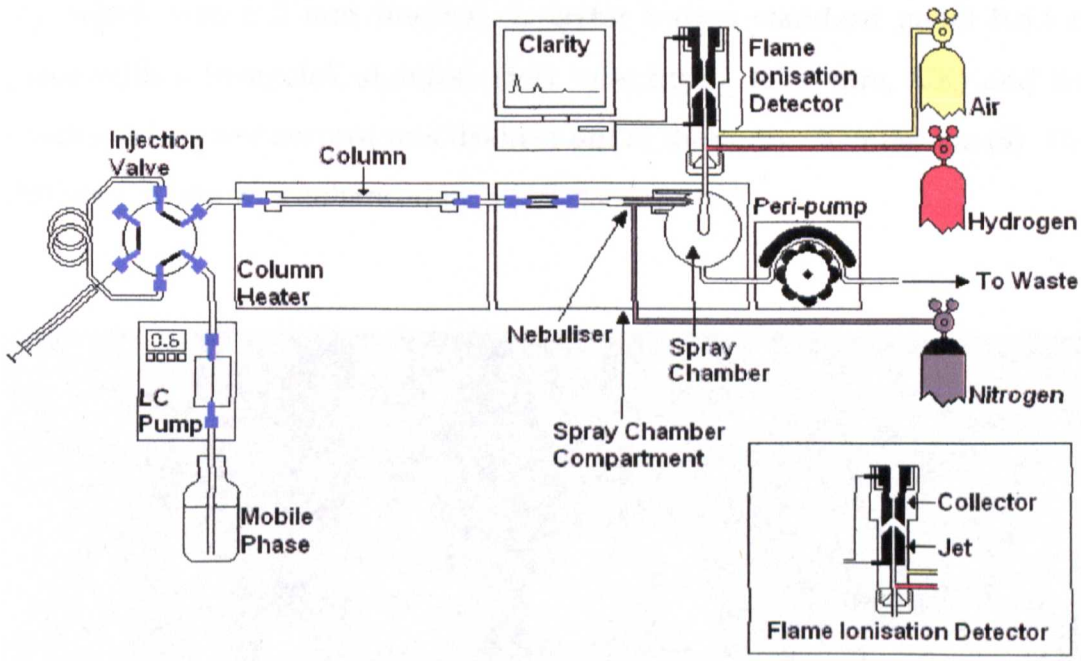

Figure 2.2. Schematic of the LC-FID equipment.

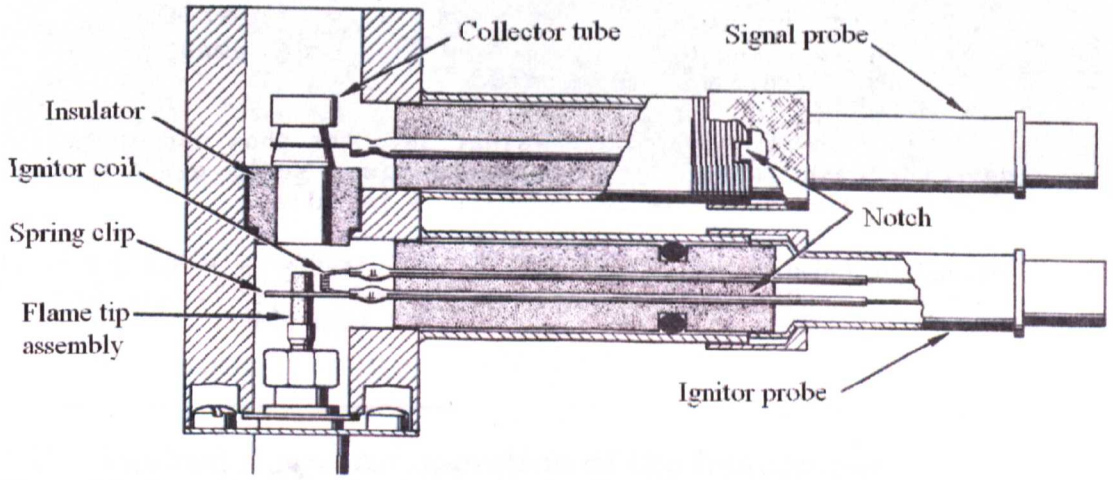

Figure 2.3. The FID cross sectional view showing the collector.

The nebulizer/spray chamber assembly (Figure 2.4) was placed between the column and the detector (FID). The nebulizer (3) receives mobile phase containing the sample via (1) and the effluent was pneumatically nebulized into the spray chamber (4). The fine aerosol was directed to the detector via

(6), which was a 2 mm internal diameter Varian standard metal held in place with a Swagelok stainless steel tube fitting (Cheshire, UK) and the condensed, coarse aerosol was drained out of the spray chamber via (5). The draining action was enhanced by a peristaltic pump.

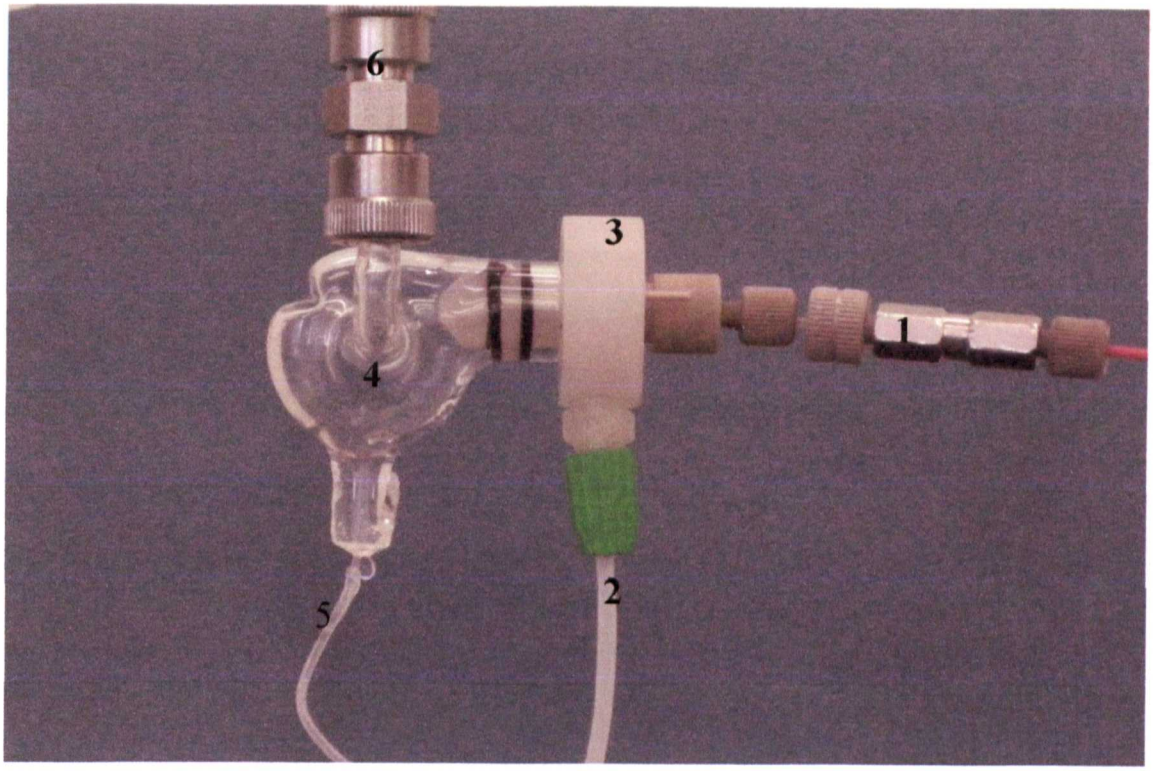

Figure 2.4. Nebulizer/spray assembly. (1) from HPLC column (2) nebulizing gas (3) nebulizer (4) spray chamber (5) condensate to drain (6) fine aerosol to detector.

2.4 Methodology and operation of the instrument

Optimization of the FID Set-up

In the laboratory set up, the only modification made to the FID was the replacement of the existing standard jet with a ceramic tube of 2 mm i.d. with a metal tip (a total length of 33 mm) to allow the free flow of the gas through the system.

The non-optimal conditions used to start off the optimization process were: collector internal diameter, 4 mm; spray chamber diameter, 30 mm; air flow, 650 mL/min; hydrogen flow, 157 mL/min; nitrogen flow, 184 mL/min and carrier water flow, 1 mL/min.

LC-FID

FID conditions applied were the same for both LC-FID and FIA-FID. However, appropriate column oven temperatures were applied for the separation of different compounds on different columns.

CHAPTER THREE

Instrumentation and the LC-FID method development

3.1 Instrumentation

The essential differences between the gas chromatograph with flame ionization detector and the LC-FID equipment are the column and the sampling systems. In the LC-FID equipment, the LC columns which are more versatile replace the GC columns. In GC, the sample is introduced into an inlet system where it is converted to a vapour for more sensitive detection. There is no heated inlet system in this configuration of the LC-FID equipment; it is replaced with a nebulizer/spray chamber assembly, incorporated between the column and the detector. The nebulizer turns the liquid sample into a form (fine aerosol) that is more amenable to treatment by a flame and improves detection. The spray chamber functions to remove coarse and coalesced fraction of the aerosol and its subsequent removal from the chamber. The nebulizer/spray assembly is shown in Figure 2.4.

The body of the nebulizer was built of an inert, Teflon material and hence can be used for aspirating acids or bases [107].

For an effective adaptation of the LC to the FID, some modifications were made to the nebulizer capillary and the jet. In order to accommodate higher eluent flows, typical of HPLC, the silica capillary in the standard MCN was replaced with a-0.009 inches stainless steel capillary (from Coopers Needle Works, Birmingham, West Midlands, UK). Besides the flow-rate compatibility, the new capillary could aspirate solutions containing dissolved salts with a reduced probability of getting blocked compared to the standard capillary [108].

The standard jet in the FID was replaced with a metal-tip ceramic jet of 2 mm internal diameter to ensure free flow of gases.

3.2 Nebulizer problems

The nebulizer, which is the sampling system, affects the variability of the FID response to a great extent. Keeping the flow-rates of gases and the detector temperature constant, variability in response can result from the following: when different nebulizers are used, the nebulizer capillary is replaced or when the capillary is partially blocked. In this current work, the first nebulizer was replaced because it was damaged and occasionally the capillary of the second one had been sonicated when blockages were observed. These can account for some observed variability in responses. The separation of the alcohols (methanol, ethanol, propanol, butanol, cyclohexanol, benzyl alcohol and m-cresol), the amines (aniline, benzylamine and pyridine) and the mixture containing 4-hydroxybenzamide, 4-hydroxybenzoic acid, benzoic acid and benzaldehyde were carried out using the first nebulizer, which was more effective and gave higher responses. The rest of the data were generated using the new nebulizer of the same design.

3.3 LC-FID development

The development of the liquid chromatography-flame ionization detection (LC-FID) method was carried out in three consecutive stages; optimization of the flame ionization detector (FID), examination of the FID responses to analytes of different volatility (volatile and non-volatile analytes) and then optimization of the LC-FID. The first two stages were carried out via flow injection analysis (FIA) in which no column was placed between the injector and detector and individual analytes were carried to the detector without passing through a column. In all the FIA experiments, an old HPLC column was placed before the injector in order to exert a back-pressure on the

pump, without which pump pulsation would produce baseline noise and cause associated analytical problems, such as high detection limits. In the third stage of the study, sample mixtures were separated on columns before detection in the FID.

3.3.1 Optimization of the FID set up

Valine, which is non-volatile, was used as the test analyte because volatile analytes such as methanol gave excessive peak tailing probably as a result of convective dispersion of the analyte in the spray chamber.

The parameters of the system that could affect the detector response were optimized. The parameters included the flame gas flows (hydrogen and air), nebulizing gas (nitrogen) flow and carrier water flow rate. Other parameters included the physical structure of the detector such as the diameters of the spray chamber and collector. The initial conditions (un-optimized) were based on trials made previously and they included: collector internal diameter, 4 mm; spray chamber diameter, 30 mm; air flow, 650 mL/min; hydrogen flow, 157 mL/min; nitrogen flow, 184 mL/min and carrier water flow, 1 mL/min. These parameters were optimized in turn; varying the parameter being studied and keeping the other initial conditions constant. Figure 3.1 and Tables 3.1 - 3.5 shows the summary of the results.

The signal strength measured as the peak area (mV.s) decreased as the carrier water flow rate was increased (Table 3.1). Flow rates of 0.5 mL/min, 1.0 mL/min and 1.5 mL/min were tested; 0.5 mL/min gave the highest signal (626.7 mV.s) but the top of the peak was noisy. However, 1.0 mL/min was chosen as the optimum because the peak was smoother. The optimized flow rate was found to be dependent on the nebulization gas flow rates. Flows higher than 1.5 mL/min gave increased baseline noise and even flame-out.

The optimum collector and spray chamber diameters were found to be 4 mm and 40 mm respectively; they gave the highest signals (Table 3.2). The shape of the spray chamber plot in Figure 3.1A shows that a diameter of 45 mm could also be used.

The optimization of air flow rate gave the results in Table 3.3. Although, flow rates of 800 mL/min and 930 mL/min gave larger peak areas, the baselines were noisy and drifted. A flow rate of 654 mL/min (optimum) gave a peak area of 411.8 mV.s with a stable baseline. The flat portion of the air flow plot in Figure 3.1B shows that this optimum is not very critical in respect of signal size.

The effect of the nebulizing gas (nitrogen) flow on the FID signal is summarized in Table 3.4. A flow rate of 250 mL/min gave the highest signal (545.5 mV.s). This flow is critical as depicted in Figure 3.1C.

Table 3.5 summarizes the optimization of hydrogen flow. The optimum flow rate was found to be 157 mL/min because it gave the strongest signal (411.8 mV.s). The shape of the hydrogen plot in Figure 3.1D shows that it is more critical than air in the operation of the FID.

The optimum flame gas flows were found to be 157 mL/minutes for hydrogen and 650 mL/min for air. These flow rates correspond to an approximate ratio of 1:4 for hydrogen and air. In GC-FID mode, a 1:10 ratio of hydrogen to air is recommended for sensitive detection [109]. Higher proportion of hydrogen flow (157 mL/minutes) with LC-FID is needed to keep the flame alight because so much wet aerosol is introduced into the detector in this set-up (FIA-FID). The need for high proportion of hydrogen to sustain the flame had been previously observed by Fogwill *et al.* [110] and Ingelse *et al.* [88] in direct liquid introduction to the FID via fused silica tube. The former used 250 mL/min of air and 100 mL/min of hydrogen while the latter used 350 mL/min of air and 100 mL/min of hydrogen.

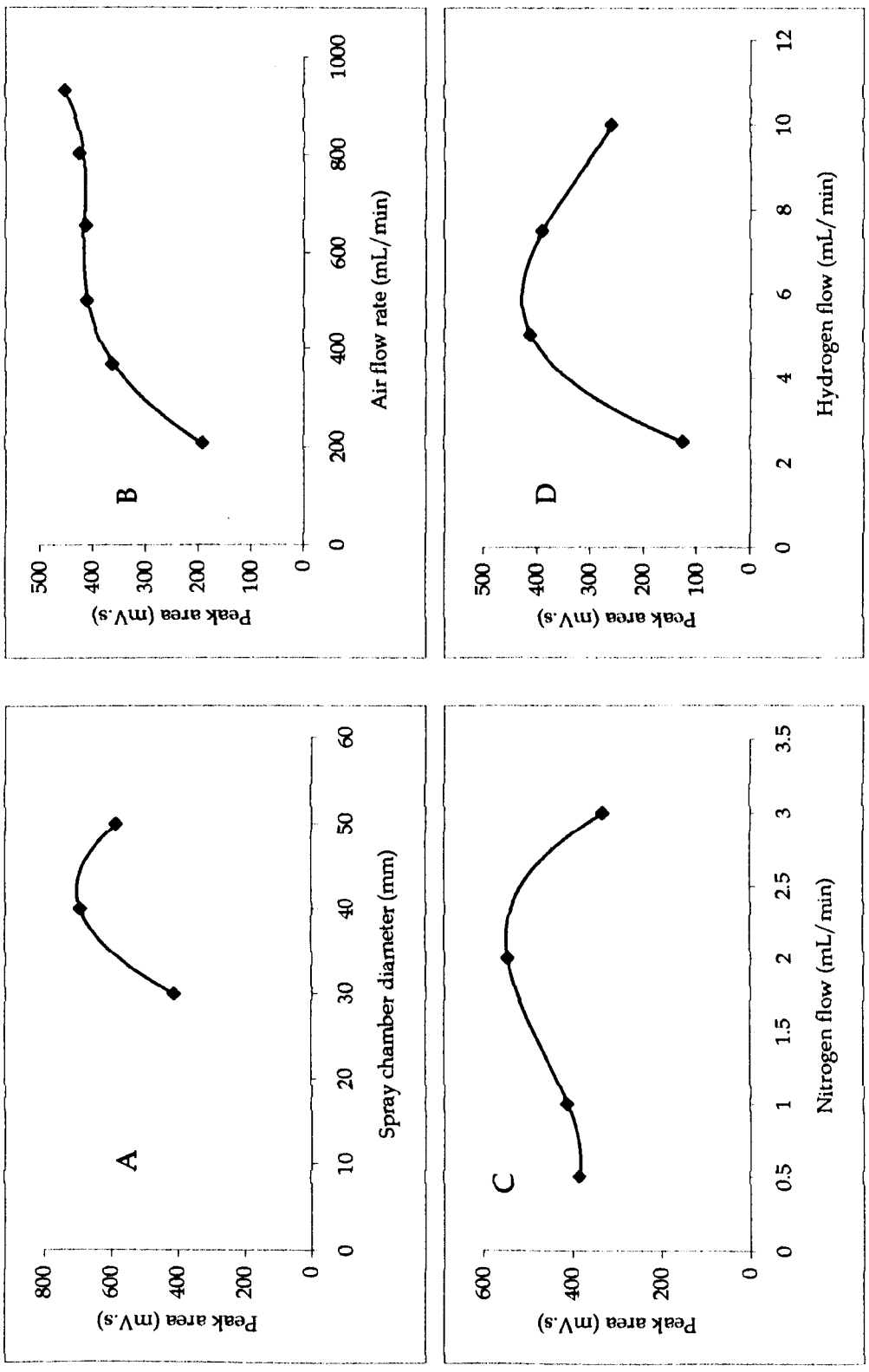

Fig 3.1. Plots showing the effect of selected parameters on FID response.

Table 3.1. The effect of carrier water flow rate on flame ionization detector signal. Test analyte, 20 µg of valine

Test parameter	Peak area in mV.s			Other parameters (kept constant)
	Mean (n=3)	SD	RSD (%)	Collector internal diameter, 4 mm; spray chamber diameter, 30 mm; air flow, 650 mL/min; hydrogen flow, 157 mL/min; nitrogen flow, 184
0.5 mL/min	626.7	1.9	0.30	
1.0 mL/min	411.8	1.6	0.39	
1.5 mL/min	393.6	2.6	0.66	

n, replicate injections; SD, Standard Deviation; RSD, Relative Standard Deviation.

Table 3.2. The effect of collector and spray chamber internal diameters on flame ionization detector signal. Test analyte, 20 µg of valine

Test parameter	Peak area in mV.s			Other parameters (kept constant)
	Mean (n=3)	SD	RSD (%)	
The effect of collector diameter				
4.00 mm, ID 29.03 mm, length	411.8	1.3	0.32	Spray chamber diameter, 30 mm; air flow, 650 mL/min; hydrogen flow, 157 mL/min; nitrogen flow, 184 mL/min and carrier water flow, 1mL/min
6.27 mm, ID 29.03 mm, length	382.9	1.9	0.50	
The effect of spray chamber diameter				
30 mm	411.8	3.0	0.73	Collector internal diameter, 4 mm; air flow, 650 mL/min; hydrogen flow, 157 mL/min; nitrogen flow, 184 mL/min and carrier water flow, 1mL/min.
40 mm	692.8	2.6	0.38	
50 mm	585.5	2.6	0.44	

n, replicate injections; SD, Standard Deviation; RSD, Relative Standard Deviation.

Table 3.3. The effect of air flow rate on flame ionization detector signal. Test analyte, 20 µg of valine

Test parameter	Peak area in mV.s			Other parameters (kept constant)
	Mean (n=3)	SD	RSD (%)	Collector internal diameter, 4 mm; spray chamber diameter, 30 mm; hydrogen flow, 157 mL/min; nitrogen flow, 184 mL/min and carrier water flow, 1mL/min.
5 psi (209 mL/min)	191.2	1.2	0.63	
10 psi (368 mL/min)	362.9	1.9	0.58	
15 psi (500 mL/min)	410.7	2.5	0.61	
20 psi (654 mL/min)	411.7	2.3	0.56	
25 psi (800 mL/min)	424.3	3.5	0.82	
30 psi (930 mL/min)	452.2	2.1	0.46	

n, replicate injections; SD, Standard Deviation; RSD, Relative Standard Deviation.

Table 3.4. The effect of nitrogen flow rate on flame ionization detector signal. Test analyte, 20 µg of valine

Test parameter	Peak area in mV.s			Other parameters (kept constant)
	Mean (n=3)	SD	RSD (%)	Collector internal diameter, 4 mm; spray chamber diameter, 30 mm; air flow, 650 mL/min; hydrogen flow, 157 mL/min; 184 mL/min and carrier water flow, 1mL/min.
0.5 bar (125 mL/min)	383.6	2.6	0.68	
1.0 bar (184 mL/min)	411.8	2.6	0.63	
2.0 bar (250 mL/min)	545.5	1.9	0.35	
3.0 bar (343 mL/min)	332.1	1.5	0.45	

n, replicate injections; SD, Standard Deviation; RSD, Relative Standard Deviation.

Table 3.5. The effect of hydrogen flow rate on flame ionization detector signal. Test analyte, 20 µg of valine

Test parameter	Peak area in mV.s			Other parameters (kept constant)
	Mean (n=3)	SD	RSD (%)	Collector internal diameter, 4 mm; spray chamber diameter, 30 mm; air flow, 650 mL/min; nitrogen flow, 184 mL/min and carrier water flow, 1mL/min.
2.5 psi (76 mL/min)	124.8	1.5	1.20	
5.0 psi (157 mL/min)	411.8	2.1	0.51	
7.5 psi (240 mL/min)	389.6	2.2	0.56	
10.0 psi (332 mL/min)	260.0	1.9	0.73	

n, replicate injections; SD, Standard Deviation; RSD, Relative Standard Deviation.

From these studies, the desirable conditions for the operation of the flame ionization detector were selected to be carrier water flow rate, 1 mL/min; hydrogen, 157 mL/min; nitrogen, 250 mL/min; air, 654 mL/min; spray chamber internal diameter, 40 mm and collector internal diameter, 4 mm. These conditions were used in the rest of the study.

3.3.2 Analyte volatility and FID response

The FID, a common gas-liquid chromatography detector, responds only weakly to non-volatile analytes but both volatile and non-volatile analytes give good response in this set up. The current set up was aerosol-based and aerosol-based detectors, such as ELSD and CAD, are limited to the analysis of non-volatile analytes and exhibit non-linear response patterns. Since the current LC-FID set up was intended to analyze volatile and non-volatile analytes, it was important to examine the response patterns of the FID for analytes of different volatility. In this section of the study, analytes were individually injected into the FID via carrier water.

a Volatile analytes

Volatile analytes [methanol (18.5 μg - 0.07 μg), propanol (21.4 μg - 0.08 μg), hexane (80 μg - 5.0 μg) and dichloromethane (46.8 μg - 2.93 μg)] were introduced into the detector via flow injection analysis mode and the calibration plots were generated. All the plots were linear and had intercepts near zero (Figure 3.2).

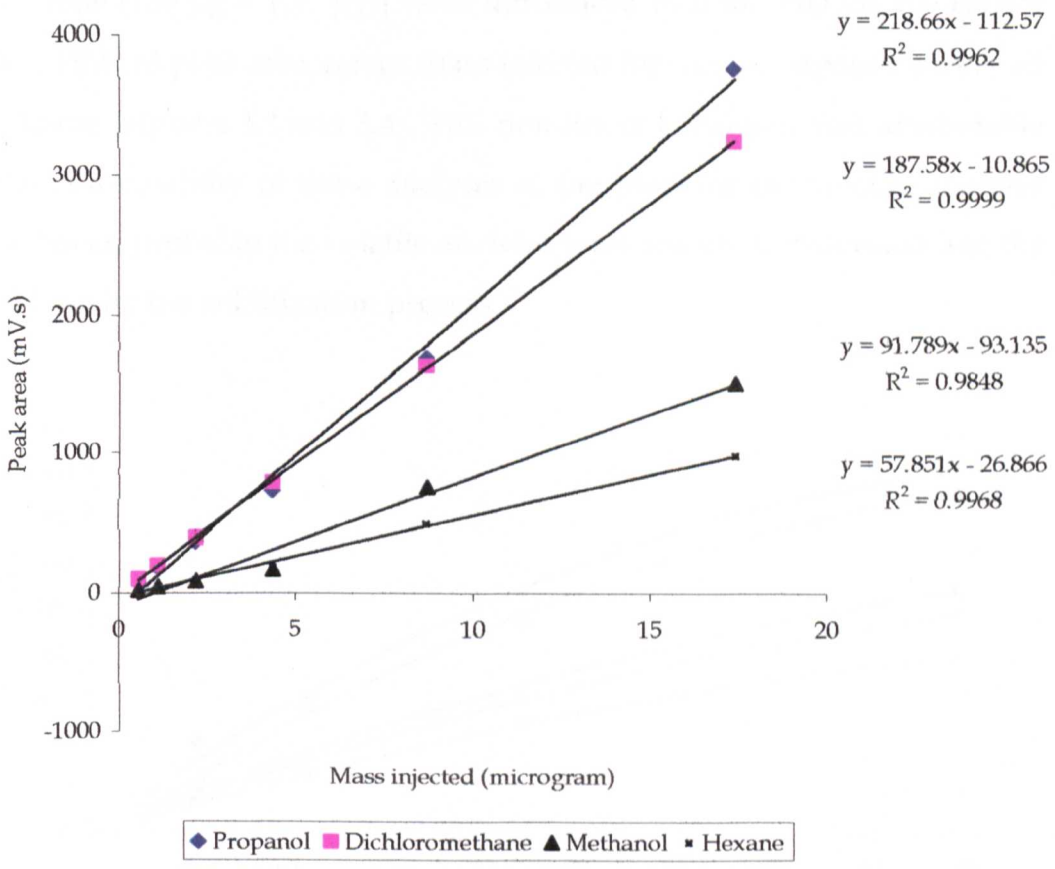

Figure 3.2. Plots showing the linear response of the FID to volatile analytes. Optimum FID conditions as in section 3.3.1 (pg 58).

The high response of dichloromethane is unexpected as halogenated compounds give low responses in GC-FID due to the short residence time in the flame which is not sufficient for the breaking of all carbon-halogen bonds, so some halogens and carbons atoms split off the molecule together [111]. The remaining CH—Cl radicals are not oxidized and hence the probability of production of a FID signal is less.

b *Non-volatile analytes*

The response patterns of non-volatile solid and liquid analytes were also studied.

Non-volatile analytes [ethylene glycol (22.2 µg – 2.78 µg), poly (ethylene glycol), 16.3 µg – 2.04 µg, resorcinol (18.0 µg – 2.25 µg), 4 –hydroxybenzoic acid (13.2 µg – 1.65 µg), 4–hydroxybenzamide (13.0 µg – 1.63 µg), maltose

and valine (160 µg – 1.25 µg)] were introduced into the FID via the carrier water. Plots of peak area versus mass injected for these compounds were all non-linear (Figures 3.3 and 3.4). This non-linear behaviour was attributable to the non-volatility of these analytes as the plots for the volatile analytes were linear; probably the volatile analytes were readily transformed into the gas phase by the nebulization process.

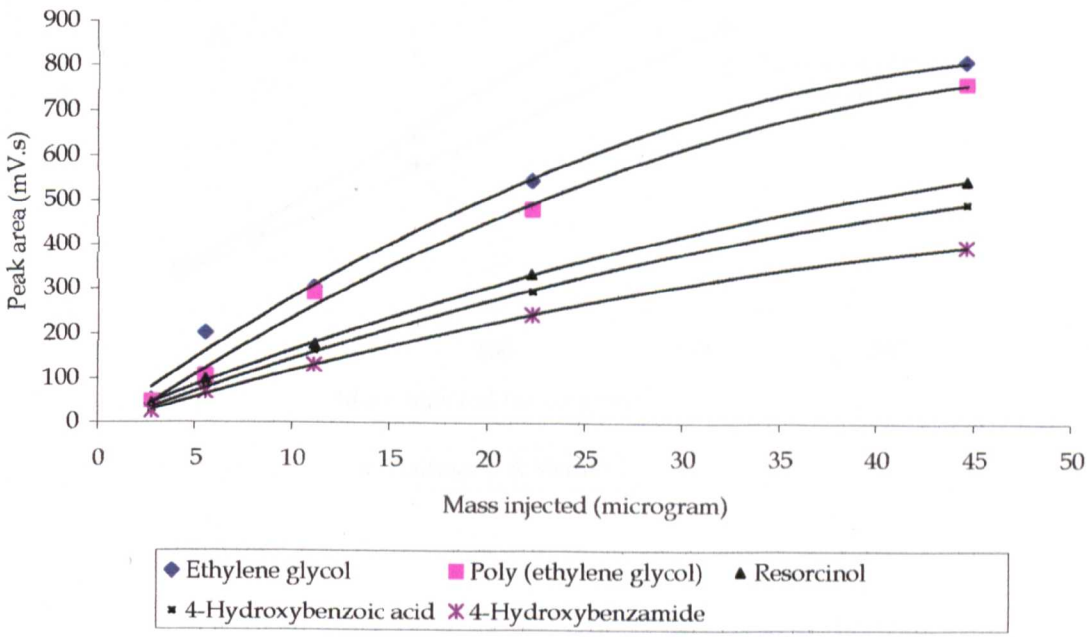

Figure 3.3. Plots showing the response pattern of the FID to non-volatile analytes [ethylene glycol and poly (ethylene glycol), resorcinol, 4-hydroxybenzoic acid, 4-hydroxybenzamide]. Optimum FID conditions as in section 3.3.1 (pg 58).

The plots of maltose and valine were linear from 160 to 20 µg (not through the origin) but non-linear from 10 – 1.25 µg (Figure 3.4). A similar non-linearity was observed but in the higher concentration region for volatile analytes by Grob *et al.* [50] in GC-FID. They explained it in terms of detector saturation; when a large amount of a compound is burned, the hydrogen flame becomes more like hydrocarbon flame, showing an increase in size. In such a situation, the ions are generated higher in the collector where the electric field is weaker, resulting in a non-linear response and detector saturation [50]. This explanation of non-linear behaviour might not hold in

this case because the high oxygen content of these compounds might reduce the height of the flame.

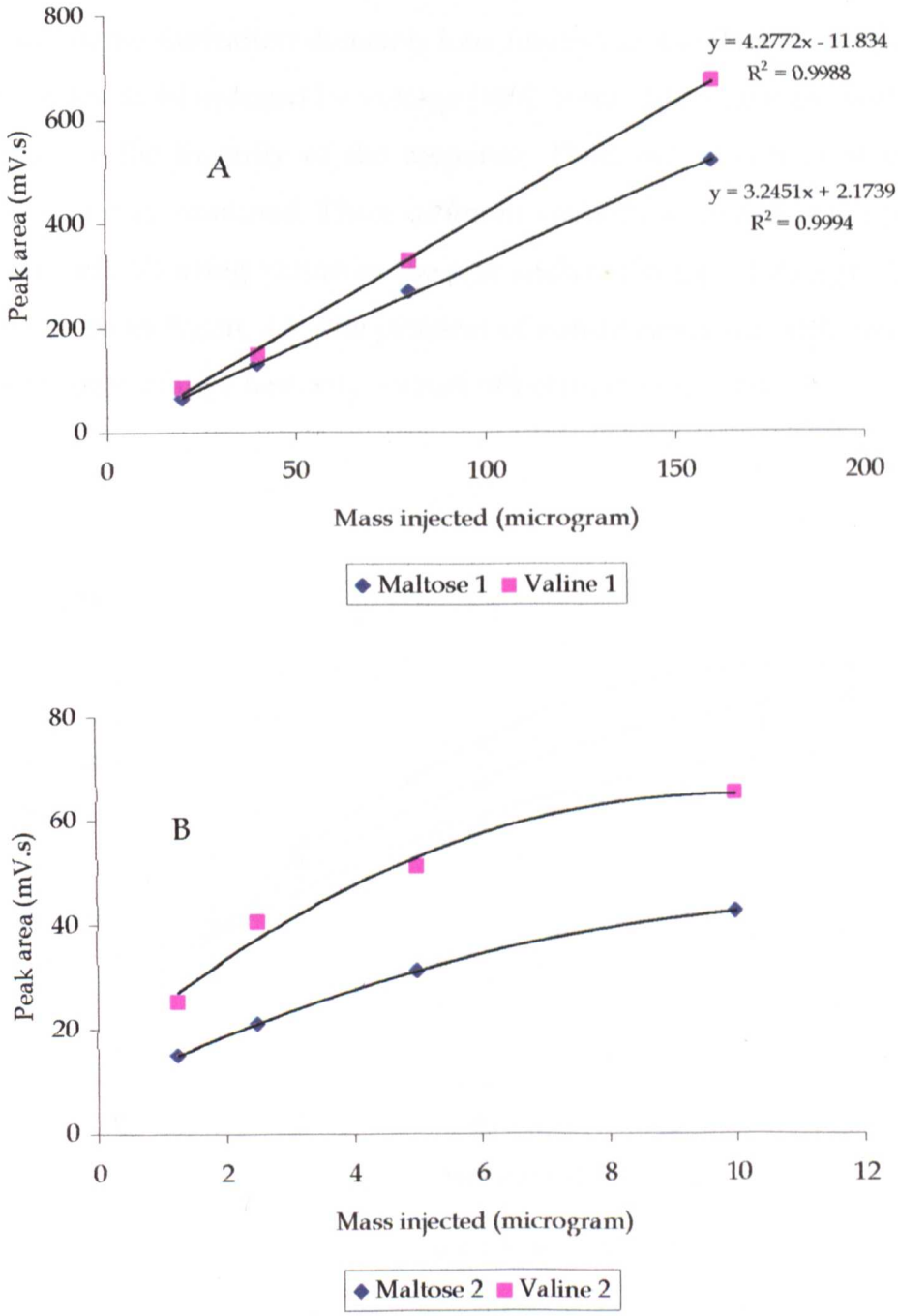

Figure 3.4. Plots showing the response pattern of the FID to maltose and valine. Optimum FID conditions as in section 3.3.1 (pg 58). Concentration ranges in A and B are 160 – 20 µg and 10 – 1.25 µg respectively.

In order to improve the linearity of the plots, the effect of voltage, collector internal diameter (which might alter the position of the flame) and mobile phase additives were examined.

Effect of voltage on linearity

In the flame ionization detector, ions formed in the flame are propelled by an electric field induced by voltage [109]. It was likely that the voltage could influence the linearity of the response. Therefore the effect of voltage on linearity was examined. Three different voltages were examined (170 V, 300 V and 400 V) using valine as the test analyte (20 µg - 1.25 µg). The results are shown in Figure 3.5. The problem of non-linearity was still observed and the voltage change had only a small effect on the response.

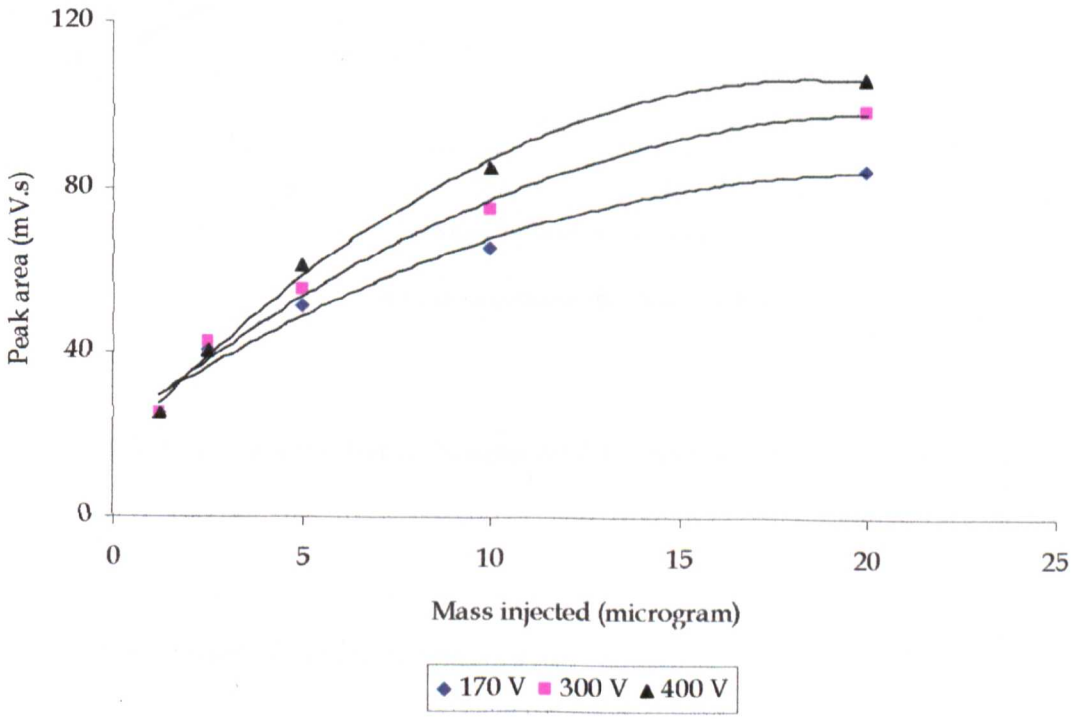

Figure 3.5. Effect of voltage on FID response of valine. Optimum FID conditions as in section 3.3.1 (pg 58).

Effect of collector internal diameter on linearity

Since ions formed in the flame, and propelled by the electric field, are collected on the surface of the collector [109], the effect of collector (Figure 2.3) internal diameter was studied using valine [20 µg - 1.25 µg (Figure 3.6)]. Collector sizes used for the test were: 6.27 mm, (i.d), 29.03 mm, length (designated wide collector); 4.00 mm, (i.d), 29.03 mm, length (designated narrow collector). The use of the wide collector increased the response slightly but the problem of non-linearity persisted.

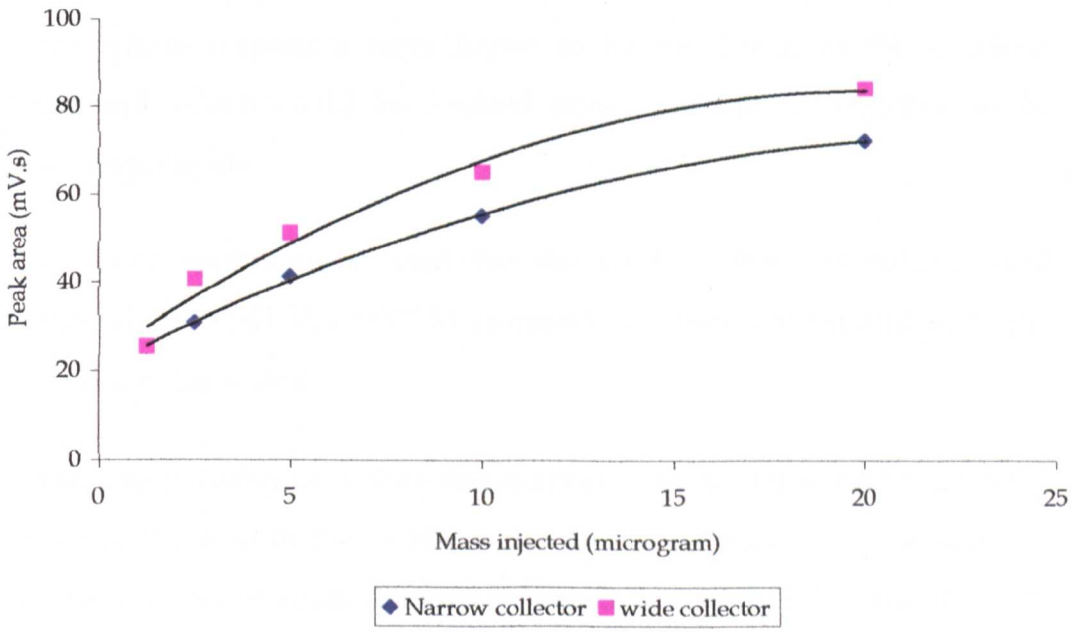

Figure 3.6. Effect of collector internal diameter on FID response. Analysis conditions as in section 3.1.

Effect of carrier water additives on linearity

The detector voltage and collector diameter, which are physical parameters, had no effect on the FID response pattern and hence, the effect of carrier water additives was studied.

FID is sensitive to molecules that are ionized in a hydrogen-air diffuse flame. As the ions are formed inside the detector, they are impelled by an electric potential towards an electrode, producing a minute current of the order of pico-amps [109]. Since the formation of ions is an integral part of FID, the effect of introducing negative and positive ions into the FID via carrier water additives was studied using ionizable (valine), non-ionizable (maltose), long-chain alcohols and the amines as test analytes.

Ionizable (valine) and non-ionizable (maltose) solid analyte

The test analytes used were valine and maltose representing the solid analytes whose responses were found to be non-linear in the previous sections and which could be ionized either positive or negative or be neutral, respectively.

Three carrier waters were used for the study: 0.0007 M sulfuric acid (corresponding to pH 3), 0.0007 M ammonia solution (corresponding to pH 9) and de-ionized water.

The response patterns for valine and maltose were found to be linear in the presence of the acid in the carrier water and non-linear in the presence of ammonia or in water alone (Figures 3.7 and 3.8). It is obvious from the plots that the presence of both ammonia and sulfuric acid reduced the sensitivity of the FID signal; the effect was more pronounced with sulfuric acid than ammonia.

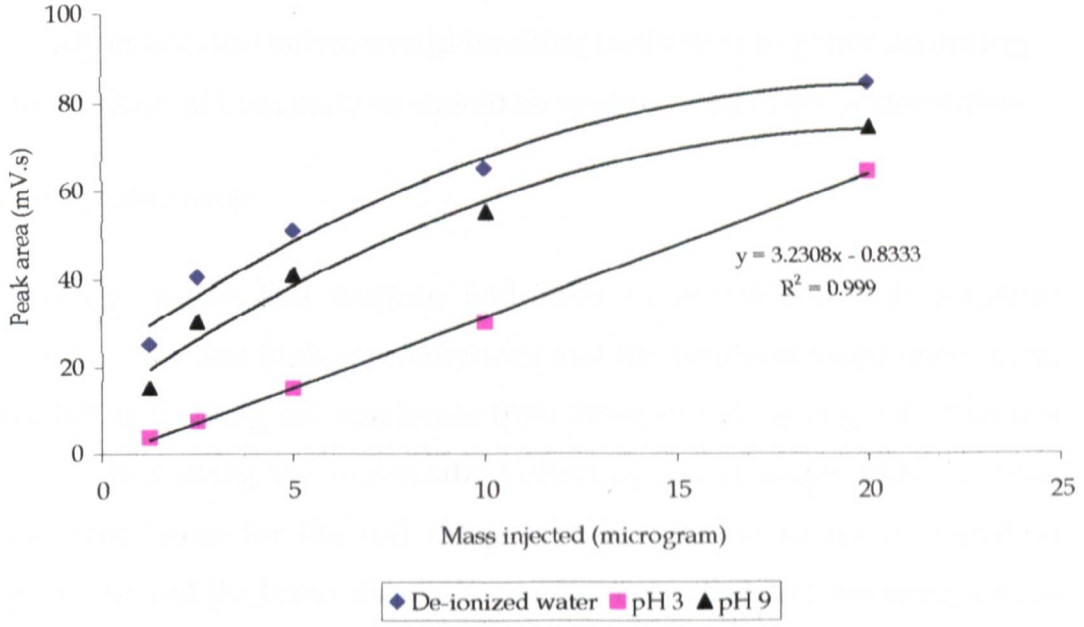

Figure 3.7. Effect of carrier water additives on FID response of valine. Optimum FID conditions as in section 3.3.1 (pg 58). Carrier waters: 0.0007 M sulfuric acid (corresponding to pH 3), 0.0007 M ammonia solution (corresponding to pH 9) and de-ionized water.

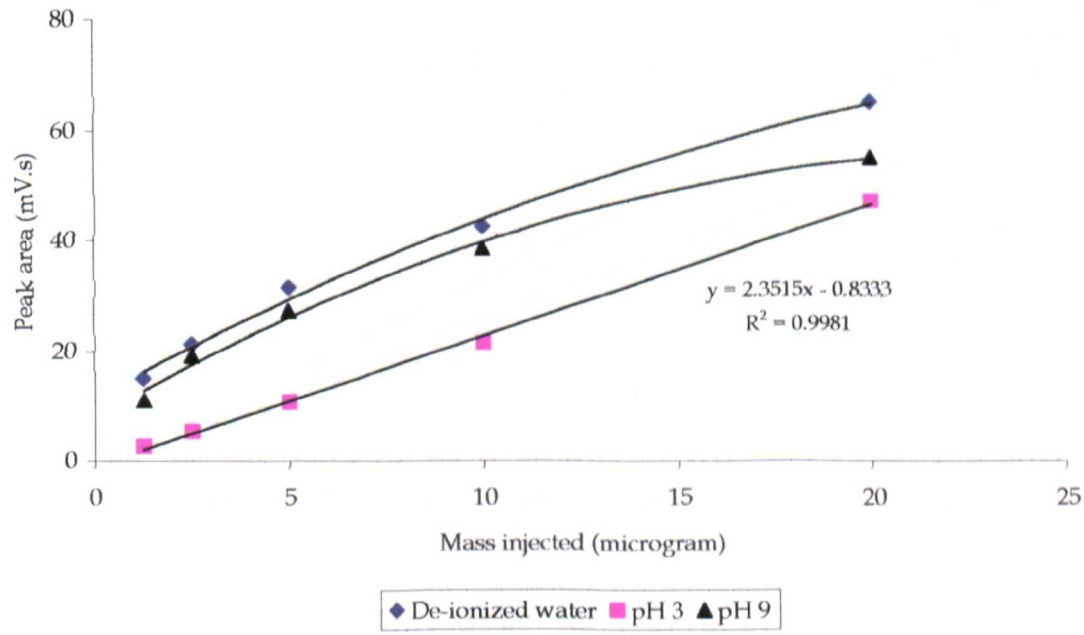

Figure 3.8. Effect of carrier water additives on FID response of maltose. Optimum FID conditions as in section 3.3.1 (pg 58). Carrier water: 0.0007 M sulfuric acid (corresponding to pH 3), 0.0007 M ammonia solution (corresponding to pH 9) and de-ionized water.

These results show that the linearization effect was not due to ionization of the analytes because valine would be either positive or negative according to the solution pH but maltose should be neutral in all three carrier waters.

Linear dynamic range

Previously, valine and maltose had been examined for their response patterns at low and high concentrations and the results showed linear plots from 160 µg to 20 µg but non-linear from 10 µg to 1.25 µg (Fig 3.4). This test was repeated using the linearization effect of carrier water additive. Both plots were linear for the full range of concentration under examination (Figure 3.9) and the linear dynamic ranges were calculated; the ranges were two orders of magnitude for both test compounds and both of the plots had an intercept close to zero.

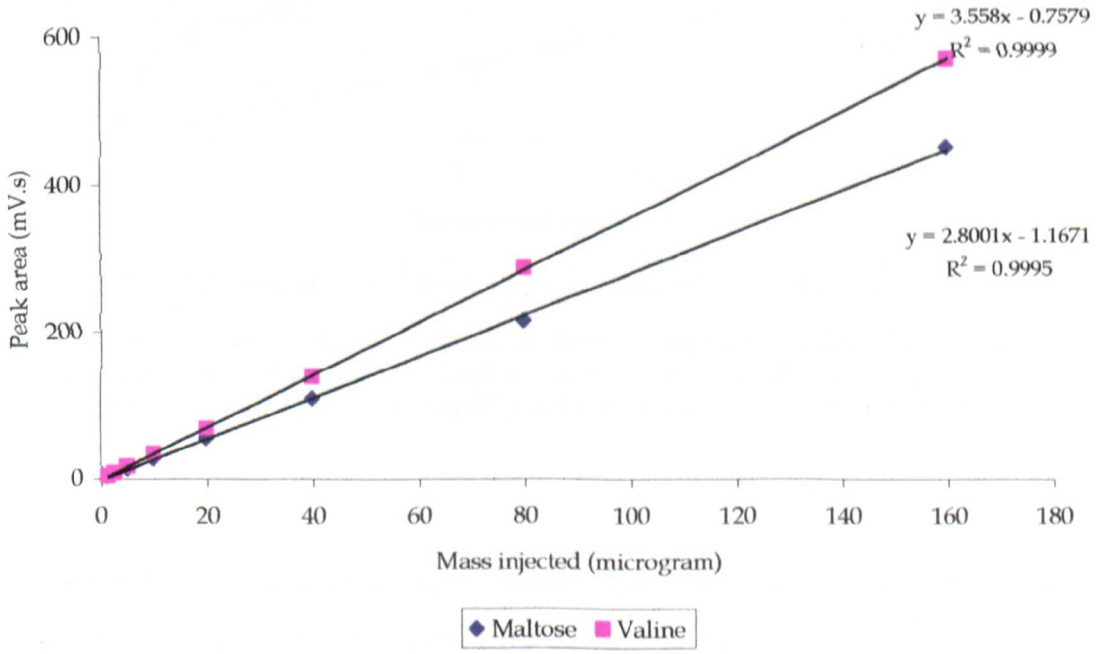

Figure 3.9. Calibration plots of maltose and valine. Optimum FID conditions as in section 3.3.1 (pg 58). Carrier water: 0.0007 M sulfuric acid.

As the presence of sulfuric acid in the eluent had been found to linearize FID response of the solids, other acids (hydrochloric, nitric and orthophosphoric) were examined to see if linearization could be obtained. The test analyte was valine (20 µg - 2.5 µg). However, a lower sample concentration range was used for orthophosphoric acid (5 µg - 0.63 µg) because the acid caused an increase in sensitivity such that the detector was overloaded with the initial concentration range.

With the presence of each of these acids in the carrier water, all the plots for valine became linear (Fig 3.10).

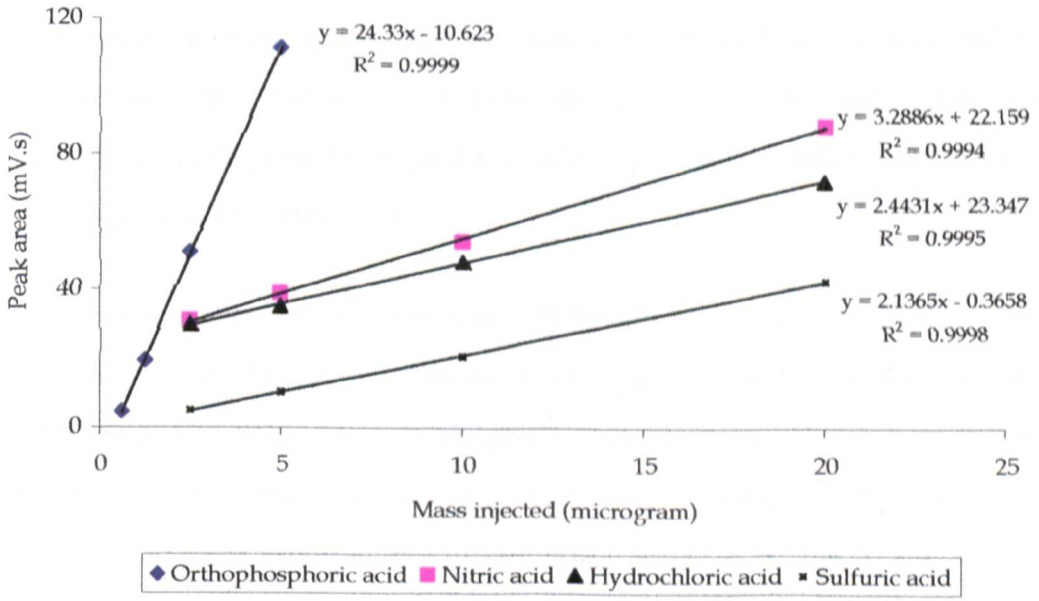

Figure 3.10. Effect of carrier water additives on the FID response of valine. Optimum FID conditions as in section 3.3.1 (pg 58). Carrier water 1 = 0.0025M H_3PO_4, carrier water 2 = 0.00225M HNO_3, carrier water 3 = 0.001M HCl and carrier water 4 = 0.00075M H_2SO_4.

The presence of sulfuric and hydrochloric acids reduced the baseline noise from 0.2 to about 0.1 mV, but that of the orthophosphoric acid increased the baseline noise from 0.2 to about 1 mV. However, the signal increased only by 2 fold with the orthophosphoric acid. The increase in noise level could be attributed to the chemistry of orthophosphoric acid at elevated temperatures such as the levels obtained in the flame. Orthophosphoric is

very stable and has essentially no oxidizing properties below 350°C - 400 °C. At elevated temperatures, pyro-orthophosphoric acid is produced (see equation below) which is fairly reactive towards metals (reduces it) and also attacks quartz [112] and could therefore had altered the surface of the collector.

$$H_3PO_4 \xrightarrow[220^{\circ}C]{\text{gentle heat}} \underset{\text{Pyrophosphoric acid}}{H_4P_2O_7} \xrightarrow[320^{\circ}C]{\text{strong heat}} \underset{\text{metaphosphoric acid}}{(HPO_3)_n}$$

Although all the four acids used as carrier water additives linearized the FID response, only sulfuric acid gave an intercept near zero; nitric and hydrochloric acids gave large positive intercepts and orthophosphoric acid gave a large negative intercept.

The linearization of the FID response of solids in the presence of sulfuric acid, nitric acid and orthophosphoric acid suggested the idea of examining the FID response using sodium sulphate and ammonium sulphate, which do not furnish protons in water, as carrier water additives. The aim of this test was to find out whether the linearization effect was due to the protons (or other cations) or the anions (sulphate, nitrate and phosphate). The calibration plots of valine were linear (Figure 3.11) in the presence of both additives indicating that the linearization effect was due to the anions and not the protons or cations; protons, sodium and ammonium ions did not cause significant differences in sensitivity and pH was therefore not the critical factor in achieving a linear response. This is probably one reason which the effect was seen with maltose as well as valine.

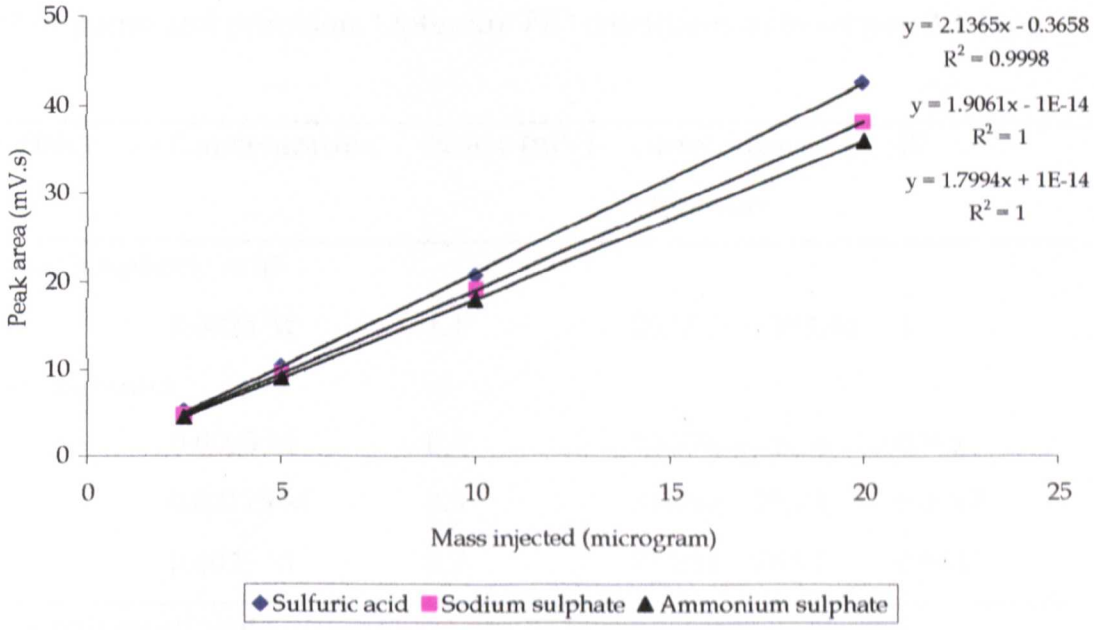

Figure 3.11. Effect of carrier water additives (salts) on the FID response of valine. Optimum FID conditions as in section 3.3.1 (pg 58). Carrier waters: 1 = 0.00075M H_2SO_4, 2 = 0.005 M Na_2SO_4 and 3 = 0.005 M $(NH4)_2SO_4$.

Following the conclusion that linearization was due to the anions such as phosphate and sulphate, it was necessary to examine the levels of concentrations needed to obtain linearity and the reproducibility of the linearization effect. Different concentrations of ammonium sulphate and orthophosphoric acid were used as the carrier water for the test (Table 3.6). The tests were repeated at different times; at intervals of one and twenty four hours. Test concentrations of valine were 200 µg to 12.5 µg and 120 µg to 7.5 µg respectively for ammonium sulphate and orthophosphoric acid.

Table 3.6. Effect of different concentrations of carrier water additives on the FID response and precision. Optimum FID conditions as in section 3.3.1 (pg 58).

Additive	Concentration	Noise (mV)	correlation equation	R^2
Orthophosphoric acid				
	0.0025 M	1.1	253.51x - 193.44	1
After 24 hours				
	0.0005 M	0.2	75.77x + 25.56	0.9987
	0.00125 M	0.3	51.95x - 25.73	0.9992
	0.0025 M	0.7	76.81x - 76.97	0.9982
Ammonium sulphate				
	0.00025 M	0.07	11.785x + 0.666	0.9999
	0.001 M	0.10	17.492x - 26.17	1
	0.0025 M	0.10	12.788x - 4.9525	1
After one hour				
	0.001 M	0.08	15.579x - 13.677	0.999
After 24 hours				
	0.001 M	0.08	16.583x - 15.432	0.9992

From Table 3.6, as little as 0.0005 M and 0.00025 M of orthophosphoric acid and ammonium sulphate respectively were needed to improve the linearity of the FID response of valine. With the orthophosphoric acid, two analyses carried out at an interval of 24 hours gave a 3-fold reduction in sensitivity (noise reduced by 1.6 fold), possibly indicating a deactivation of the collector surface. Using ammonium sulphate as additive was more reproducible than orthophosphoric acid; there was no significant change in sensitivity [slope of regression (peak area vs mass injected) equation] between the two runs carried out at an interval of 24 hours.

Long-chain alcohols

The response patterns of non-volatile liquid analytes (decyl alcohol and glycerol) were examined. The plots of both analytes were non-linear and curved like the plots of the other non-volatile analytes previously seen. The non-linear behaviour of the FID towards these compounds was attributable to their low-volatility; they do not readily go into the gas phase during the pneumatic nebulization as was the case with the solid analytes.

The calibration plot of decyl alcohol was curved without an acid-additive in the carrier water [Fig 3.12A, plot 1 (36.0 μg - 2.25 μg)]. However, using 0.00075 M of sulfuric acid as carrier water (Fig 3.12 A, plot 2) and the addition of 20 μL of 39.2% sulfuric acid to the sample (Fig 3.12 A, plot 3) linearized the plot.

The calibration plot of glycerol was also curved [Fig 3.12 B, plot 1 (58 μg - 0.91 μg)]. Using 0.00075 M of sulfuric acid as the carrier water suppressed the signals of the five lowest concentration levels such that only the two top levels were measured and so, calibration could not be made. But the addition of 20 μL of 39.2% sulfuric acid to the sample linearized the plot [Figure 3.12 B, plot 2 (62 μg - 7.75 μg)].

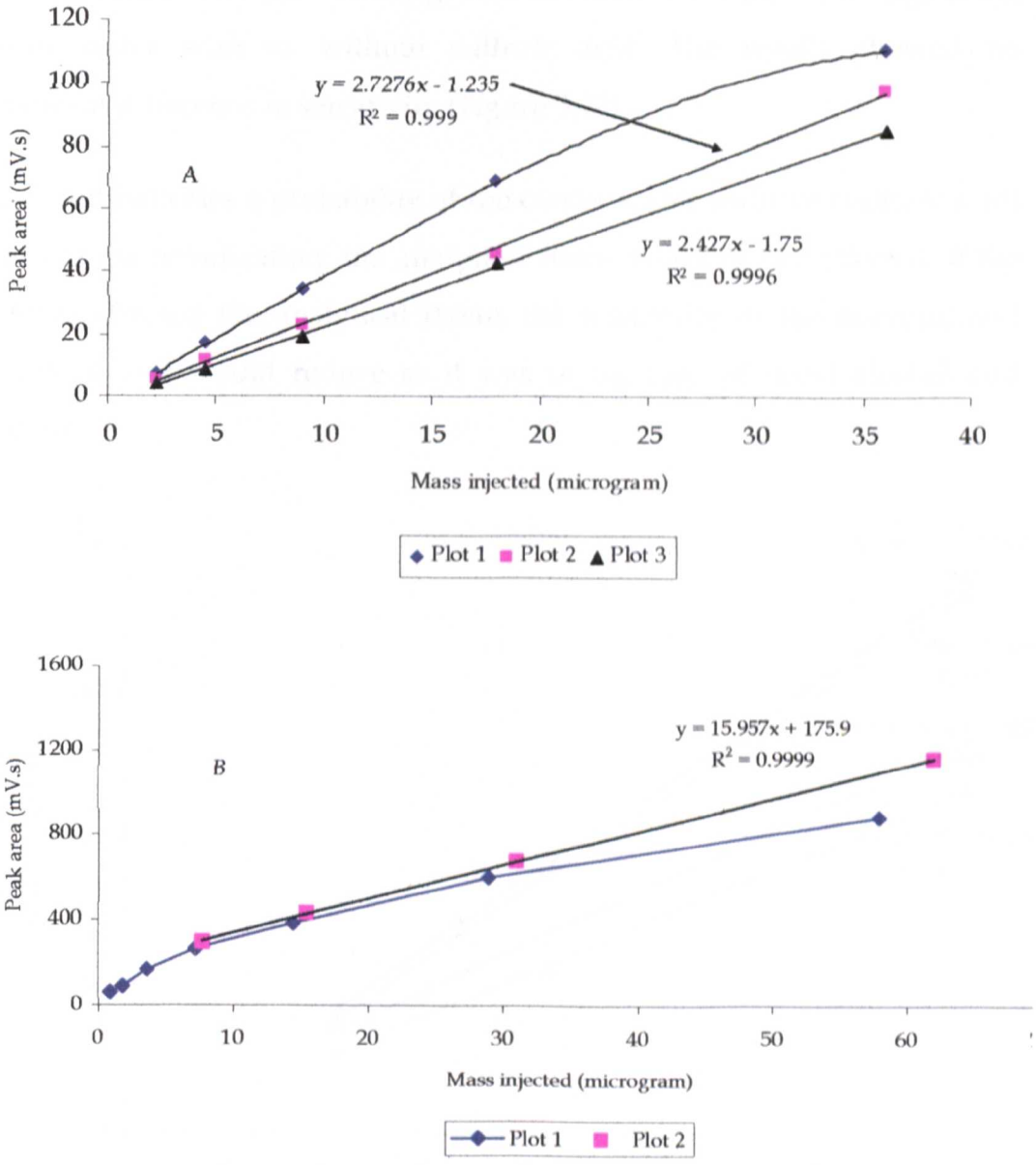

Figure 3.12. Plots showing the response patterns of the FID to non-volatile liquid analytes. Optimum FID conditions as in section 3.3.1 (pg 58). Decyl alcohol (A): 1, eluent without acid additive; 2, eluent with acid additive and 3, acid in sample. Glycerol (B): 1, eluent without acid additive and 2, acid in sample.

Since decyl alcohol and glycerol are moderately volatile, it became analytically important to examine the effect of these carrier water additives on the sensitivity of the FID towards more volatile analytes such as m-cresol and benzyl alcohol. On this reasoning, calibration curves were generated for

benzyl alcohol (85.6 µg – 21.4 µg) and m-cresol (85.6 µg – 21.4 µg) using carrier water with or without sulfuric acid. The results showed no significant difference in sensitivity (Figure 3.13).

The result indicates a probability of the carrier water additive (sulfuric acid) affecting the nebulization; the analytical flame might not be affected. If the additive affected the analytical flame, the sensitivity of the m-cresol and benzyl alcohol would reduce as it was in the case of decyl alcohol and glycerol.

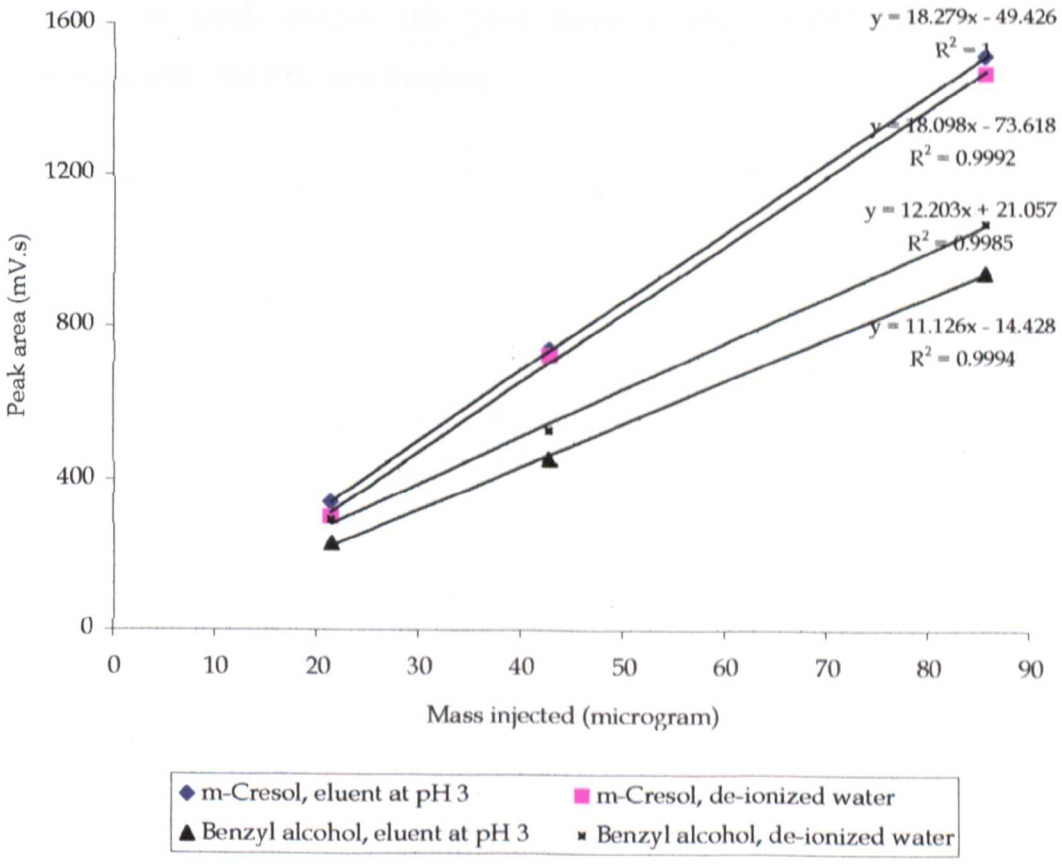

Figure 3.13. Effect of carrier water additive (sulfuric acid) on the response of moderately volatile analytes. Optimum FID conditions as in section 3.3.1 (pg 58).

Aliphatic amines and amino alcohols

A number of aliphatic amines and amino alcohols gave unexpected responses, that is, the FID calibration plots were non-linear using 0.00075 M sulfuric acid as the carrier water (Figure 3.14). Another surprising issue was the peak shapes of the amines; the peak shapes of all the long-chain amines were better (Figure 3.16) than those of the short-chain amines (3.15). Comparing these figures, it is obvious that peak shape improved with an increase in the carbon-to-basic nitrogen ratio. Since the analysis was done in the FIA mode, independent of analyte-column interactions which might result in poor peak shape, the poor peak shapes might be due to interferences with the FID mechanism.

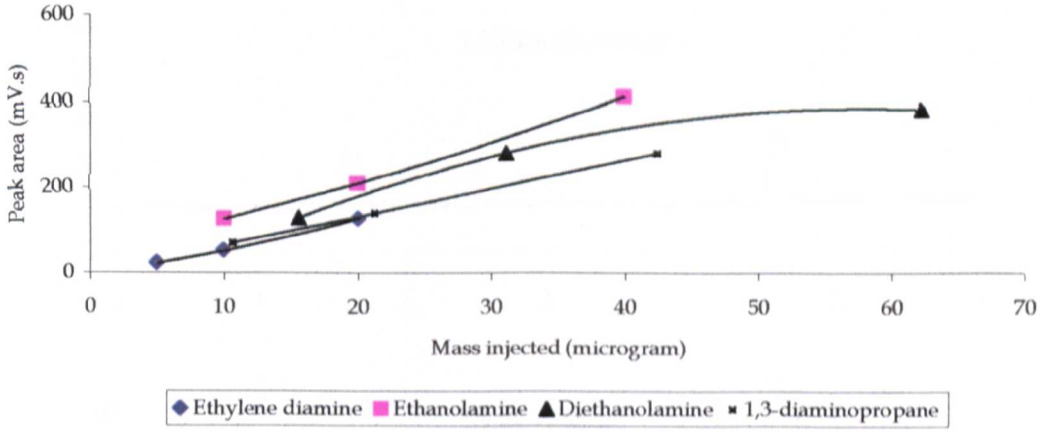

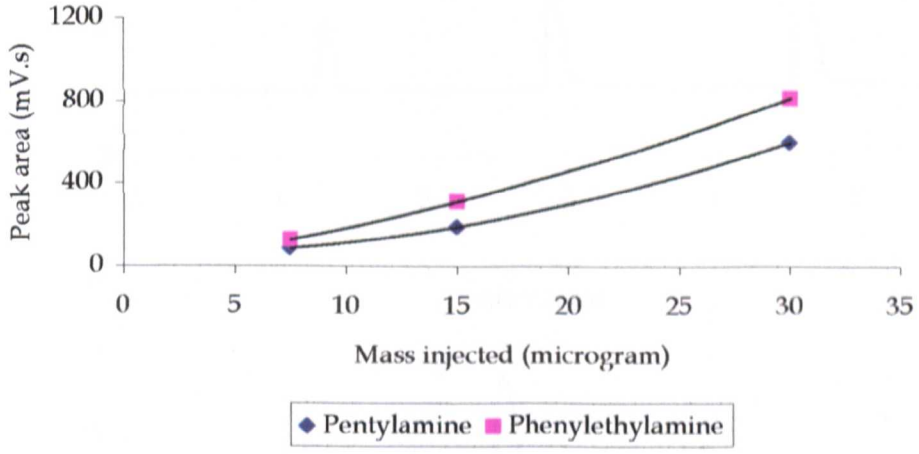

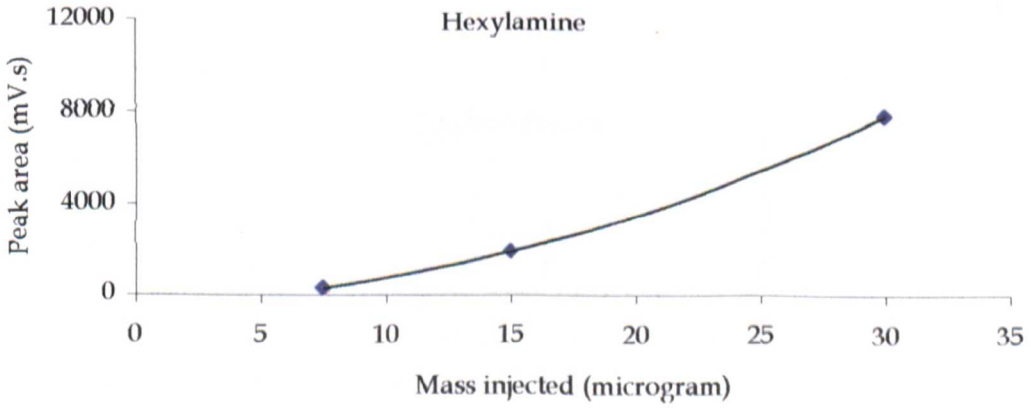

Figure 3.14. Calibration plots of amines. Carrier water, 0.00075 M sufuric acid. Optimum FID conditions as in section 3.3.1 (pg 58).

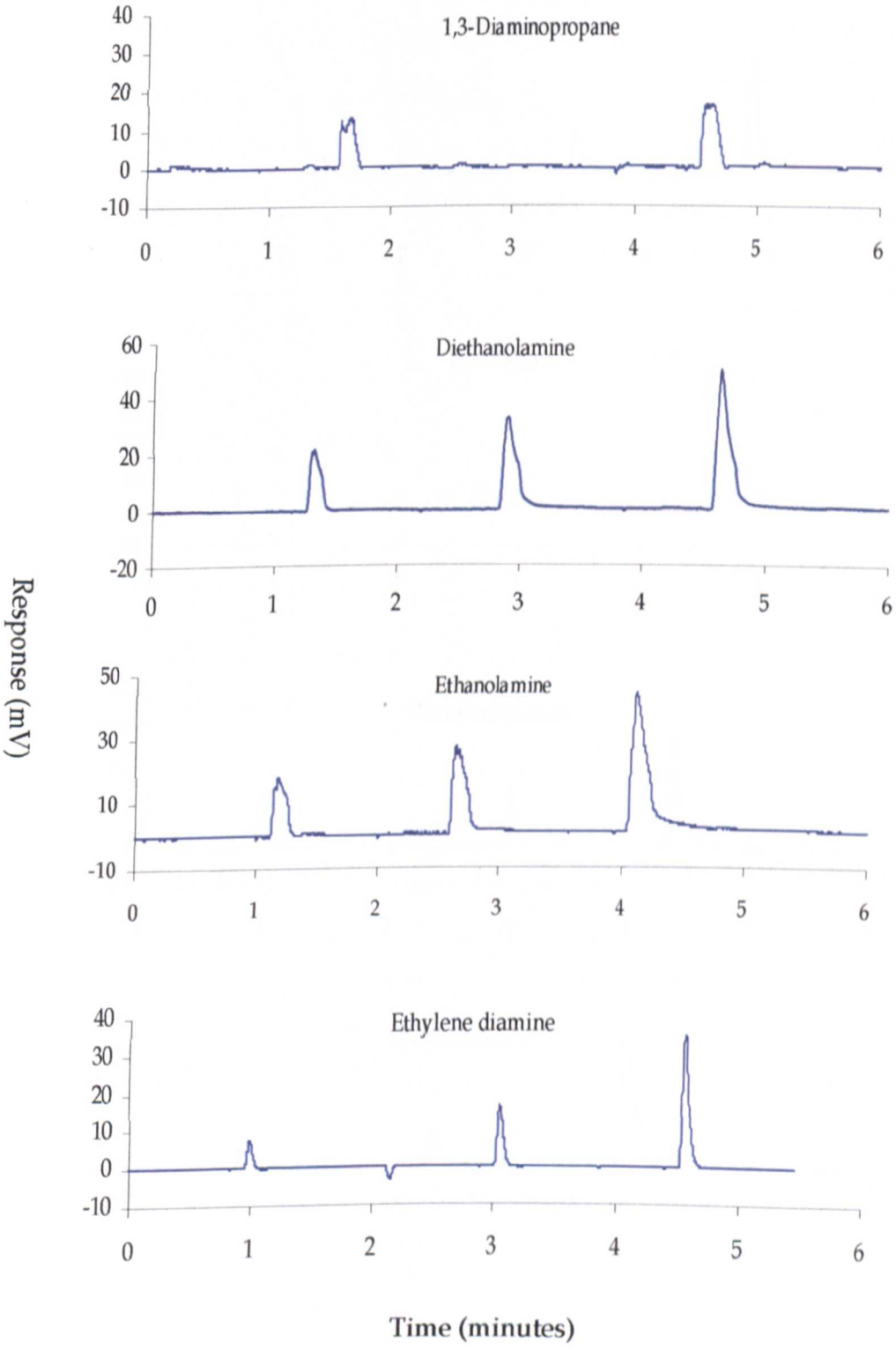

Figure 3.15. Peak shapes of short-chain amines using FIA with a 0.00075 M aqueous sulfuric acid as the carrier water. Optimum FID conditions as in section 3.3.1 (pg 58).

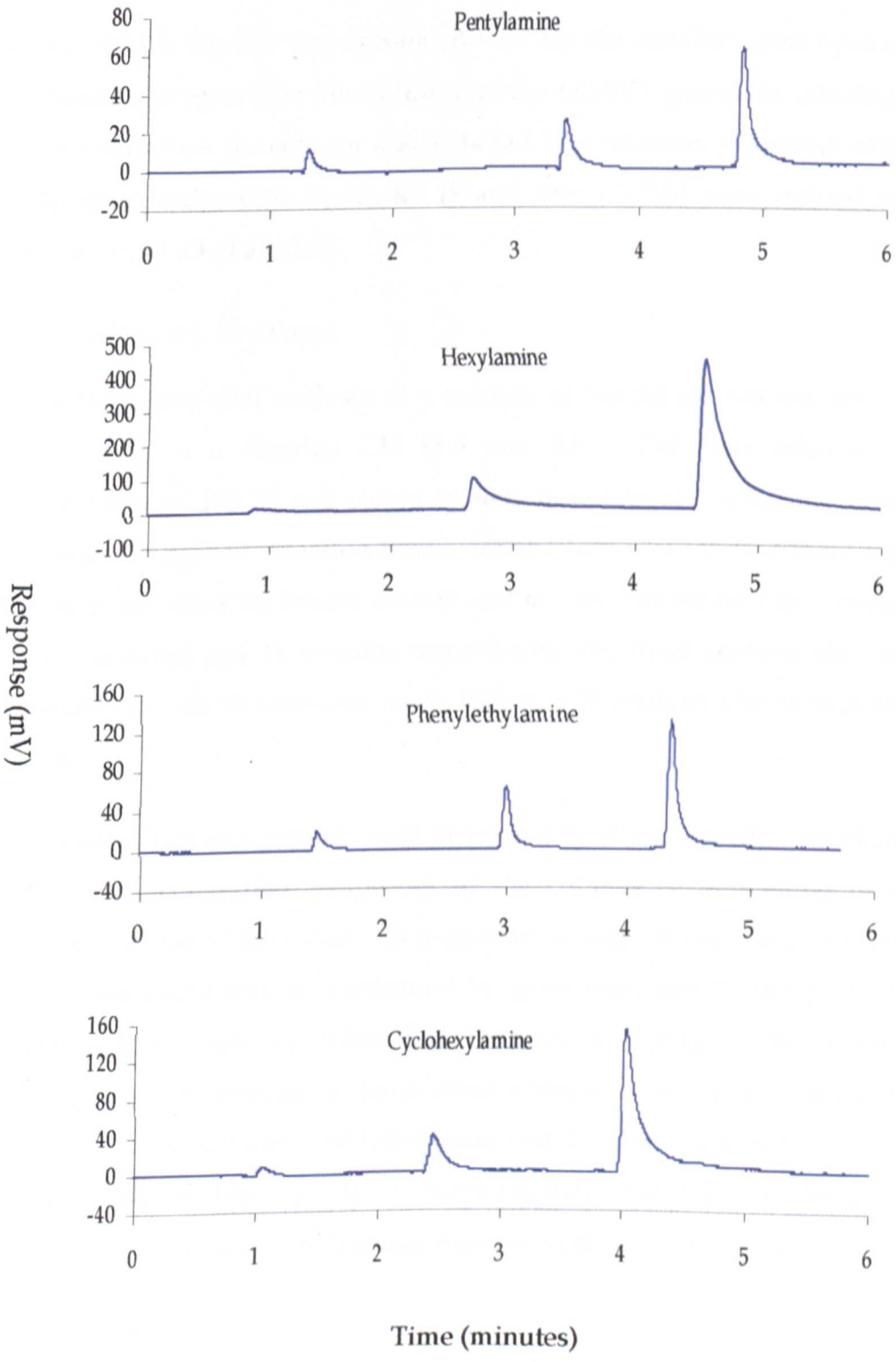

Figure 3.16. Peak shapes of long-chain amines using FIA with a 0.00075 M aqueous sulfuric acid as the carrier water. Optimum FID conditions as in section 3.3.1 (pg 58).

3.3.3 Columns study for the LC-FID system

In section 3.1, the FID was optimized via FIA; the variables were optimized without an integral part (the column) of the LC-FID system. In this stage of the optimization, the column was included. The retention properties of three columns (Xbridge C18, Xterra RP 18 and Xterra RP 8) were studied using both aryl and alkyl alcohols.

a Xbridge C18 column

The consecutive trial analyses of a mixture of benzyl alcohol and m-cresol by LC-FID on a Xbridge C18 (3.5 µm, 4.6 x 150 mm) column at a temperature of 100 °C and eluent (water) flow-rate of 1 mL/min showed dramatic changes in retention times. The mixture was injected three times; the retention times for benzyl alcohol and m-cresol in the first two analyses were 5 minutes and 11 minutes respectively. The third analysis showed a dramatic decrease in retention times, that is, both analytes eluted in about 2 minutes.

The marked loss of retention could be caused by either a permanent change in the chromatographic properties of the column or de-wetting of the stationary phase of the column (a temporary change in column properties). The former cause may be confirmed by generating van t' Hoff plots (log retention factor versus absolute temperature). A change in the slopes of these plots will indicate a permanent change in the chromatographic properties of the column. The latter cause may be confirmed by flushing the column with an eluent of high percent organic solvent and if the loss of retention is restored by the flushing, then de-wetting is the culprit.

van t' Hoff plot

The relationship between the retention factor, k, and the temperature is given by the van't Hoff equation:

$$k = -(\Delta H^0 / RT) + (\Delta S^0 / R) + \ln \Phi$$

The equation predicts that a plot of ln k versus 1/T will be a straight line with a slope of $-(\Delta H^0 / R)$ and an intercept of $[(\Delta S^0 / R) + \ln \Phi]$, provided that $\ln \Phi$ (phase ratio, defined as the ratio between the volume of stationary phase and the volume of the mobile phase) is independent of temperature. If the stationary phase or the analyte undergoes changes in conformation at a certain temperature, the enthalpy and entropy of the retention properties will change, and the van't Hoff plot will show a change in the slope and the intercept at the transition temperature [49, 113].

The study was conducted by analyzing different analytes under different column temperatures while the retention factors were calculated. The first set of analytes used for the study included methyl benzoate, acetophenone, anisole, propiophenone. The second set of analytes included butyl phenyl ketone and butyrophenone. Temperatures used for the study ranged from 60 °C to 100 °C except for the second set of analytes (100 °C to 160 °C). The van't Hoff plots and the regression equations are shown in Figure 3.17 and Table 3.7 respectively.

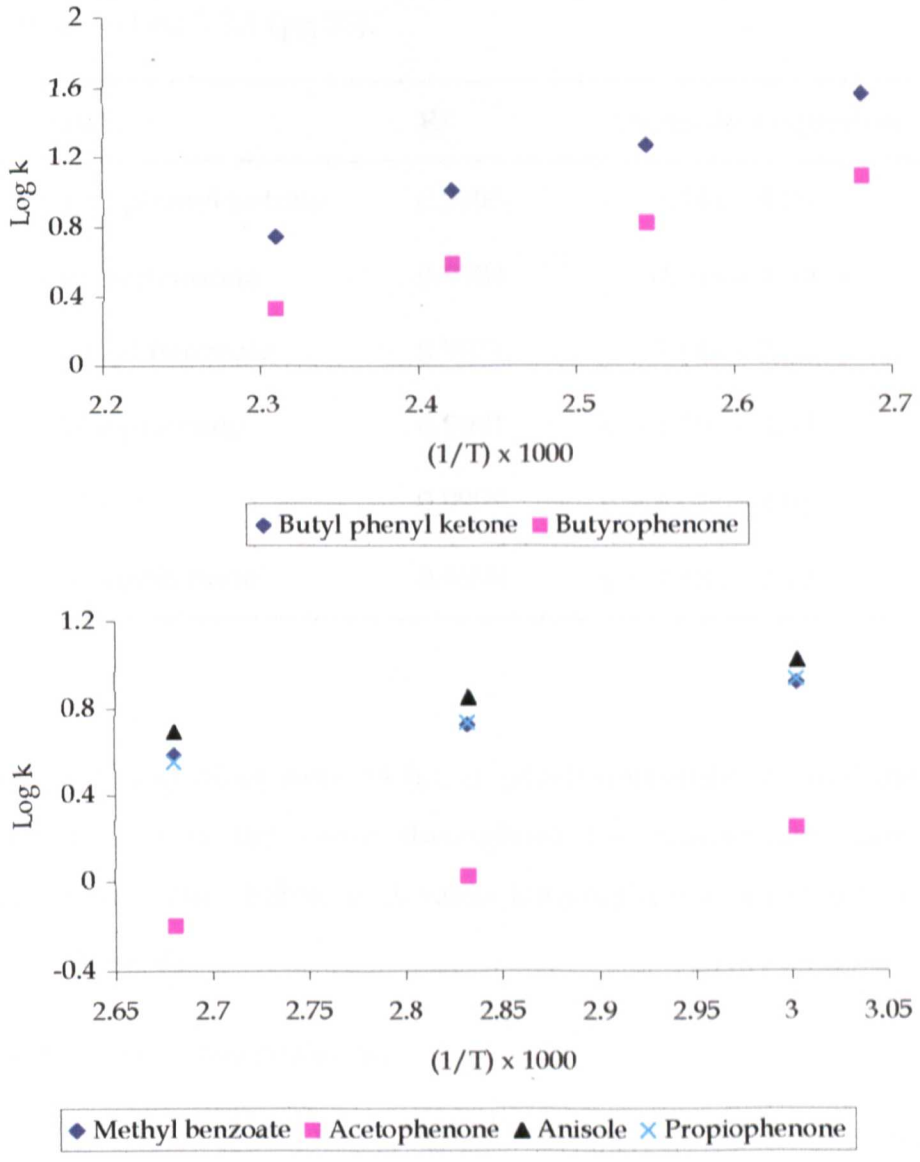

Figure 3.17. van't Hoff plots of alkyl aryl ketones and aromatic analytes on Xbridge C18 (3.5 µm, 4.6 x 150 mm). Test temperatures for methyl benzoate, acetophenone, anisole, propiophenone ranged from 60 °C to 100 °C. Test temperatures for butyl phenyl ketone and butyrophenone ranged from 100 °C to 160 °C. Flow rate of eluent, 1mL/min. Optimum FID conditions as in section 3.3.1 (pg 58).

Table 3.7. Change of retention factor with temperature for analytes on Xbridge C18 column. Data based on Figure 3.7. Optimum FID conditions as in section 3.3.1 (pg 58).

Analyte	R^2	Regression equation
Butyl phenyl ketone	0.9993	y = 2.18x - 4.29
Butyrophenone	0.9984	y = 2.01x - 4.30
Methyl benzoate	0.9971	y = 1.04x - 2.21
Acetophenone	0.9991	y = 1.39x - 3.93
Anisole	0.9998	y = 1.02x - 2.03
Propiophenone	0.9999	y = 1.18x - 2.61

The van't Hoff plots were all linear which demonstrated that the retention mechanism was the same throughout the temperature ranges under investigation and therefore elevated temperature was not the cause of the loss of retention.

Column regeneration by flushing

Since the van t' Hoff plots were linear, suggesting a de-wetting of the stationary phase or phase collapse to a stable condition, the effect of solvent was examined.

The column was regenerated by flushing with 50% methanol on a conventional HPLC system for 3 hours and then with 100% water for 1 hour at room temperature. After this column regeneration process, the test mixture was injected three times at a column temperature of 100 °C and eluent flow of 1 mL/minutes. Benzyl alcohol and m-cresol were eluted between 10 and 20 minutes in the first run (Figure 3.18). The retention times decreased in the second run; the analytes eluted between 5 and 12 minutes

(Figure 3.19). The analytes eluted in about 2 minutes in the third run (Figured 3.20).

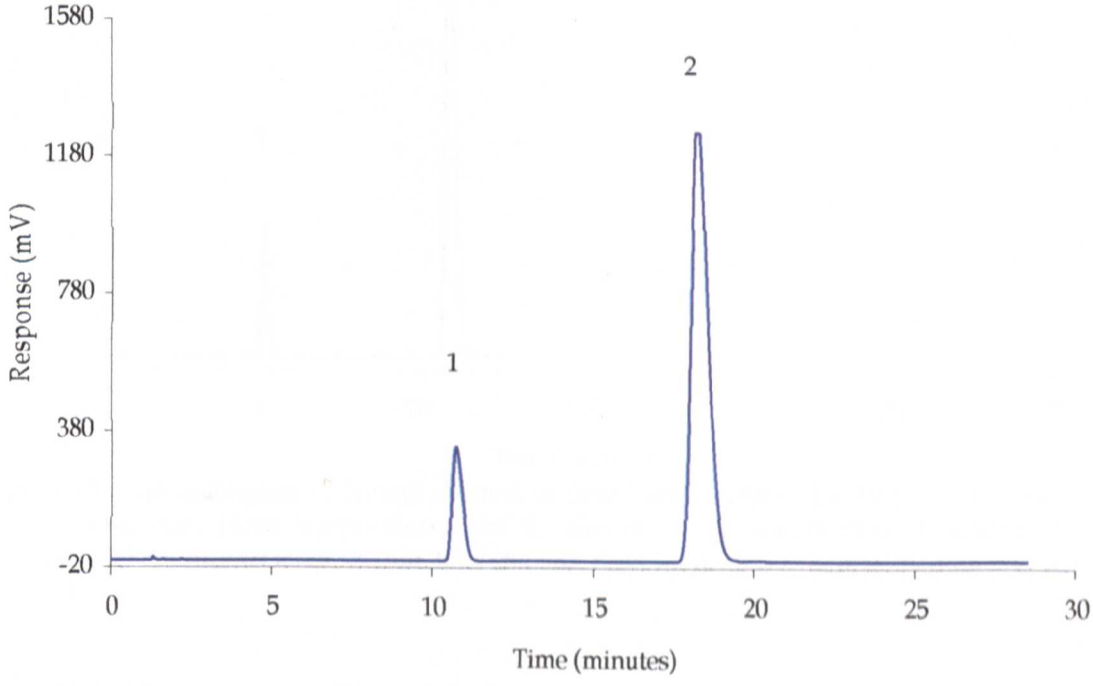

Figure 3.18. Chromatogram of benzyl alcohol, m-cresol on Xbridge C18, 3.5 µm, 4.6 x 150 mm - **first run**. Oven temperature, 100 °C. Eluent (100% water) flow, 1 mL/min. Optimum FID conditions as in section 3.3.1 (pg 58). Peak identity: 1 = benzyl alcohol and 2 = m-cresol.

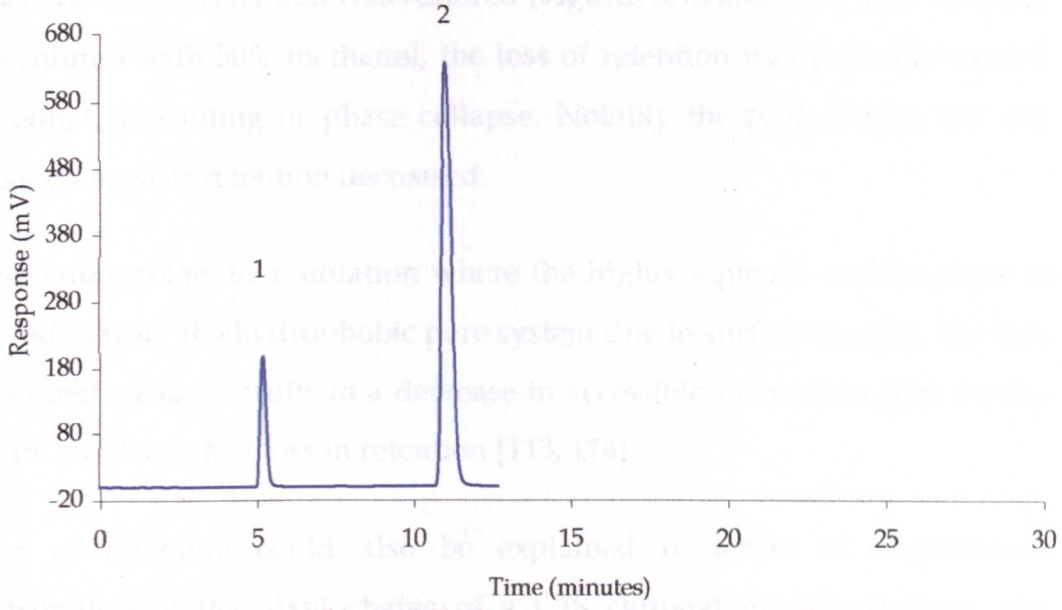

Figure 3.19. Chromatogram of benzyl alcohol, m-cresol on Xbridge C18, 3.5 µm, 4.6 x 150 mm - **second run**. Oven temperature, 100 °C. Eluent (100% water) flow, 1 mL/min. Optimum FID conditions as in section 3.3.1 (pg 58). Peak identity: 1 = benzyl alcohol and 2 = m-cresol.

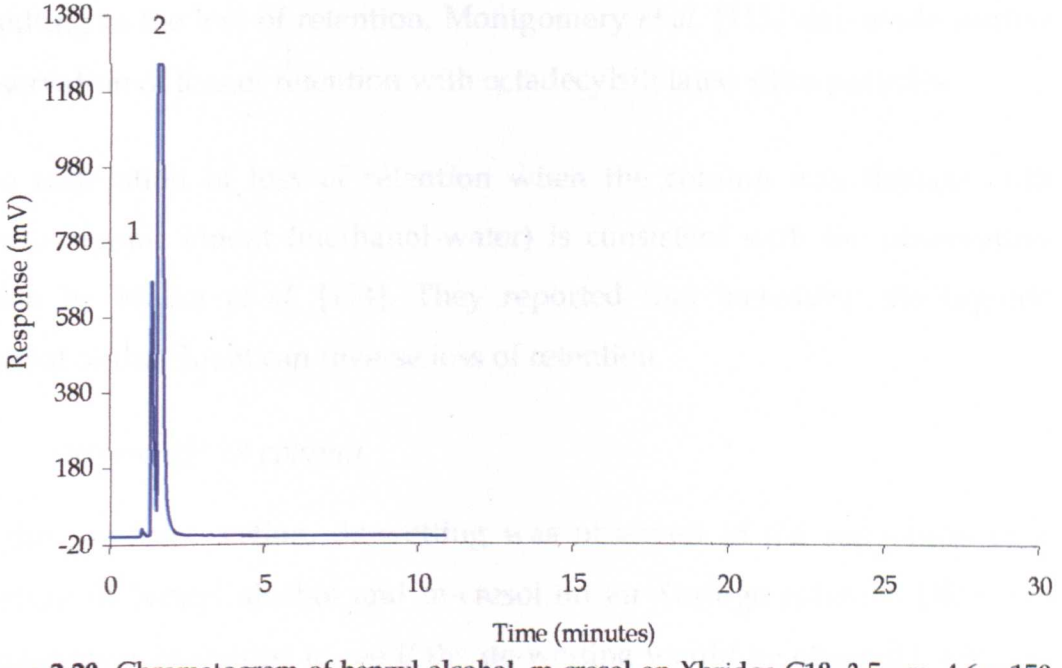

Figure 3.20. Chromatogram of benzyl alcohol, m-cresol on Xbridge C18, 3.5 µm, 4.6 x 150 mm - **third run**. Oven temperature, 100 °C. Eluent (100% water) flow, 1 mL/min. Optimum FID conditions as in section 3.3.1 (pg 58). Peak identity: 1 = benzyl alcohol and 2 = m-cresol.

Since the loss of retention was restored (Figures 3.18 and 3.19) after flushing the column with 50% methanol, the loss of retention was probably caused by either de-wetting or phase collapse. Notably the peak shapes did not broaden even as retention decreased.

De-wetting refers to a situation where the highly aqueous mobile phase is excluded from the hydrophobic pore system due to surface tension. The loss of wetted surface results in a decrease in accessible interaction sites for the solute and leads to a loss in retention [113, 114].

Loss of retention could also be explained in terms of orientational distribution of the alkyl chains of a C18 chromatographic surface. The chains are depicted as lying flat on the surface for an aqueous mobile phase but are extended toward the surface normal in the presence of a wetting mobile phase such as methanol [114 - 116]. When the alkyl chains are lying flat, the hydrophobic interaction of the analytes and the chains is reduced, resulting in the loss of retention. Montgomery *et al.* [115] also made similar observation of loss of retention with octadecylsilylated silica particles.

The restoration of loss of retention when the column was flushed with hydro-organic eluent (methanol-water) is consistent with the observation made by Walter *et al.* [114]. They reported that increasing the organic content of the eluent can reverse loss of retention.

b *Xterra RP 18 column*

In the previous section, de-wetting was observed in the separation of a mixture of benzyl alcohol and m-cresol on an Xbridge column. The same mixture was examined to see if the de-wetting would be observed with the Xterra RP 18 (3.5 µm, 4.6 x 150 mm) column.

Before the analysis of the alcohols, the chromatographic status of the column was investigated by injecting benzyl alcohol, 2-phenyl ethanol, 3-phenyl propanol and 4-phenyl butanol individually. The analyses were

carried out under the following conditions: column temperature, 100 °C and eluent (water) flow, 1 mL/min. The peaks of all the analytes were sharp, indicating that the column was in good condition (Figure 3.21).

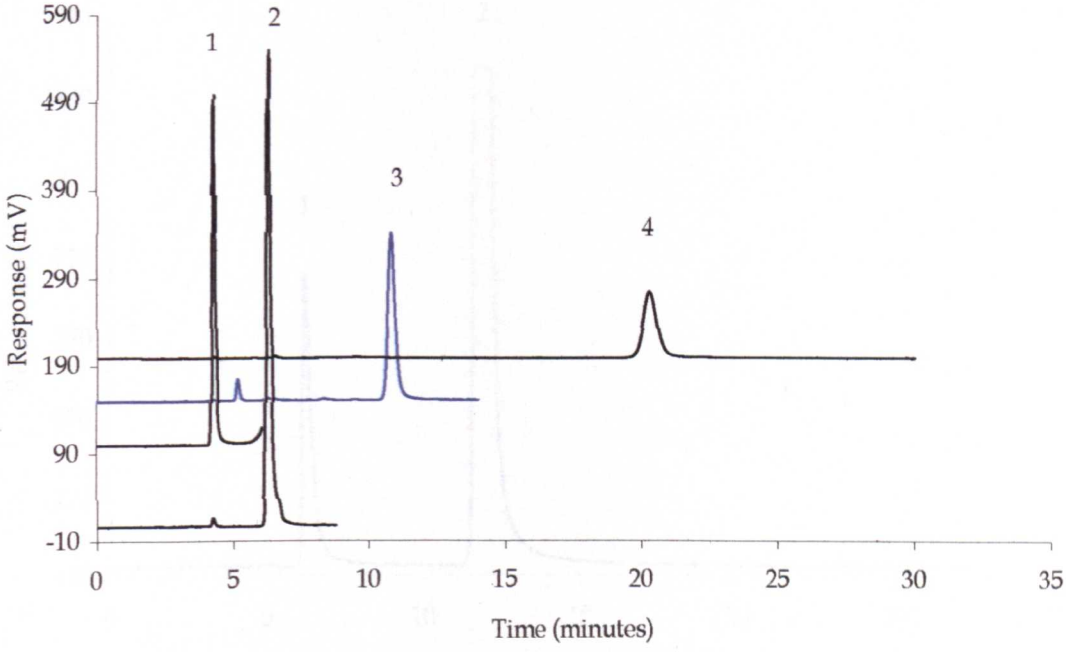

Figure 3.21. Chromatograms of benzyl alcohol and substituted aryl alcohols on Xterra RP 18, 3.5 µm, 4.6 x 150 mm. Oven temperature, 100 °C. Eluent (100% water) flow, 1 mL/min. Optimum FID conditions as in section 3.3.1 (pg 58). Peak identity: 1 = benzyl alcohol, 2 = 2-phenyl ethanol, 3 = 3-phenyl propanol and 4 = 4-phenyl butanol.

Following the confirmation of the good status of the column, the mixture (benzyl alcohol and m-cresol) was injected twice. The conditions of analyses included: column temperature, 100 °C and eluent flow, 1 mL/minutes. The first chromatogram recorded good peak shapes for both analytes (Figure 3.22). The peak shapes were poor and the retention times decreased in the second run (Figure 3.23).

The poor peak shapes in Figure 3.23 were suspected to be due to a partial de-wetting of the stationary phase in aqueous mobile phase. After the column was flushed with 50% methanol for 3 hours and then 100% water

for 1 hour, the pre-heating coil (the coiled tube before the column) was removed so that the eluent would reach the column colder. The mixture was injected four times at an interval of thirty minutes and the resulting superimposed-chromatograms are shown in Figure 3.24. The result showed repeatability in peak shapes and retention times for the four injections.

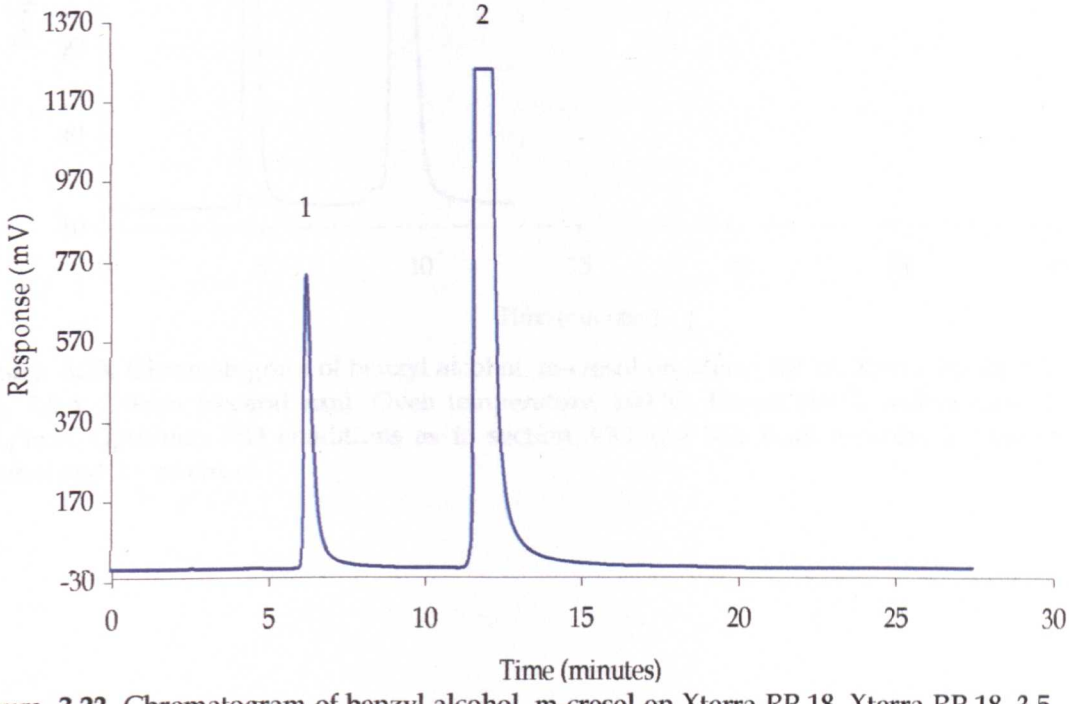

Figure 3.22. Chromatogram of benzyl alcohol, m-cresol on Xterra RP 18, Xterra RP 18, 3.5 µm, 4.6 x 150 mm **(first run)**. Oven temperature, 100 °C. Eluent (100% water) flow, 1 mL/min. Optimum FID conditions as in section 3.3.1 (pg 58). Peak identity: 1 = benzyl alcohol and 2 = m-cresol.

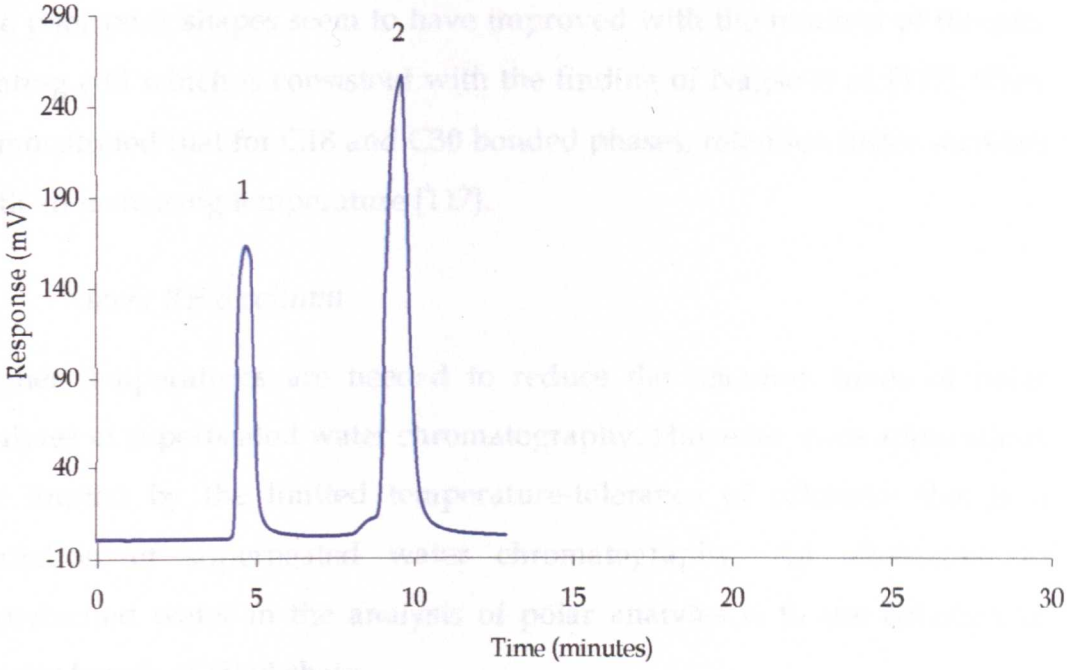

Figure 3.23. Chromatogram of benzyl alcohol, m-cresol on Xterra RP 18, Xterra RP 18, 3.5 µm, 4.6 x 150mm **(second run)**. Oven temperature, 100 °C. Eluent (100% water) flow, 1 mL/min. Optimum FID conditions as in section 3.3.1 (pg 58). Peak identity: 1, benzyl alcohol and 2 = m-cresol.

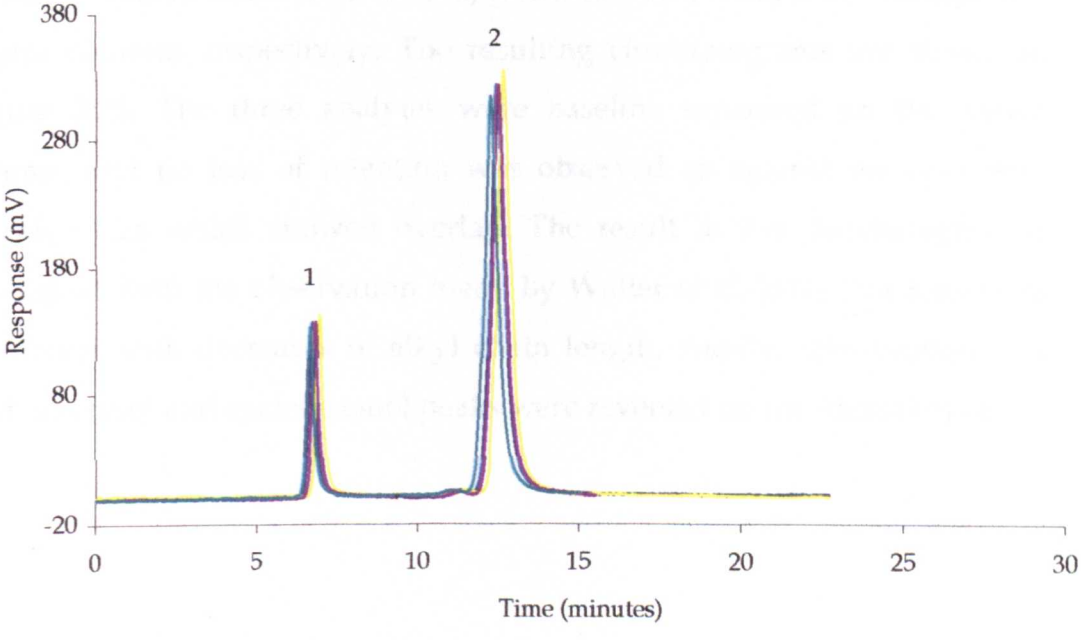

Figure 3.24. Chromatogram of benzyl alcohol, m-cresol on Xterra RP 18 with no preheating coil 3.5 µm, 4.6 x 150mm. Oven temperature, 100 °C. Eluent (100% water) flow, 1 mL/min. Optimum FID conditions as in section 3.3.1 (pg 58). Peak identity: benzyl alcohol and 2 = m-cresol.

The poor peak shapes seem to have improved with the removal of the pre-heating coil which is consistent with the finding of Nagae *et al.* [117]. They demonstrated that for C18 and C30 bonded phases, retention losses increase with an increasing temperature [117].

c Xterra RP 8 column

Higher temperatures are needed to reduce the retention times of polar analytes in superheated water chromatography. However, such applications are limited by the limited temperature-tolerance of columns; this is a limitation of superheated water chromatography. An alternative to superheated water in the analysis of polar analytes is to use columns of shorter length of alkyl chain.

In order to reduce analyte retention capacity of the column, an Xterra RP 8 column with shorter chain length was examined. A mixture of benzyl alcohol, m-cresol and cyclohexanol was separated on Xterra RP 8 (3.5 µm, 4.6 x 150 mm) column and compared to Xbridge C18 (3.5 µm, 4.6 x 150 mm) at 100 °C. Eluent flows were 0.7 mL/min and 1 mL/min on the Xbridge and Xterra columns respectively. The resulting chromatograms are shown in Figure 3.25. The three analytes were baseline separated on the Xterra column and no loss of retention was observed as against the case with Xbridge C18 which showed overlap. The result in the chromatogram is consistent with the observation made by Walter *et al.* [114] that retentions are lower with decreases in alkyl chain length. Another observation was that, m-cresol and cyclohexanol peaks were reversed on the Xterra column.

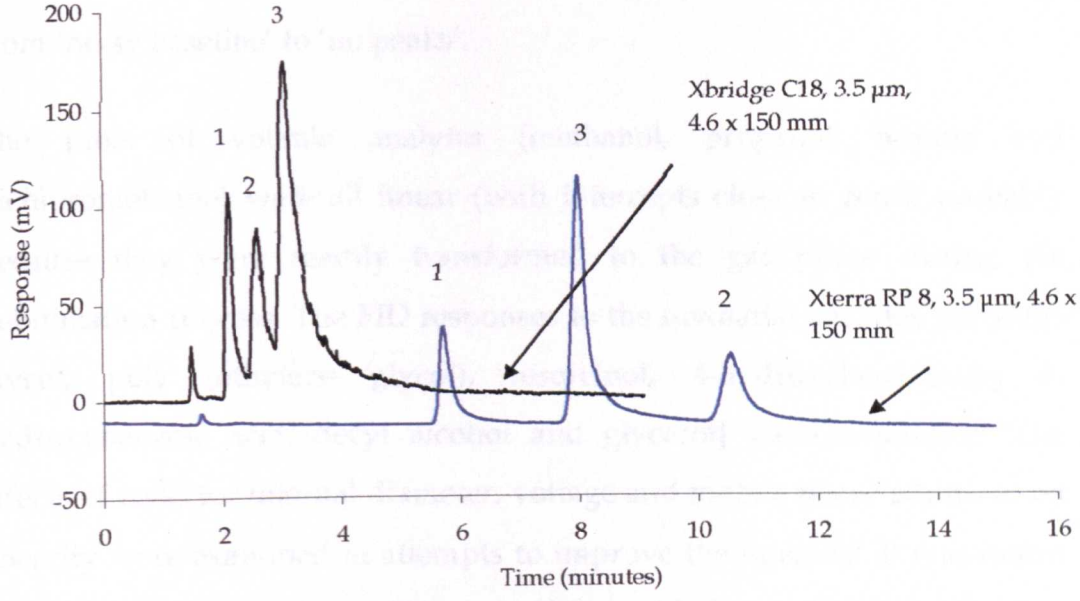

Figure 3.25. Chromatograms of benzyl alcohol, m-cresol and cyclohexanol on Xbridge C18, 3.5 µm, 4.6 x 150 mm. Eluent flow, 0.7 mL/min. Xterra RP 8, 3.5 µm, 4.6 x 150 mm. Eluent flow, 1 mL/min. Oven temperature, 100 °C. Eluent, 100% water. Optimum FID conditions as in section 3.3.1 (pg 58). Peak identity 1 = benzyl alcohol, 2 = m-cresol and 3 = cyclohexanol.

3.4 An overview

From the results of this section, the following conclusions can be made. Hydrogen is more critical than air in the operation of the FID. A mutual dependence exists between the flame gas flows and the nebulizing gas flow and the latter depends on carrier water flow (interactive effects). The proportion of hydrogen flow was higher than that recommended and usually used for gas liquid chromatography in order to keep the flame lit; this observation is consistent with the findings previously made by different researchers [88, 91, 110].

The most critical part of the set-up is the nebulizer-spray chamber unit; the interface between the liquid chromatography and flame ionization detector. The nebulizer should spray well so that the eluent can be transformed into

fine aerosol for sensitive detection. Problems with nebulization can range from 'noisy baseline' to 'no peaks'.

The plots of volatile analytes (methanol, propanol, hexane and dichloromethane) were all linear (with intercepts close to zero), probably because they were readily transformed to the gas phase during the nebulization process. The FID responses to the involatile analytes [ethylene glycol, poly (ethylene glycol), resorcinol, 4-hydroxybenzamide, 4-hydroxybenzoic acid, decyl alcohol and glycerol] were non-linear. The effects of collector internal diameter, voltage and mobile phase additives on linearity were examined in attempts to improve the linearity. It was found that only mobile phase additives (sulfuric acid, hydrochloric acid, nitric acid, sulfuric acid, hydrochloric acid, nitric acid and orthophosphoric acid) linearized the plots; collector and voltage had no significant effect.

Sulfuric acid gave an intercept close to zero, hydrochloric and nitric acids gave positive intercepts and oorthophosphoric acid gave a negative intercept. However, the linearization effects were accompanied with different levels of reduction in sensitivity; sulfuric acid > hydrochloric acid > nitric. Ammonium and sodium sulphates also exhibited the linearization effect with reductions in sensitivity; ammonium sulphate > sodium sulphate > sulfuric acid suggesting that anions were more significant than cations and pH in the linearization process. The reduction in sensitivity could be due to poor aerosol production in the presence of the anions; this is consistent with the observation (acid-induced reduction in aerosol production) made by Grotti *et al.* [96].

The reproducibility of the linearization effect was studied at a time difference of 24 hours with orthophosphoric acid and ammonium sulphate. The sensitivity reduced from 253 mV.s to 76 mV.s, with the former additive and approximately 17 mV.s to 16 mV.s with the latter additive. Although

the use of ammonium sulphate gave lower response, it gave more reproducible results than orthophosphoric acid.

A similar pattern of linearization effect was observed with involatile liquid analytes (decyl alcohol and glycerol). However, when the responses of more volatile liquid analytes (m-cresol and benzyl alcohol) were examined with and without additives, the plots were all linear and there was no significant difference in sensitivities indicating that the linearization effect might be due to an enhancement in the nebulization when additives were used.

The calibration plots of the amines were non-linear even with acid in the carrier water. Besides, the peak shapes were found to improve with an increase in the carbon-to-basic nitrogen ratio.

Changing the configuration of the system from FIA-FID to LC-FID did not affect the working of the FID; the optimized conditions for the FID were still effective. However, loss of retention was observed in some cases in the LC-FID optimization process; loss of retention was separation problems and not detector problem.

CHAPTER FOUR

Applications of the LC-FID method

In chapter three, the FID operating conditions were optimized via the FIA-FID. It was found that the detector responses were linear for the volatile analytes but the responses for the non-volatile analytes were linear only in the presence of selected anions in the eluent. Having established the conditions for the general operation of the LC-FID, the methods were applied to the separation of analytes of different functional groups in the LC-FID mode; different analytes (aliphatic alcohols, substituted aryl alcohols, amines, amino acids, organic acids and sugars) were separated on suitable columns. The relative responses of the different functional groups were also compared with those of the GC-FID responses especially the alcohols.

4.1 Alcohols

The sensitivities of GC-FID and LC-FID were compared using the alcohols.

4.1.1 Separation of aliphatic and aromatic alcohols by GC-FID

A set of alcohols, from methanol to m-cresol was examined by GC-FID and found that all seven analytes were baseline resolved (Figure 4.1) at a temperature programme of 30 °C – 160 °C; 10 °C/min. Calibration studies were carried out and the resulting plots are shown in Figures 4.2 and 4.3. A summary of the limits of detections [calculated by (3*standard error in y-axis)/sensitivity] are shown in Table 4.1. This formula for limits of detection was used in the rest of the study.

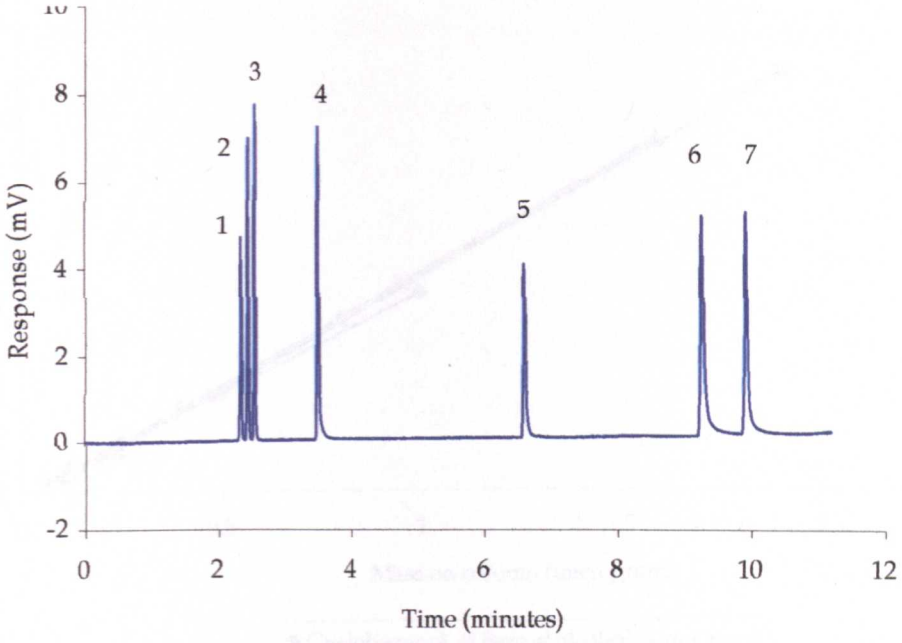

Figure 4.1. GC-FID chromatogram of aliphatic and aromatic alcohols. Conditions: column, HP-5 (Crosslinked 5% Ph Me Siloxane) 30 m x 0.32 mm x 0.25 µm film thickness; hydrogen flow, 55 mL/min; air flow, 375 mL/min and carrier gas (helium) flow, 0.44 mL/min; injector temperature, 250 °C and detector temperature, 200 °C. Temperature programme, 30 °C – 160 °C, 10 °C/minutes. Peaks: 1 = methanol; 2 = ethanol; 3 = propanol; 4 = butanol; 5 = cyclohexanol; 6 = benzyl alcohol and 7 = m-cresol.

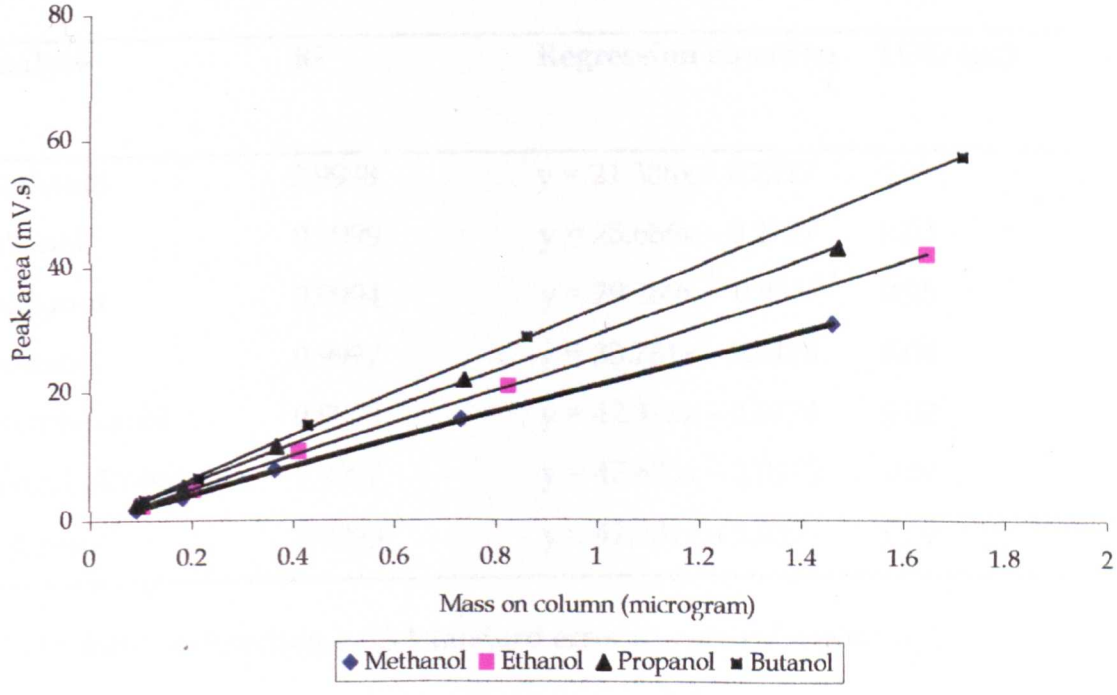

Figure 4.2. Calibration plots of aliphatic alcohols. GC-FID data. Analysis conditions as in Fig 4.1.

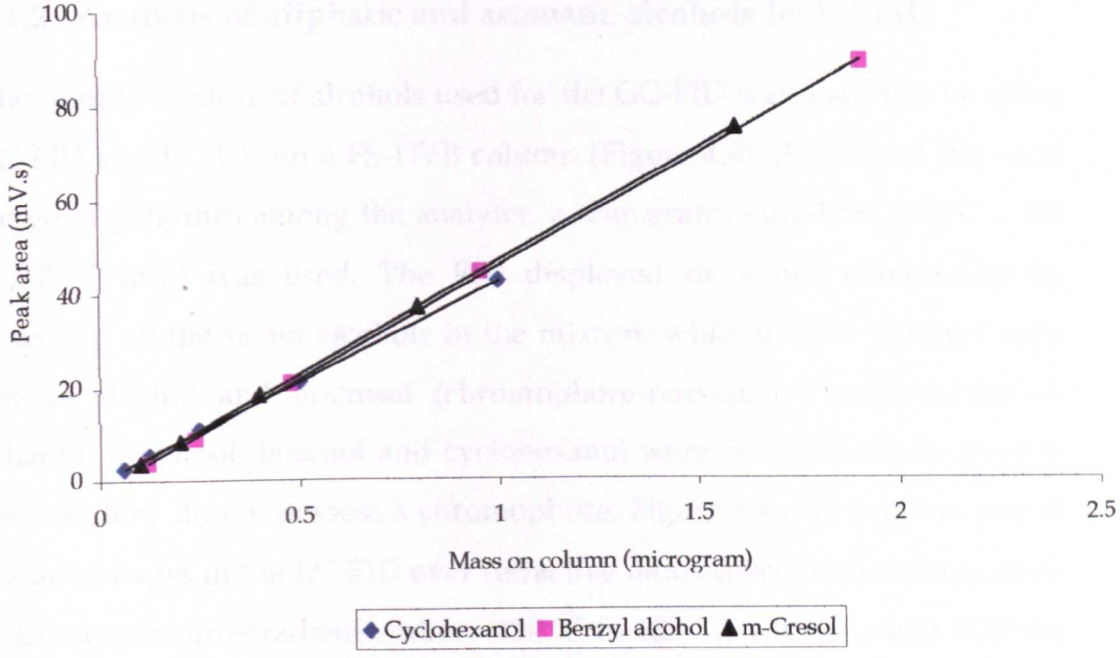

Figure 4.3. Calibration plots of aromatic alcohols. GC-FID data. Analysis conditions as in Fig 4.1.

Table 4.1. LODs for GC-FID analysis of aliphatic and aromatic alcohols + regression (peak area vs mass on column) data based on Figures 4.2 and 4.3. Analysis conditions as in Fig 4.1

Analyte	R^2	Regression equation	LOD (µg)
Methanol	0.9998	y = 21.388x – 0.2227	0.03
Ethanol	0.9999	y = 25.686x – 0.2787	0.03
Propanol	0.9994	y = 29.289x + 0.0327	0.05
Butanol	0.9997	y = 33.781x – 0.3478	0.04
Cyclohexanol	0.9999	y = 42.498x – 0.0724	0.02
Benzyl alcohol	0.9997	y = 47.625x – 2.0143	0.04
m-Cresol	0.9999	y = 47.731x – 1.0307	0.02

LOD = limit of detection = [(3 *standard error in y-axis)/sensitivity]

4.1.2 Analysis of aliphatic and aromatic alcohols by LC-FID

The sample mixture of alcohols used for the GC-FID was analyzed by using LC-FID and LC-UV on a PS-DVB column (Figure 4.4). Because of the wide range of polarities among the analytes, a temperature gradient (120°C – 180 °C, 7 °C/min) was used. The FID displayed its wider universality by detecting all the seven alcohols in the mixture while the UV detected only benzyl alcohol and m-cresol (chromophore-possessing) only; methanol, ethanol, propanol, butanol and cyclohexanol were not detected by the UV because they do not possess a chromophore. Figure 4.4 also displays one of the advantages of the LC-FID over refractive index detector; it is compatible with temperature-gradient elution (120 °C to 180 °C) whereas with RID the temperature change would cause a big shift in baseline.

The analysis of these alcohols by GC-FID was faster [Fig 4.1 (run time = 10 min)] and more efficient than LC-FID.

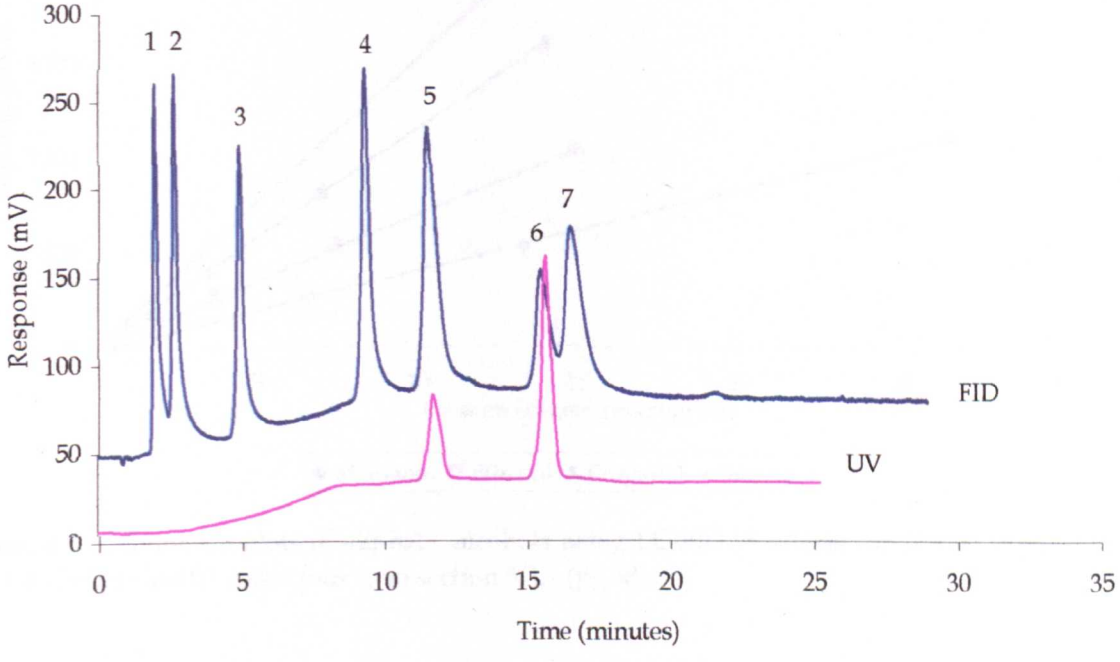

Figure 4.4. Chromatograms of aliphatic and aromatic alcohols on PS-DVB (4.6 x 150 mm column). Oven temperature, 120 °C to 180 °C at 7 °C/minutes. Eluent (100% water) flow, 1 mL/min. Detection, FID and UV (λ = 220 nm). Optimum FID conditions as in section 3.3.1 (pg 58). Peak identity: 1 = methanol; 2 = ethanol; 3 = propanol; 4 = butanol; 5 = benzyl alcohol; 6 = m-cresol and 7 = cyclohexanol.

Calibration studies were carried out on the two detectors; FID results are shown in Figures 4.5 and 4.6 and UV results are shown in Figure 4.7. The regression lines were reasonably linear (regression coefficients greater than 0.99) except, surprisingly the UV line for benzyl alcohol. Detection limits for these analytes were about 1.2 µg for both detectors; the GC-FID limits of detections (Table 4.1) were about 10 fold lower than those of LC-FID (Table 4.2). The slopes (sensitivities) increased with the number of carbon as expected with FID; from methanol to butanol (Table 4.2). The sensitivity of benzyl alcohol (about 35) is lower than that of cyclohexanol (about 102). This is expected because the FID sensitivity reduces with aromatic compounds [50].

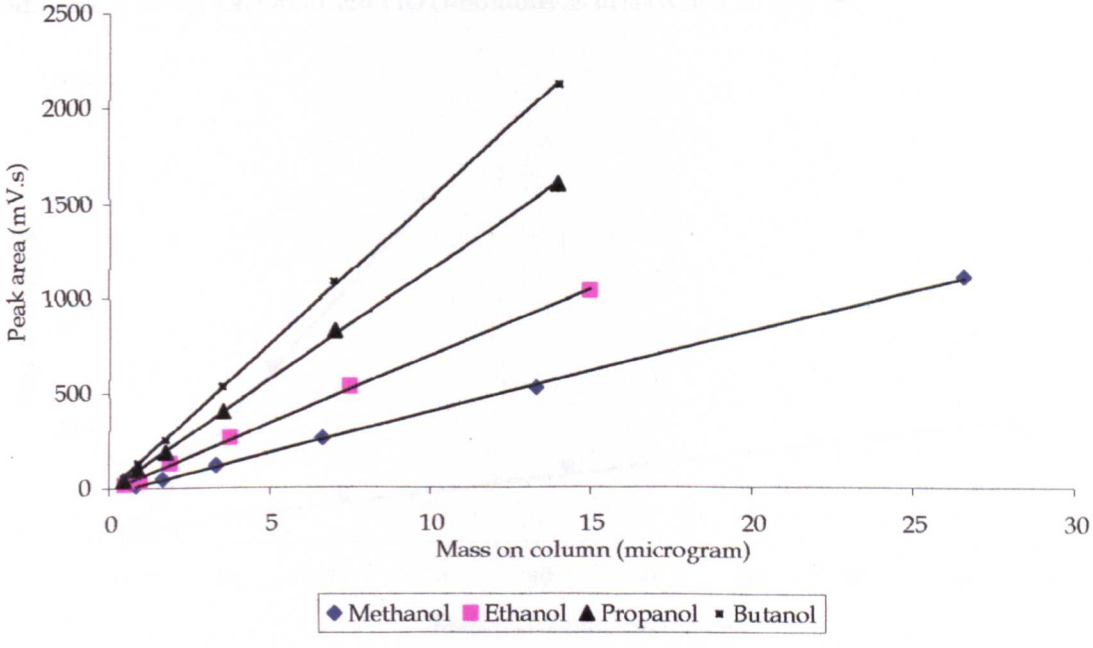

Figure 4.5. Calibration plots of aliphatic alcohols using LC-FID. Analysis conditions as in Fig 4.4. Optimum FID conditions as in section 3.3.1 (pg 58).

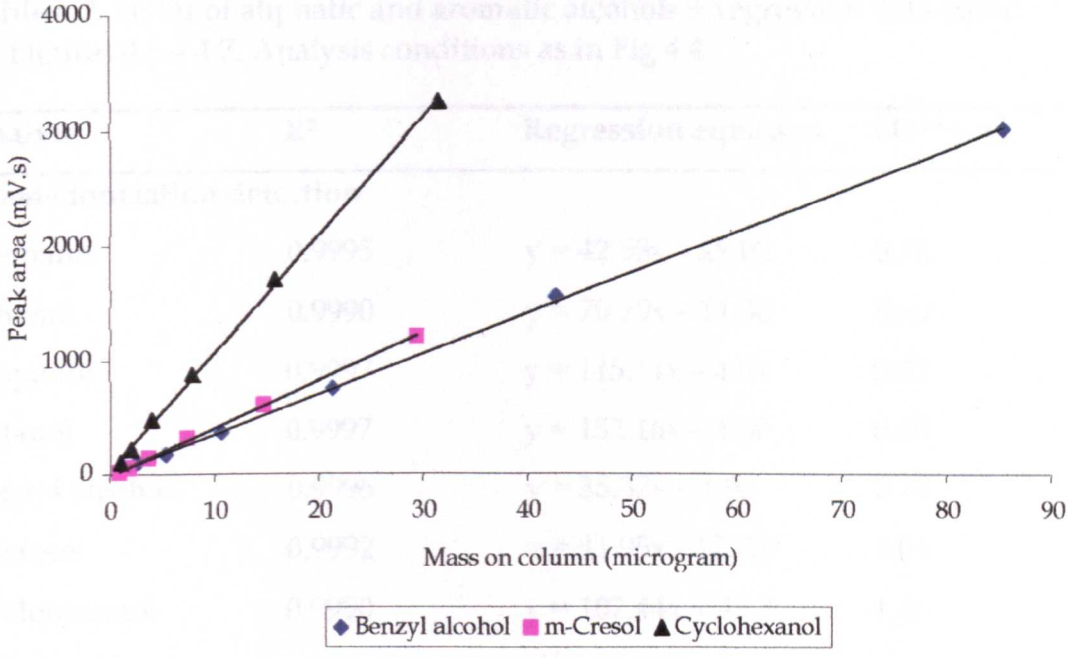

Figure 4.6. Calibration plots of cyclohexanol and aromatic alcohols using LC-FID. Analysis conditions as in Fig 4.4. Optimum FID conditions as in section 3.3.1 (pg 58).

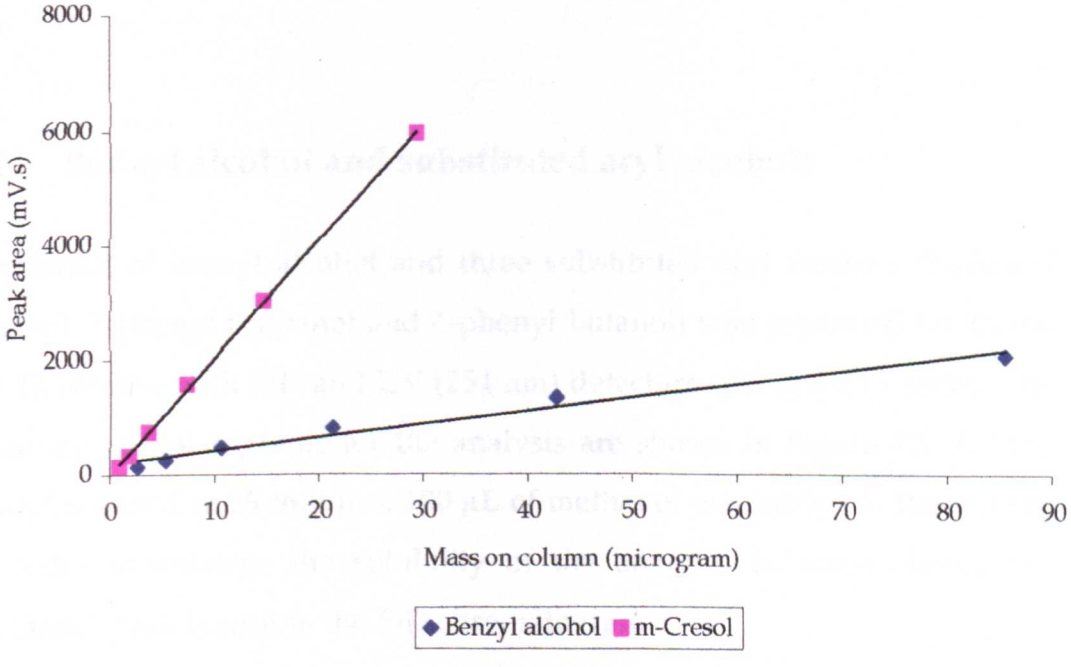

Figure 4.7. Calibration plots of aromatic alcohols using LC-UV at 220 nm. Analysis conditions as in Fig 4.4.

Table 4.2. LODs of aliphatic and aromatic alcohols + regression data based on Figures 4.5 – 4.7. Analysis conditions as in Fig 4.4

Analyte	R^2	Regression equation	LOD (µg)
Flame ionization detection			
Methanol	0.9995	y = 42.58x – 28.02	0.78
Ethanol	0.9990	y = 70.29x – 11.38	0.60
Propanol	0.9997	y = 115.11x – 4.91	0.32
Butanol	0.9997	y = 152.16x – 4.60	0.30
Benzyl alcohol	0.9996	y = 35.37x – 1.96	2.15
m-cresol	0.9992	y = 41.95x - 12.75	1.04
Cyclohexanol	0.9990	y = 102.44x + 45.3	1.26
UV detection			
Benzyl alcohol	0.9734	y = 22.77x + 199.49	17.01
m-cresol	0.9995	y = 203.83x + 1.77	0.83

4.2 Benzyl alcohol and substituted aryl alcohols

A mixture of benzyl alcohol and three substituted aryl alcohols (2-phenyl ethanol, 3-phenyl propanol and 4-phenyl butanol) was separated on Xterra RP 18 column with FID and UV (254 nm) detectors connected in series. The resulting chromatograms for the analysis are shown in Figure 4.8. All the analytes eluted in 59 minutes. 100 µL of methanol was added to the sample in order to enhance the solubility of the analytes in water; hence the methanol peak is seen in the FID chromatogram.

Calibration studies were carried out and the resulting plots are shown in Figure 4.9 (FID) and Figure 4.10 (UV). A summary of the regression equations and detection limits are shown in Table 4.3. Both detectors have comparable detection limits for these analytes, reflecting the weak,

unconjugated phenyl chromophore, although it is not clear why the response for 2-phenyl ethanol should be so much lower.

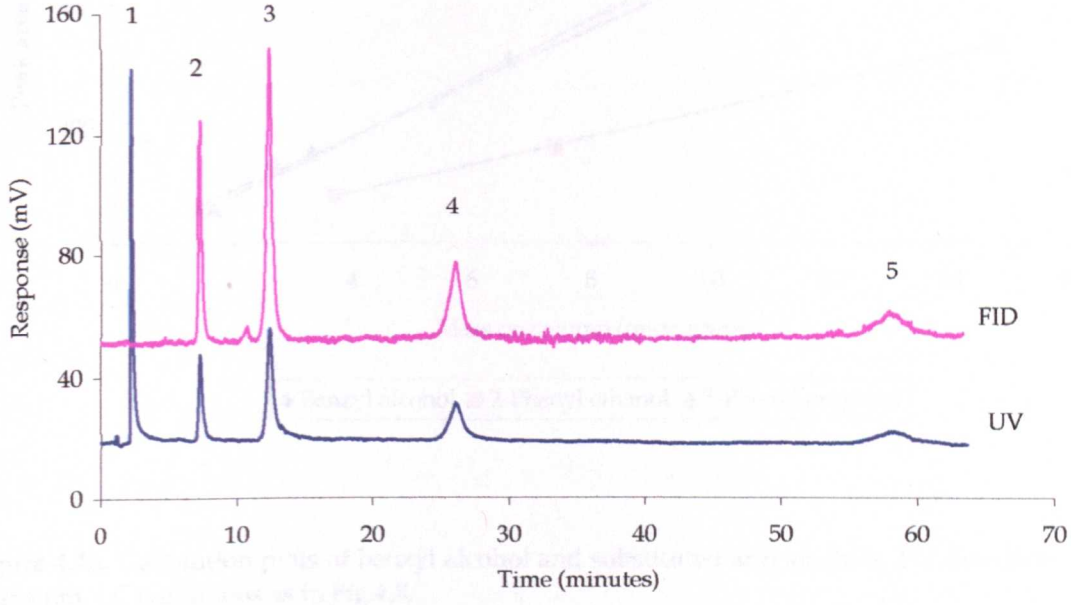

Figure 4.8. Chromatograms of benzyl alcohol and substituted aryl alcohols on Xterra RP 18 (3.5 µm, 4.6 x 150 mm). Oven temperature, 100 °C. Eluent (100% water) flow, 1 mL/min. UV wavelength, 254 nm. Optimum FID conditions as in section 3.3.1 (pg 58). Peak identity: 1 = methanol; 2 = benzyl alcohol; 3 = 2-phenyl ethanol; 4 = 3-phenyl propanol and 5 = 4-phenyl butanol.

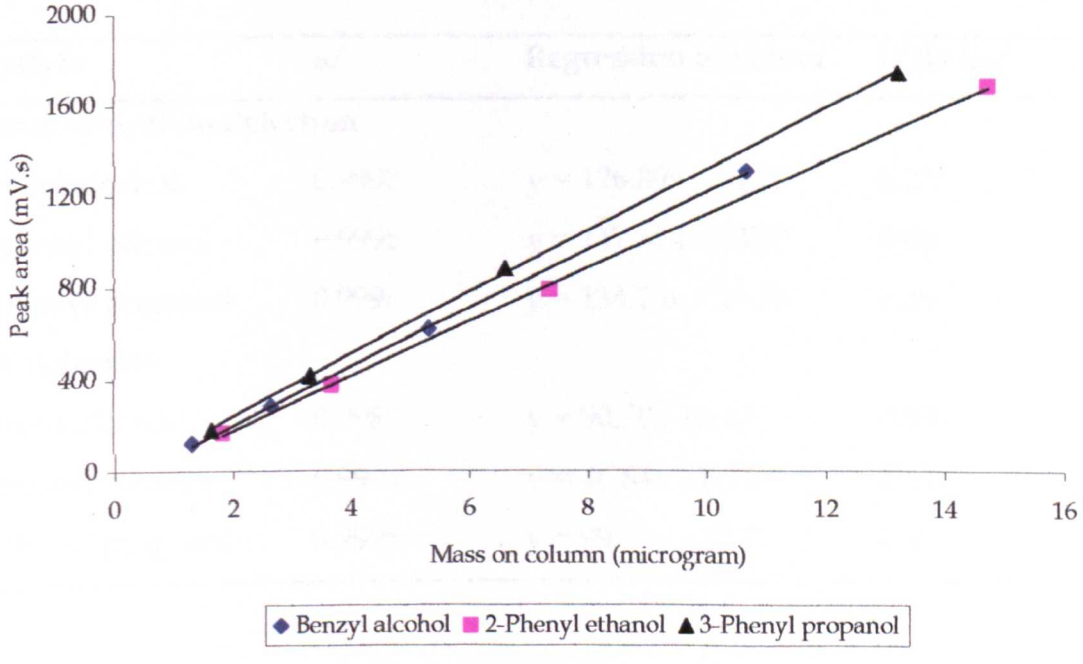

Figure 4.9. Calibration plots of benzyl alcohol and substituted aryl alcohols. LC conditions as in Fig 4.8. Optimum FID conditions as in section 3.3.1 (pg 58).

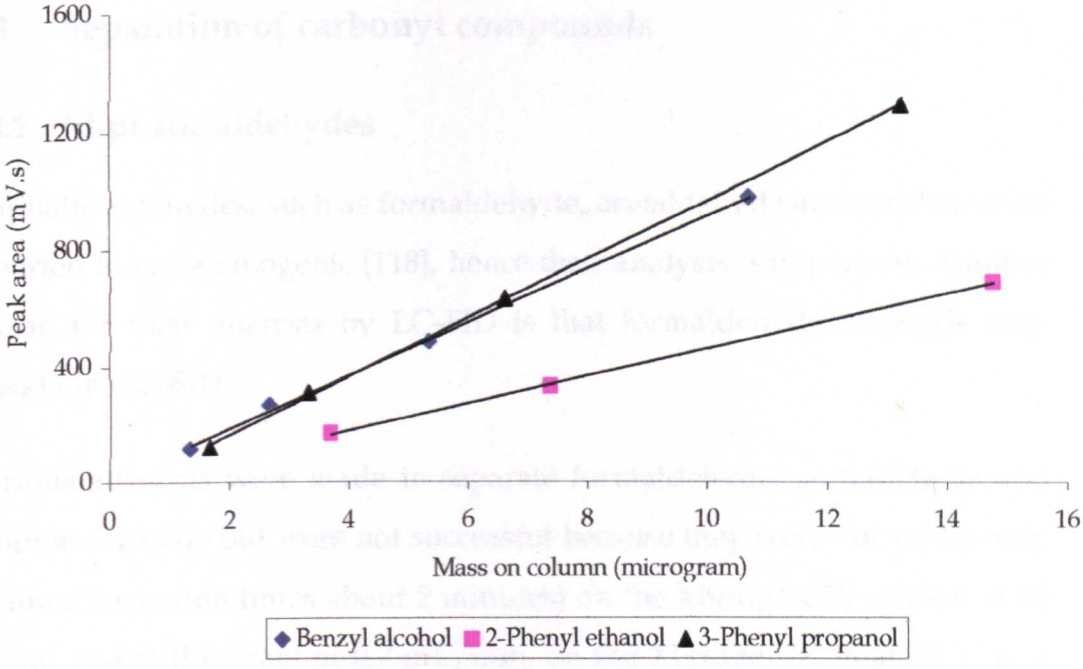

Figure 4.10. Calibration plots of benzyl alcohol and substituted aryl alcohols. UV detection at 254 nm. LC conditions as in Fig 4.8.

Table 4.3. LODs of benzyl alcohol and substituted aryl alcohols + regression (peak area vs mass on column) data based on Figures 4.9 and 4.10. LC conditions as in Fig 4.8

Analyte	R^2	Regression equation	LOD (µg)
Flame ionization detection			
Benzyl alcohol	0.9998	y = 126.89x – 54.78	0.23
2-phenyl ethanol	0.9995	y = 117.39x – 58.80	0.46
3-phenyl propanol	0.9996	y = 134.25x – 29.76	0.39
UV detection			
Benzyl alcohol	0.9988	y = 90.70x +6.67	0.53
2-phenyl ethanol	0.9994	y = 46.84x – 8.16	0.61
3-phenyl propanol	0.9996	y = 99.74x – 32.77	0.38

4.3 Separation of carbonyl compounds

4.3.1 Aliphatic aldehydes

Aliphatic aldehydes, such as formaldehyde, acetaldehyde and acrolein were reported to be carcinogenic [118], hence their analysis is important. Another reason for their analysis by LC-FID is that formaldehyde responds only weakly in GC-FID.

Various attempts were made to separate formaldehyde, acetaldehyde and propionaldehyde but were not successful because they were not sufficiently retained (retention times about 2 minutes) on the Xbridge C18 column at 80 °C and eluent flow rate of 0.7 mL/min, on the Xbridge RP 18 at 40 °C and eluent flow rate of 1 mL/minute, on the Xterra MS C18 at 80 °C and eluent flow rate of 1 mL/minute and on the Xterra RP 8 at 40 °C and eluent flow rate of 1 mL/minute. The weak retention and hence lack of selectivity of these columns can be attributed to their polarity.

However, these compounds were baseline separated on PS-DVB column at reasonable retention times (Figure 4.11) because PS-DVB is more hydrophilic compared to alkylated C18 columns with a higher effective carbon loading.

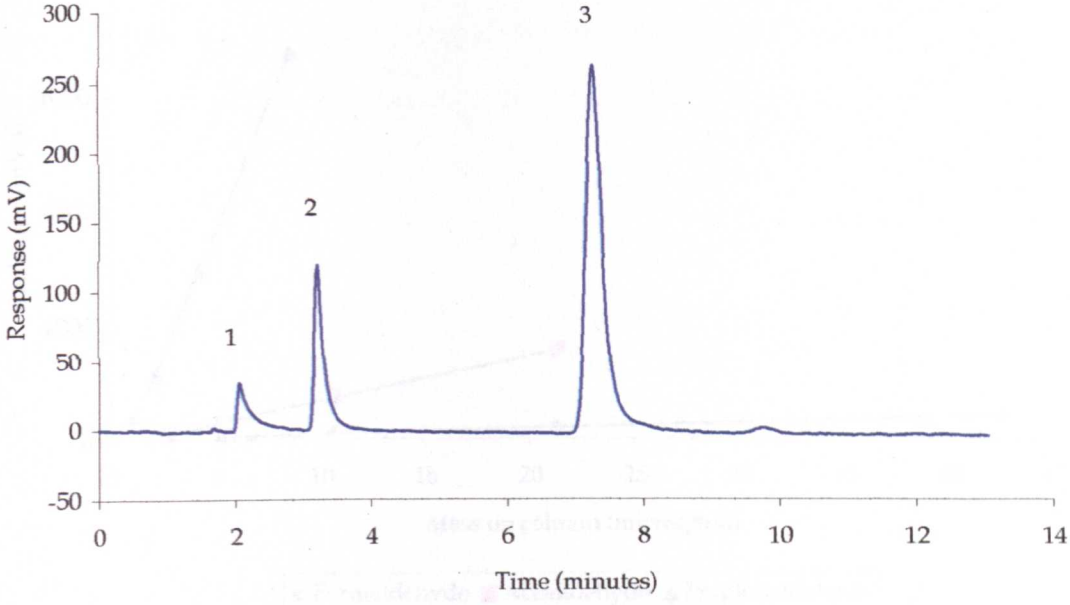

Figure 4.11. Chromatogram of aliphatic aldehydes on PS-DVB, 4.6 x 150 mm column at 160 °C. Eluent (100% water) flow, 1 mL/min. Optimum FID conditions as in section 3.3.1 (pg 58). Peak identity: 1 = formaldehyde; 2 = acetaldehyde and 3 = propionaldehyde.

The compounds were detected without derivatization, demonstrating one of the advantages of LC-FID over common HPLC detectors like UV and fluorescence. The compounds lack strong UV- or fluorescence-absorbing groups which call for derivatization before detection by UV or fluorescence. LC-FID also has an advantage over GC-FID in respect of formaldehyde analysis because it has been reported that GC-FID has a low response for formaldehyde [119].

Calibration plots were generated by serial dilutions and the plots are shown in Figure 4.12. The sensitivity increased with an increase in carbon number as expected and the sensitivity of formaldehyde is very low; the same observation made in GC-FID. Detection limits were also calculated (Table 4.4).

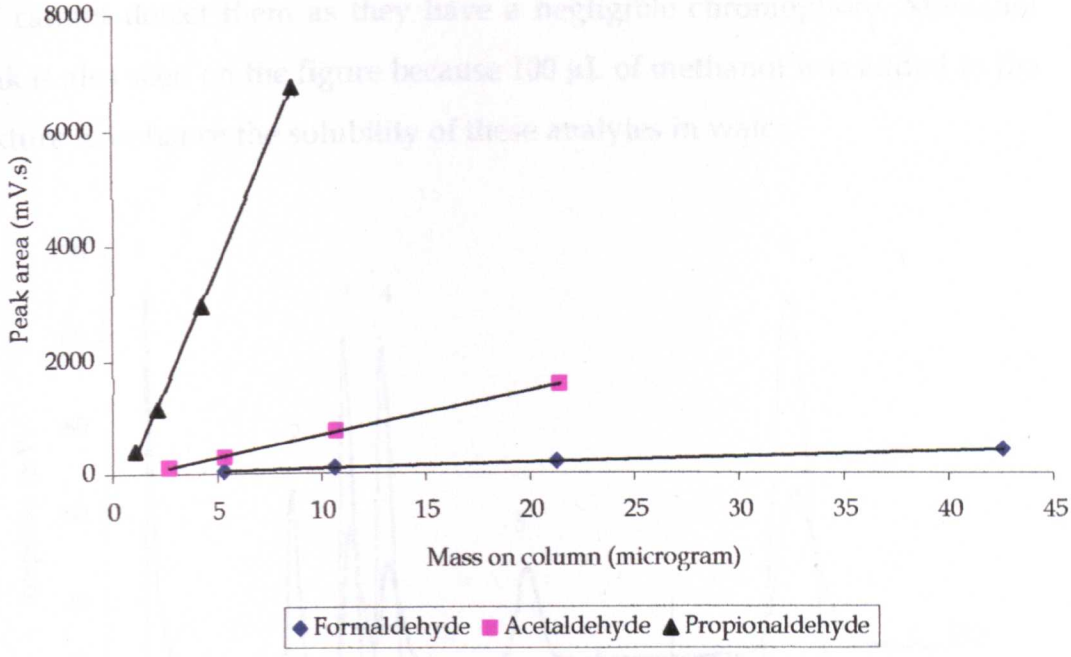

Figure 4.12. Calibration plots of aliphatic aldehydes. LC conditions as in Fig 4.11. Optimum FID conditions as in section 3.3.1 (pg 58).

Table 4.4. LODs of aliphatic aldehydes + regression (peak area vs mass on column) data based on 4.12. Conditions as in Fig 4.11

Analyte	R^2	Regression equation	LOD (µg)
Formaldehyde	1	y = 9.92x – 5.84	0.21
Acetaldehyde	0.9992	y = 78.60x – 106.34	0.83
Propionaldehyde	0.9990	y = 854.95x – 615.71	0.38

4.3.2 Ketones

A mixture of ketones containing aliphatic (2-hexanone, 2-heptanone) and aromatic (o-methyl-acetophenone, propiophenone, butyrophenone) was separated with 0.00075 M sulfuric acid as the eluent on Xbridge C18 column. Both flame ionization detection (FID) and UV detection at 254 nm were employed for the analysis (Figure 4.13). 2-Hexanone and 2-heptanone are not seen on the UV chromatogram because at the measurement wavelength,

UV cannot detect them as they have a negligible chromophore. Methanol peak is also seen on the figure because 100 µL of methanol was added to the mixture to enhance the solubility of these analytes in water.

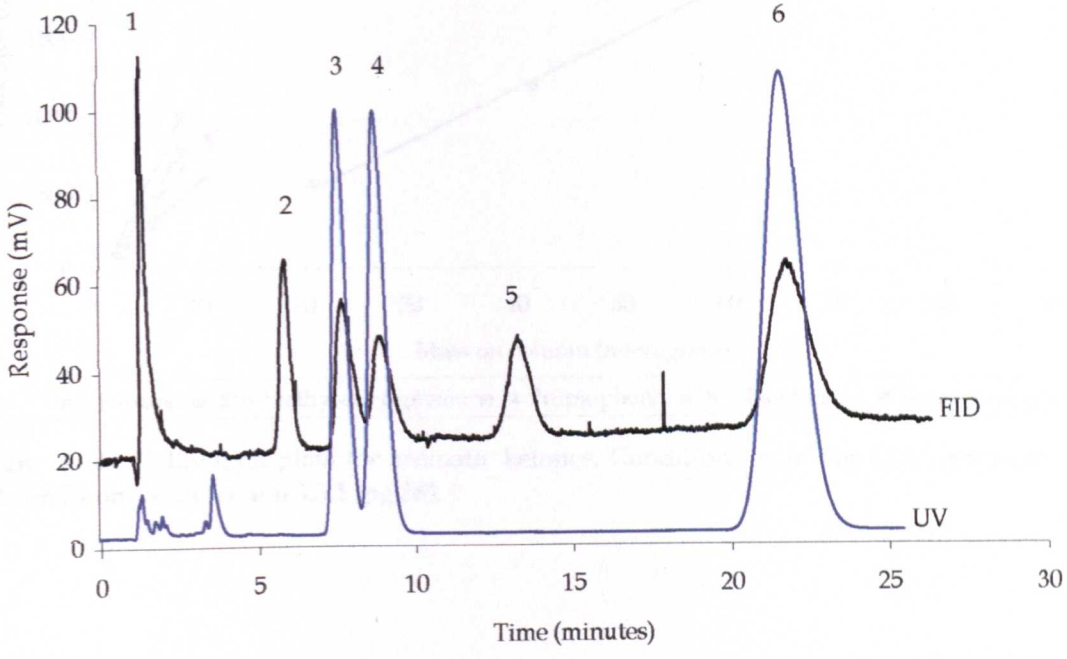

Figure 4.13. Chromatograms of aliphatic and aromatic ketones on Xbridge C18, 3.5 µm, 4.6 x 150 mm. Oven temperature, isothermal at 130 °C. Eluent (0.00075 M sulfuric acid) flow, 1 mL/min. Optimum FID conditions as in section 3.3.1 (pg 58). Peak identity: 1 = methanol; 2 = 2-hexanone; 3 = o-methyl-acetophenone; 4 = propiophenone; 5 = 2- heptanone and 6 = butyrophenone.

Calibration study was carried out for this analysis; both with FID and UV. Since the analytes have low volatility, sulfuric acid was added to the eluent to linearize the FID plots. The plots were reasonably linear [Figures 4.14 (FID) and 4.15 (UV)] and a summary of the detection limits are given in Table 4.5. From the table, the UV detector is more sensitive than the FID as evident from the slopes of their calibration plots. The values of their sensitivities also show that the FID responses of the aromatic compounds are less than those of the aliphatic ones.

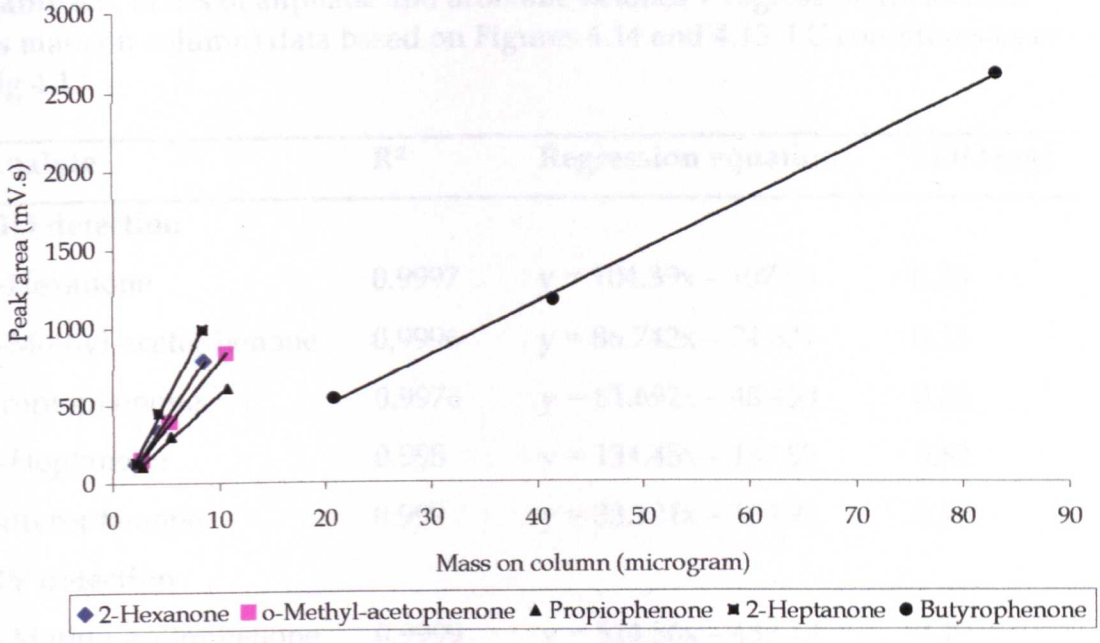

Figure 4.14. Calibration plots for aromatic ketones. Conditions as in Fig 4.13. Optimum FID conditions as in section 3.3.1 (pg 58).

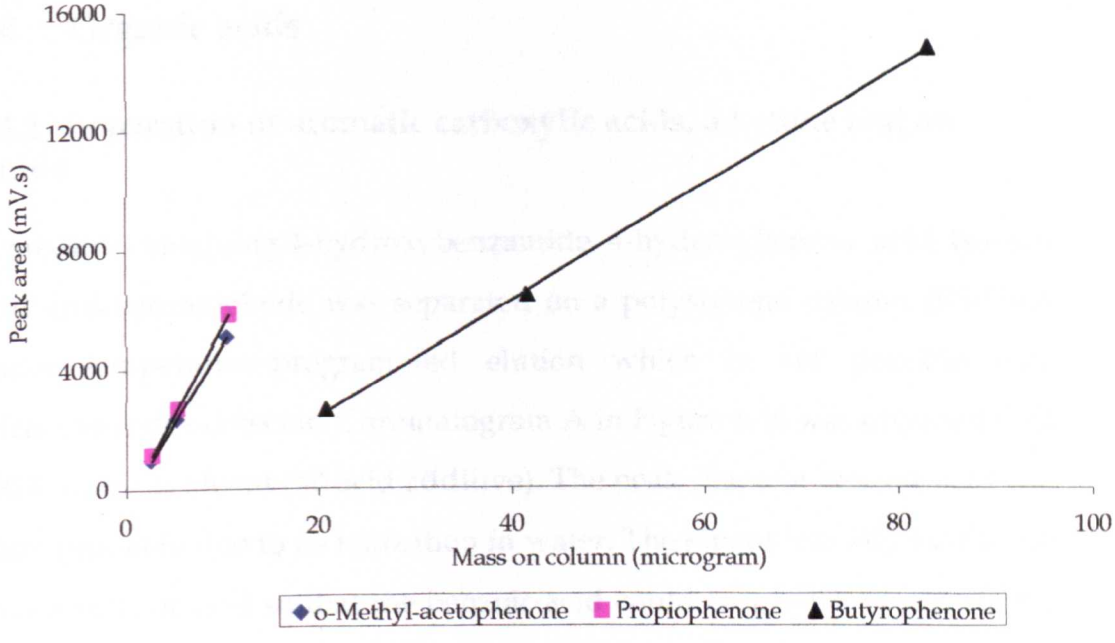

Figure 4.15. Calibration plots for aromatic ketones, UV detection. Conditions as in Fig 4.13.

Table 4.5. LODs of aliphatic and aromatic ketones + regression (peak area vs mass on column) data based on Figures 4.14 and 4.15. LC conditions as in Fig 4.13

Analyte	R^2	Regression equation	LOD (µg)
FID detection			
2-Hexanone	0.9997	y = 104.39x - 107.96	0.25
o-Methyl-acetophenone	0.9996	y = 86.742x - 74.631	0.33
Propiophenone	0.9976	y = 61.692x - 48.454	0.85
2-Heptanone	0.998	y = 134.45x - 137.92	0.62
Butyrophenone	0.999	y = 33.121x - 169.93	4.17
UV detection			
o-Methyl-acetophenone	0.9999	y = 524.56x - 432.13	0.17
Propiophenone	0.9999	y = 588.52x - 463.89	0.14
Butyrophenone	0.9997	y = 194.33x - 1497.60	2.33

4.4 Organic acids

4.4.1 Separation of aromatic carboxylic acids, a ketone and an amide

A mixture containing 4-hydroxybenzamide, 4-hydroxybenzoic acid, benzoic acid and benzaldehyde was separated on a polystyrene column (PS-DVB) under temperature-programmed elution which is not possible with refractive index detector. Chromatogram A in Figure 4.16 was obtained with 100% water as eluent (no acid additive). The peak shape of benzoic acid was poor, probably due to its ionization in water. The eluent was adjusted to pH 3 with sulfuric acid so that the benzoic acid could be pre-protonated in the eluent before getting to the detector. The peak shape of benzoic acid improved with the acidified eluent (Figure 4.16 B). All the analytes eluted in 25 minutes. Figure 4.16 also showed that benzaldehyde ran faster in the acidified eluent.

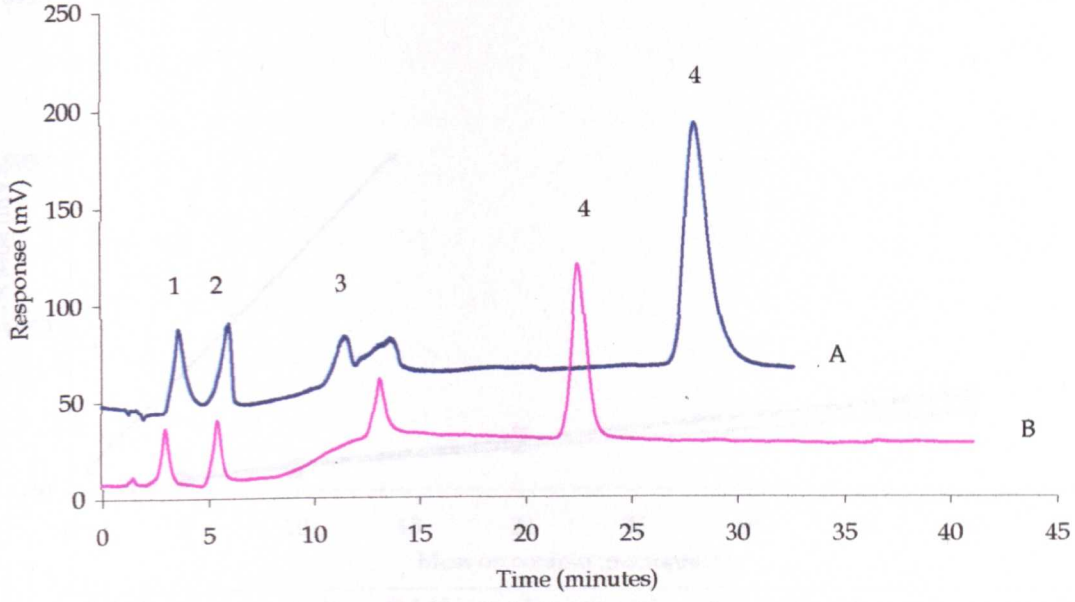

Figure 4.16. PS-DVB (4.6 x 150 mm) column. Oven program: 120 °C for 2 minutes, increased to 180 °C at 4 °C/min. A: Eluent, 100% water. B: Eluent (water adjusted to pH 3 with sulfuric acid). Flow, 1 mL/min. Optimum FID conditions as in section 3.3.1 (pg 58). Peak identity: 1 = 4-hydroxybenzamide; 2 = 4-hydroxybenzoic acid; 3 = benzoic acid and 4 = benzaldehyde.

The calibration plots and the summary containing regression equations and limits of detection are shown in Figure 4.17 and Table 4.6 respectively. The table shows that the sensitivities of 4-hydroxybenzamide, 4-hydroxybenzoic acid and benzoic acid are lower than that of benzaldehyde. This could be explained in terms of volatility because all the analytes are solids except benzaldehyde.

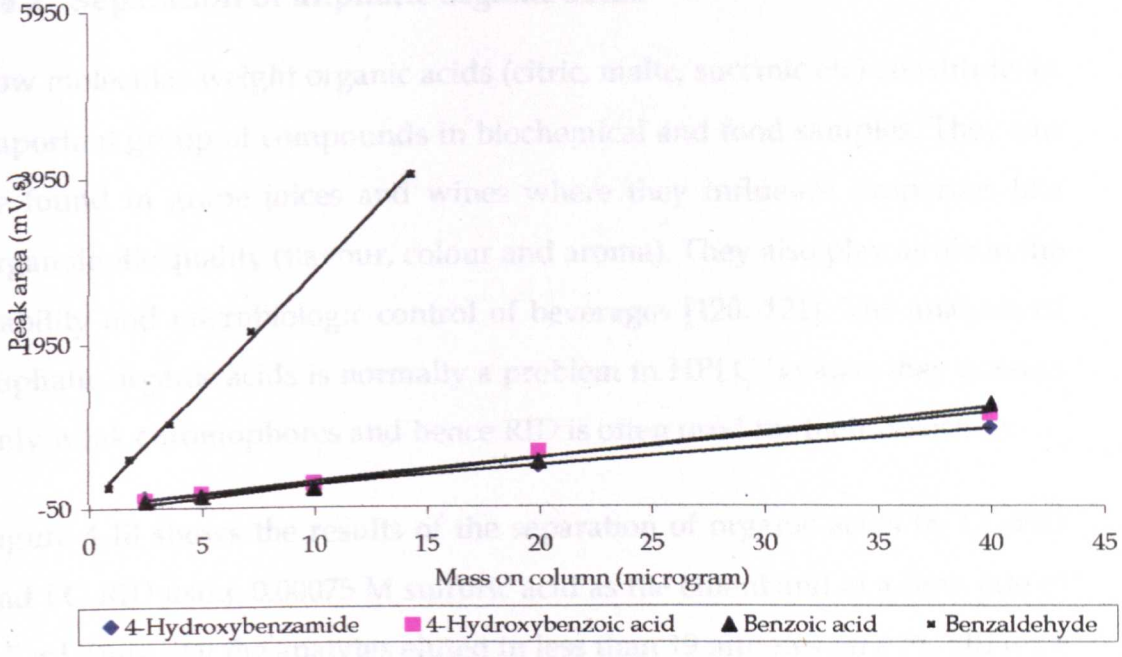

Figure 4.17. LC conditions as in Fig 4.16. Optimum FID conditions as in section 3.3.1 (pg 58).

Table 4.6. LODs + regression (peak area vs mass on column) data based on Figure 4.17. LC conditions as in Fig 4.16

Analyte	R^2	Regression equation	LOD (µg)
4-Hydroxybenzamide	0.9989	y = 22.71x + 1.7	1.79
4-Hydroxybenzoic acid	0.9911	y = 28.27x + 17.02	1.44
Benzoic acid	0.9910	y = 31.60x – 87.03	5.03
Benzaldehyde	0.9984	y = 279.36x + 2.75	0.77

4.4.2 Separation of aliphatic organic acids

Low molecular weight organic acids (citric, malic, succinic etc) constitute an important group of compounds in biochemical and food samples. They can be found in grape juices and wines where they influence properties like organoleptic quality (flavour, colour and aroma). They also play a role in the stability and microbiologic control of beverages [120, 121]. The analysis of aliphatic organic acids is normally a problem in HPLC because they possess only weak chromophores and hence RID is often used for their detection.

Figure 4.18 shows the results of the separation of organic acids by LC-FID and LC-RID using 0.00075 M sulfuric acid as the eluent and at a flow rate of 0.5 mL/min. All the analytes eluted in less than 19 minutes on a PL HiPlex 8 µm H column at 60 °C.

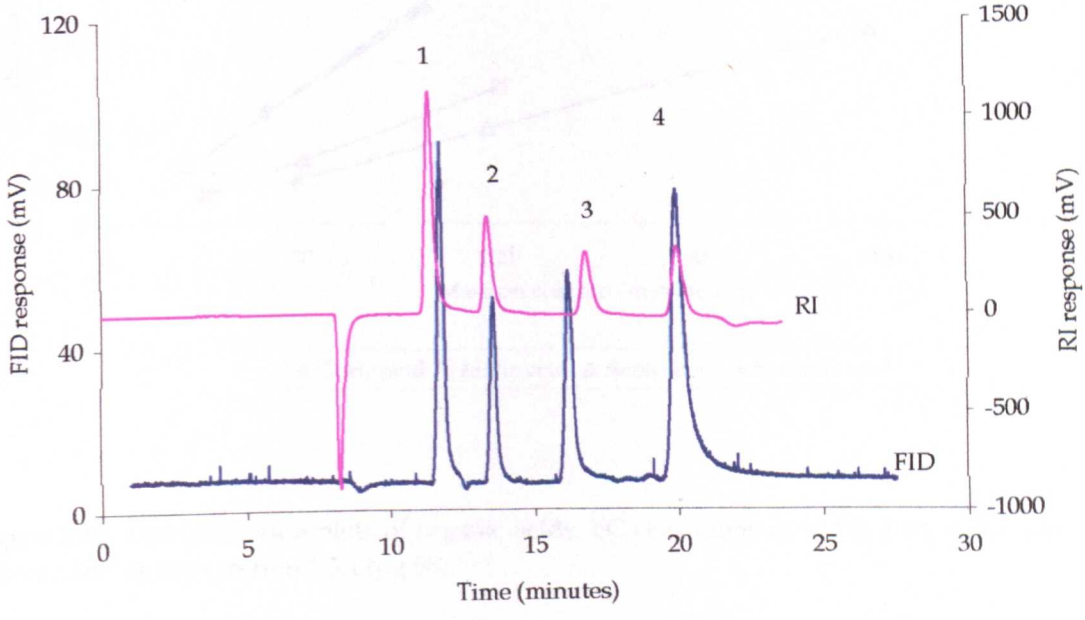

Figure 4.18. Chromatograms of organic acids on PL HiPlex 8 µm H (300 x 7.7 mm) column. Oven temperature, 60 °C; eluent (0.00075 M sulfuric acid) flow, 0.5 mL/min. Detection, FID and RID. Optimum FID conditions as in section 3.3.1 (pg 58). Peak identity: 1 = citric acid; 2 = malic acid; 3 = succinic acid and 4 = acetic acid.

Figures 4.19 and 4.20 are the calibration plots for the FID and RID respectively. The summary of the limits of detection are shown in Table 4.7. The FID sensitivities are low because they have very low carbon-to-oxygen ratios and all are solids. Malic and acetic acids are even lower because they have lower carbon-to-oxygen ratios compared to citric and succinic acid. In GC-FID, formic and acetic acids also give weak relative responses for the same reason.

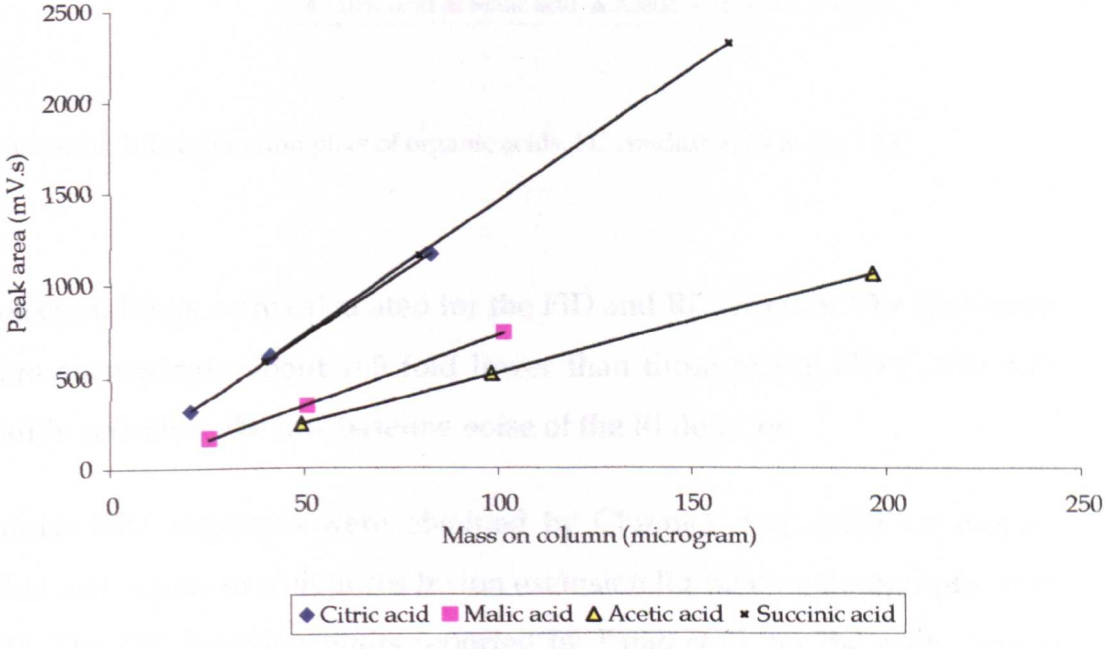

Figure 4.19. FID calibration plots of organic acids. LC conditions as in Fig 4.18. Optimum FID conditions as in section 3.3.1 (pg 58).

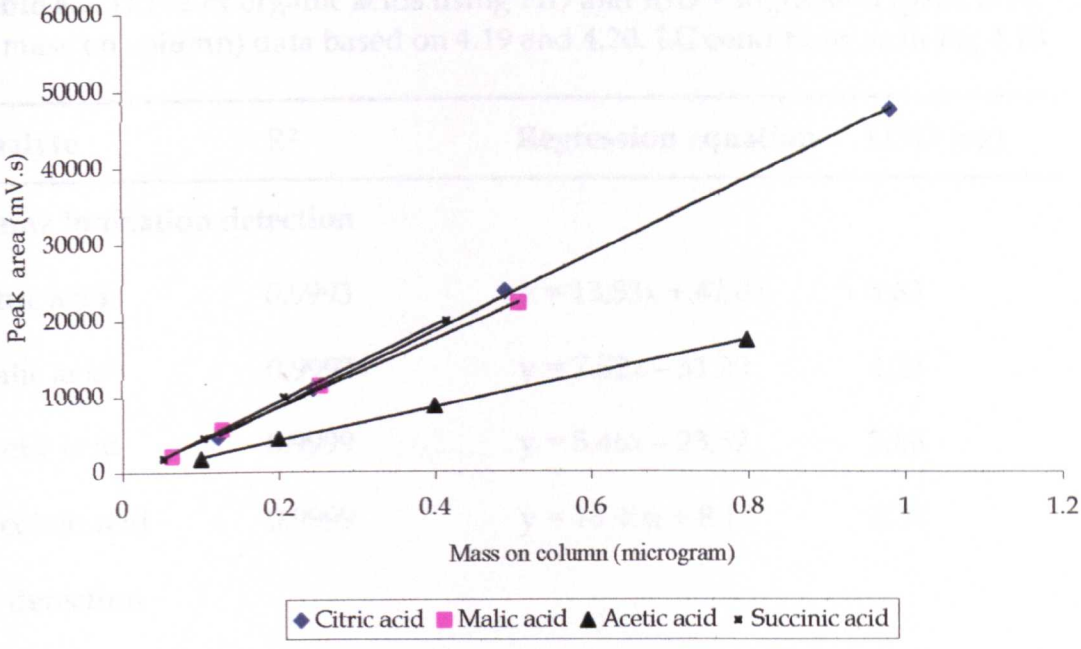

Figure 4.20. RID calibration plots of organic acids. LC conditions as in Fig 4.18.

Detection limits were calculated for the FID and RI detectors. The RID limits were surprisingly about 100 fold lower than those of the FID (Table 4.7); mainly reflecting the low baseline noise of the RI detector.

Similar RID responses were obtained by Chinnici *et al.* [122] for organic acids and sugars in fruit juices by ion exclusion liquid chromatography with RID. The UV detection limits reported by Fabio *et al.* for the acids ranged from 0.007 – 0.102 µg. Mato *et al.* [120] determined organic acids and found detection limits of 0.001 – 0.006 µg with UV detection at 185 nm.

Table 4.7. LODs of organic acids using FID and RID + regression (peak area vs mass on column) data based on 4.19 and 4.20. LC conditions as in Fig 4.18

Analyte	R^2	Regression equation	LOD (µg)
Flame ionization detection			
Citric acid	0.9993	y = 13.53x + 42.01	3.63
Malic acid	0.9993	y = 7.52x - 31.20	4.25
Acetic acid	0.9999	y = 5.46x - 23.57	2.66
Succinic acid	0.9999	y = 14.45x + 8.13	2.38
RI detection			
Citric acid	0.9996	y = 49765x - 1282	0.03
Malic acid	0.9985	y = 44840x + 387.45	0.03
Acetic acid	0.9991	y = 22233x + 303.48	0.03
Succinic acid	0.9995	y = 50267x - 732.67	0.01

4.5 The amines

4.5.1 Aromatic

A mixture of pyridine, aniline and benzylamine was analyzed isothermally at 180 °C by LC-FID on PS-DVB column (Figure 4.21).

The calibration plots and limits of detection are shown in Figure 4.22 and Table 4.8 respectively.

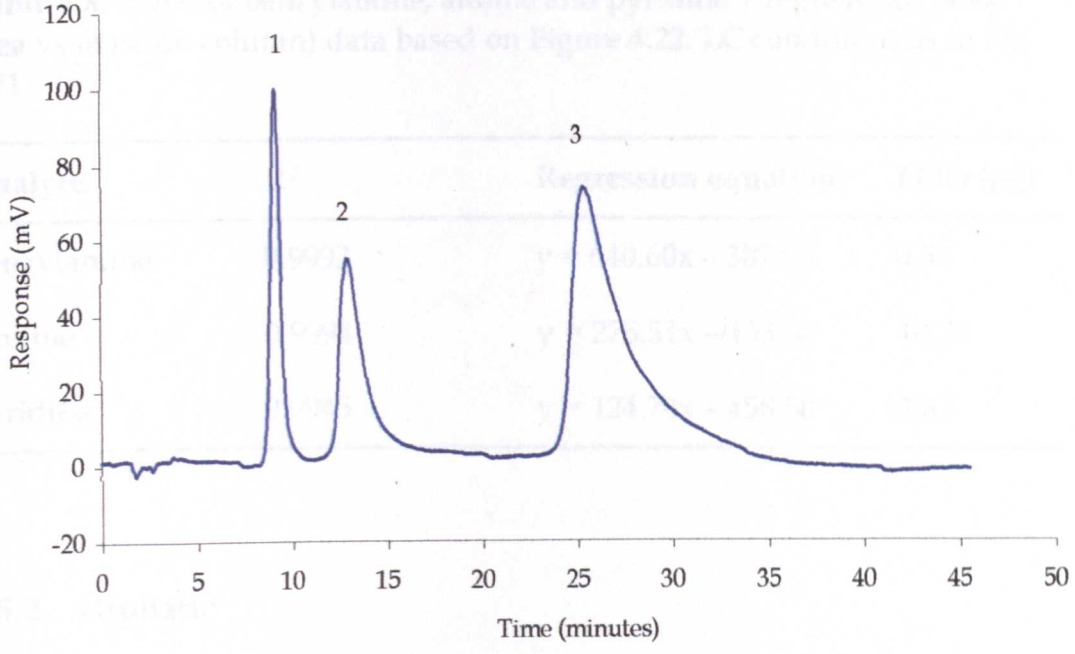

Figure 4.21. Chromatogram of aromatic amines on PS-DVB (150 x 4.6 mm) column. Oven temperature, isothermal at 180 °C. Eluent flow, 1 mL/minutes. Optimum FID conditions as in section 3.3.1 (pg 58). Peak identity: 1 = pyridine; 2 = aniline and 3 = benzylamine.

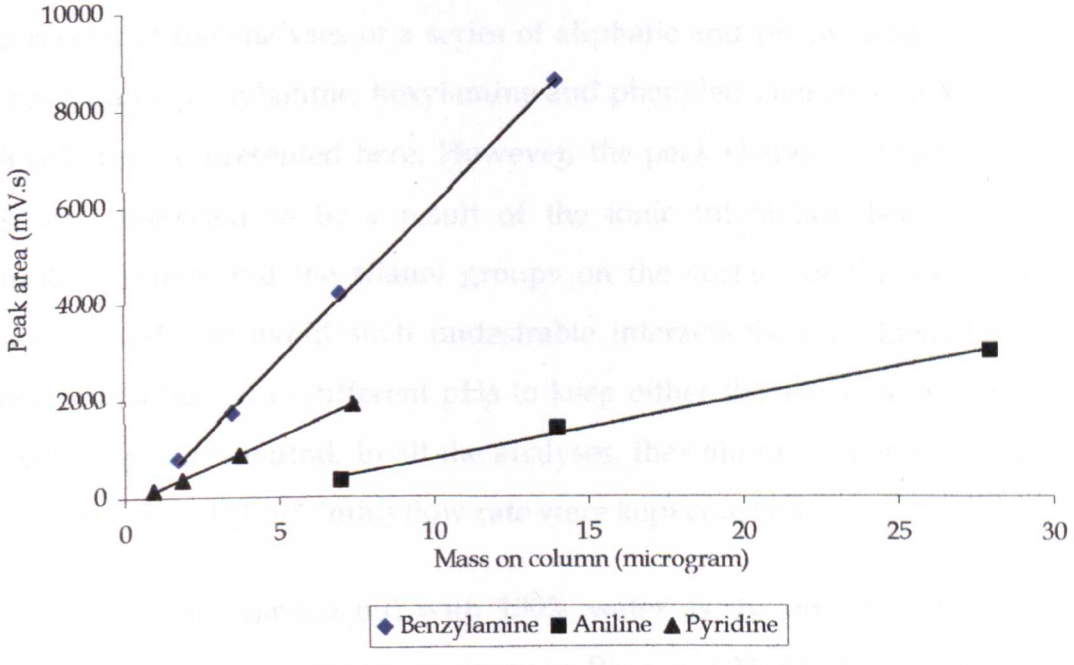

Figure 4.22. Calibration plots of benzylamine, aniline and pyridine. LC conditions as in Fig 4.21. Optimum FID conditions as in section 3.3.1 (pg 58).

Table 4.8. LODs of benzylamine, aniline and pyridine + regression (peak area vs mass on column) data based on Figure 4.22. LC conditions as in Fig 4.21

Analyte	R^2	Regression equation	LOD (µg)
Benzylamine	0.9993	y = 640.60x - 387.95	0.52
Aniline	0.9994	y = 275.51x - 133.50	10.23
Pyridine	0.9945	y = 124.74x - 458.58	3.83

4.5.2 Aliphatic

Although aryl amines could also be detected by UV, aliphatic amines have no chromophore and can only be detected by the FID.

The results of the analyses of a series of aliphatic and phenyl alkyl amines (benzylamine, pentylamine, hexylamine and phenylethylamine) on Xbridge C18 column are presented here. However, the peak shapes were poor and this was suspected to be a result of the ionic interaction between the ionisable amines and the silanol groups on the surface of the stationary phase. In order to avoid such undesirable interactions, the eluent (100% water) was adjusted to different pHs to keep either the analytes neutral or the silanol groups neutral. In all the analyses, the column temperature (100 °C) and the eluent (1 mL/min) flow rate were kept constant.

The first run was carried out with 100% water as the eluent without an additive and the peak shapes were poor (Figure 4.23 A). The poor peak shapes could be explained in terms of the ionic interaction between the partially protonated amines and residual silanol groups at pH (6.50) of the eluent [123].

The second run was carried out in an acidic eluent (adjusted to pH 3 with sulfuric acid); the result is shown in Figure 4.23 B. The sample was made up

in the eluent in order to avoid distortion of peak shapes that could result from difference in mobility between sample and eluent. Since these analytes have pKa of over 8, use of low pH should eliminate the ion-exchange interaction between the silanol and analytes because at this pH, the silanol groups should be sufficiently neutral and the analytes positively charged [124]. The chromatogram was found to be worse.

The persistence of the poor peak shapes with eluent at low and intermediate pHs suggested an option of separating these analytes in an eluent adjusted to pH 11. The pH of the eluent was adjusted with ammonia which is permitted with Xbridge material and the sample mixture was constituted in the eluent. At this pH, the silanol groups and the analytes should be negatively charged and neutral respectively, thereby eliminating the possibility of the undesirable interaction between the silanol groups and analytes. The peak shapes were still poor (Figure 4.24 A).

The pH of the eluent was then adjusted to 11 with sodium hydroxide (NaOH) instead of ammonia and the sample made up in the eluent. The peak shapes were poor (Figure 4.24 B) but better than those generated with the eluent at pH 3. The peak shapes were similar to those generated with the eluent at intermediate pH (4.23 A) but the retention times were longer.

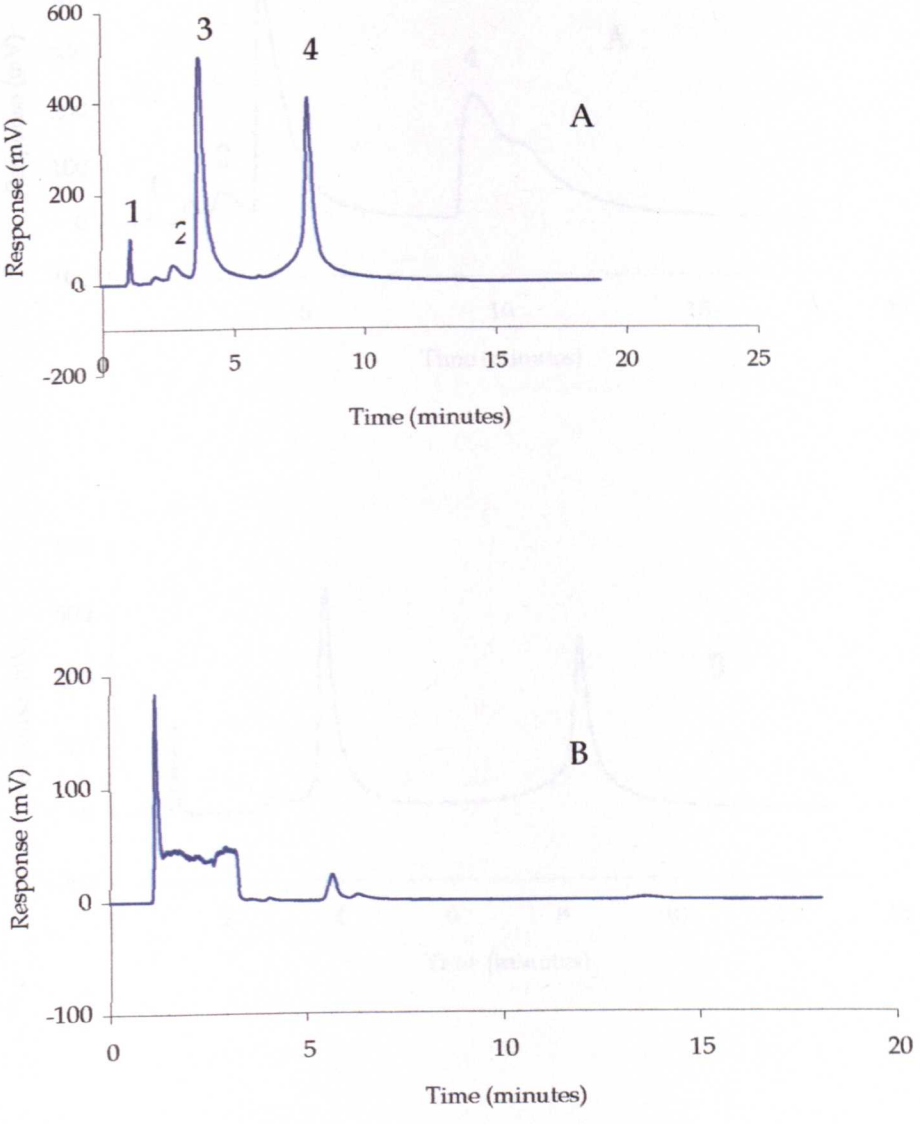

Figure 4.23. Chromatograms of amines. Xbridge C18, 3.5 µm, 4.6 x 150 mm. Column temperature, 100 °C. A = eluent, 100% water; B = eluent at pH 3 and sample in eluent. Optimum FID conditions as in section 3.3.1 (pg 58). Peaks: 1 = benzylamine, 2 = phenylethylamine, 3 = pentylamine and 4 = hexylamine.

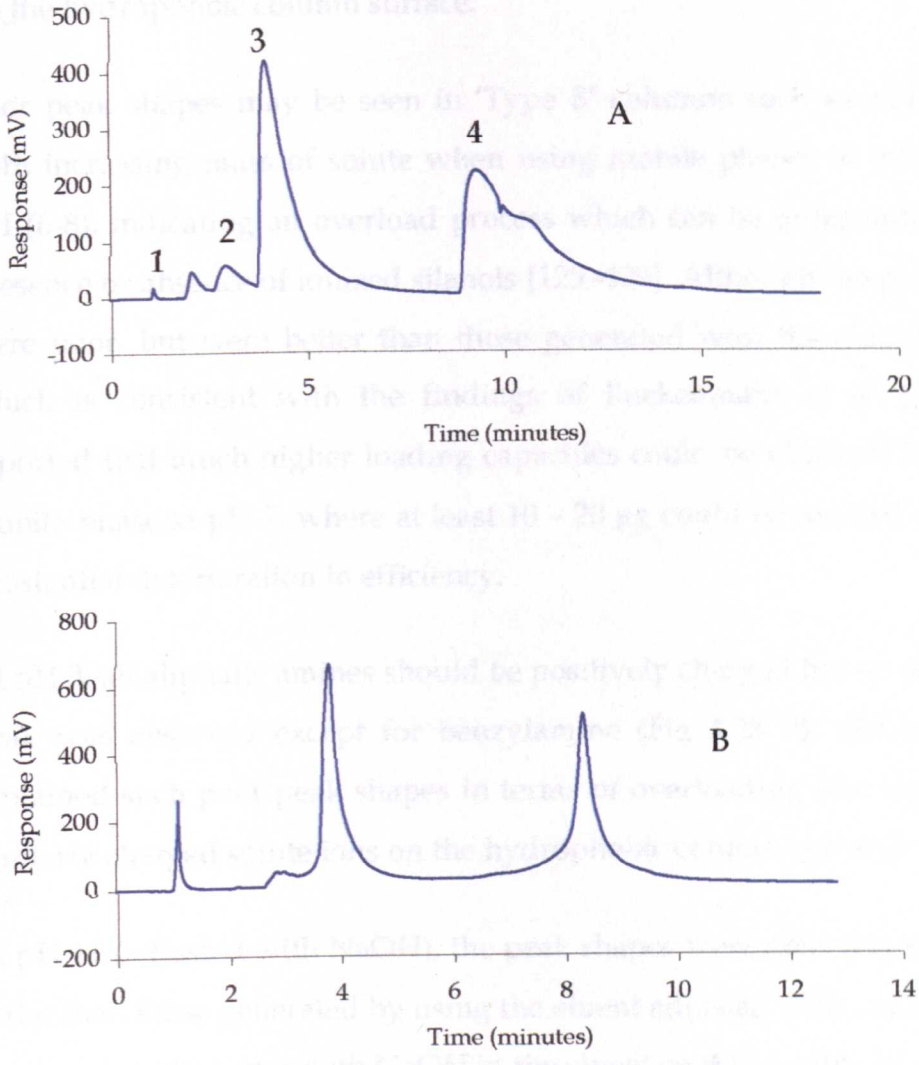

Figure 4.24. Chromatograms of amines. Xbridge C18, 3.5 µm, 4.6 x 150 mm. Column temperature, 100 °C. A = eluent at pH 11 and sample in eluent; B = eluent [200 mL water + 200 µL (0.02 M NaOH)] and sample in eluent. FID conditions and peak identification as in Figure 4.23.

In all the eluents used, either the ionization of the silanol groups or analytes should have been suppressed, eliminating the possibility of ionic interaction between the former and the latter. Since these measures did not improve the peak shapes, the poor peak shapes could be explained in terms of sample

overload [125, 126] caused by the repulsion of similarly charged solute ions on the hydrophobic column surface.

Poor peak shapes may be seen in 'Type B' columns such as Xbridge C18 with increasing mass of solute when using mobile phases of intermediate pH (6-8), indicating an overload process which can be independent of the presence or absence of ionized silanols [125 -129]. Although the peak shapes were poor, but were better than those generated with the eluent at pH 3 which is consistent with the findings of Buckenmaier *et al.* [130] who reported that much higher loading capacities could be obtained by using a mobile phase at pH 7, where at least 10 – 20 µg could be injected without a substantial deterioration in efficiency.

At pH 3, all aliphatic amines should be positively charged but no discernible peak was observed except for benzylamine (Fig 4.23 B). McCalley [128] explained such poor peak shapes in terms of overloading (the repulsion of similarly charged solute ions on the hydrophobic column surface).

At pH 11 (adjusted with NaOH), the peak shapes were poor (Fig 4.24 B) but better than those generated by using the eluent adjusted with ammonia. The improved peak shapes with NaOH in the eluent could possibly be explained in terms of the competitive interactions of Na^+ ions with ionized (negatively charged) silanols, giving the reduced tailing [127].

Using the eluent adjusted to pH 11 with NaOH, two detectors were connected in series for monitoring the analysis; FID and UV at 254 nm (Figure 4.25).

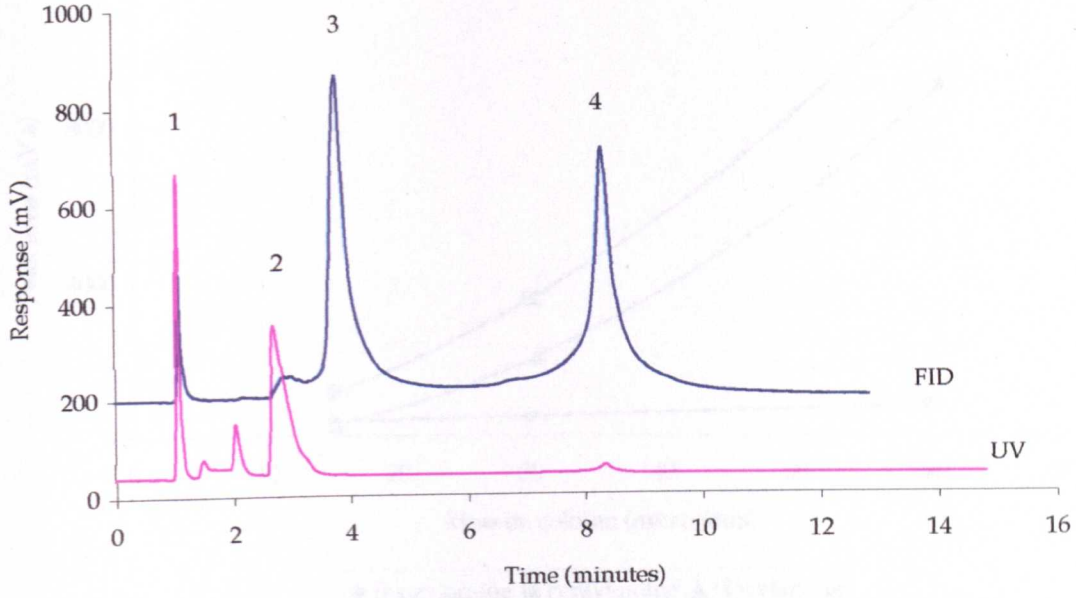

Figure 4.25. Chromatograms of amines on Xbridge C18, 3.5 µm, 4.6 x 150 mm. Column temperature, 100 °C. Sample diluted in eluent. Eluent (200 mL water + 200 µL [0.02 M NaOH]) flow, 1 mL/min. Optimum FID conditions as in section 3.3.1 (pg 58). Peaks: 1 = benzylamine, 2 = phenylethylamine, 3 = pentylamine and 4 = hexylamine.

The FID calibration plots for benzylamine was linear but those of pentylamine and hexylamine were curved (Figure 4.26). No calibration was carried out for phenylethylamine because the response (peak) was too low.

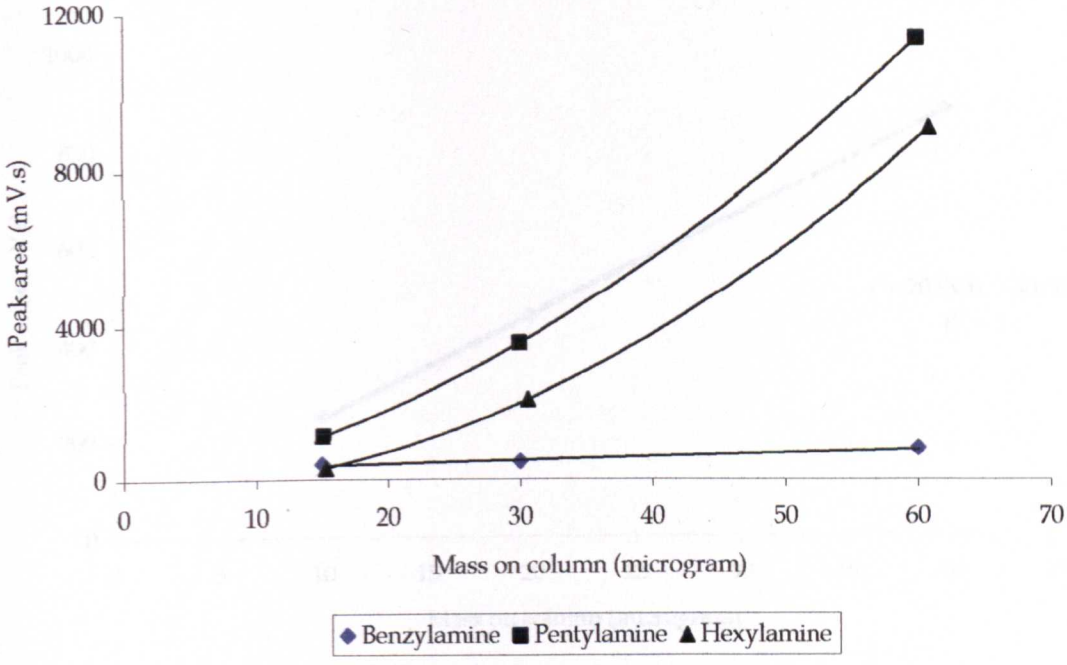

Figure 4.26. FID calibration plots of benzylamine, pentylamine and hexylamine. Conditions as in Fig 4.25. Optimum FID conditions as in section 3.3.1 (pg 58).

Since the FID calibration plots of the amines were non-linear, hexylamine calibration was repeated with the addition of sulfuric acid to the mobile phase to make it linear but the plot was still non-linear. Surprisingly, the plot became linear (Figure 4.27) when 20 µL of 39.2% sulfuric acid was added to the sample (hexylamine).

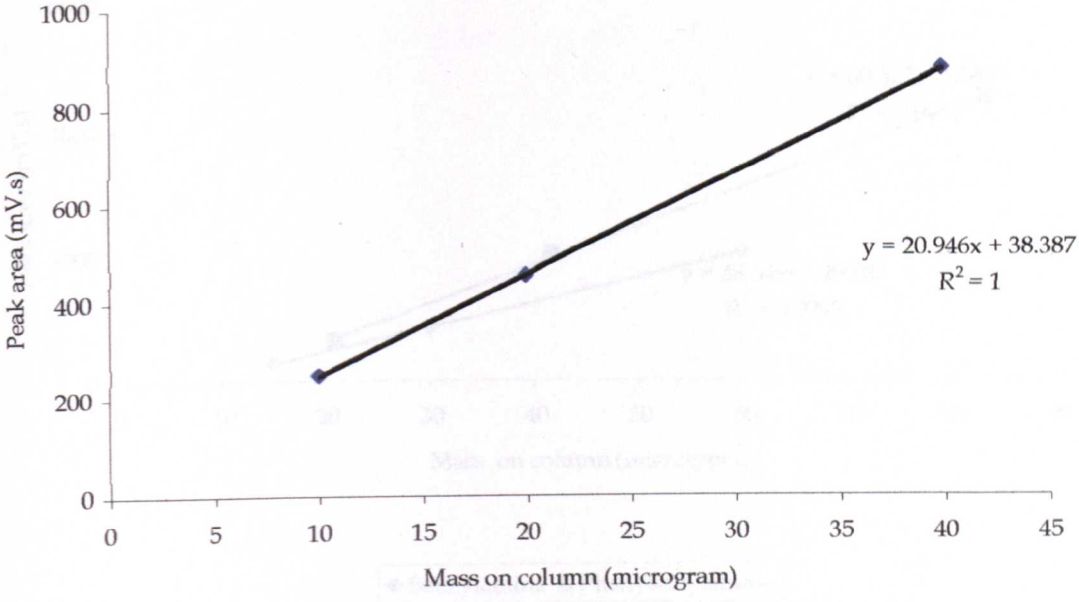

Figure 4.27. Linear plot of hexylamine in acidified water. Other conditions as in Figure 4.25.

The UV calibration plots for benzylamine and phenylethylamine are shown in Figure 4.28; both plots were linear and the detection limits for benzylamine and phenylethylamine were 0.74 and 3.98 µg respectively.

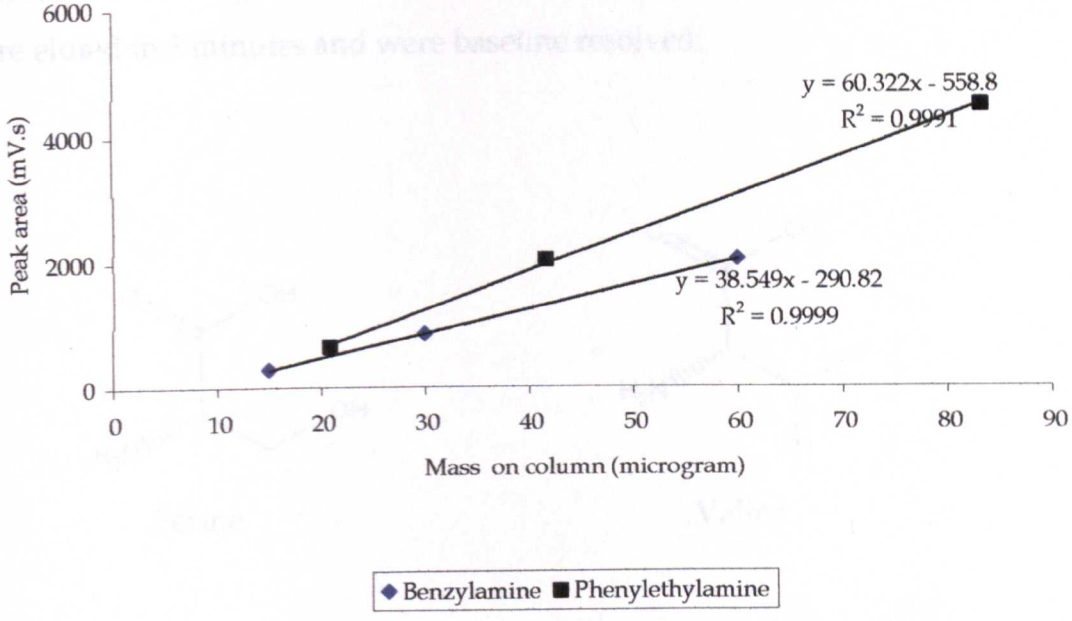

Figure 4.28. UV calibration plots of benzylamine and phenylethylamine. Conditions as in Fig 4.25.

4.6 Amino Acids

The analysis of amino acids in body fluids, such as urine and blood is important in the diagnosis and treatment of some diseases. In the food industries, amino acid levels are measured in order to check the quality of the final products. The compositional analysis of amino acids in proteins and peptides is essential in the study of the primary structures in biochemistry [131]. Most amino acids lack a chromophore and cannot be detected by UV detectors without derivatization.

This section presents the results of the separation of selected amino acids; serine, valine, isoleucine and phenylalanine (Figure 4.29); the acids are non-chromophore-containing compounds except phenylalanine. The analysis was carried out under the following conditions: column, Xterra RP 8 (3.5 µm, 4.6 x 150 mm); oven temperature, 50 °C; eluent (0.00075 M sulfuric acid) flow, 0.7 mL/min. Monitoring detectors were FID, UV at 206 nm and the

refractive index. Figure 4.30 shows the results of the analysis. The acids were eluted in 5 minutes and were baseline resolved.

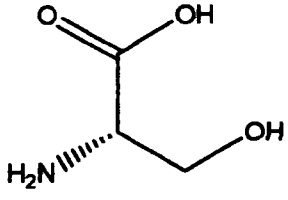

Serine

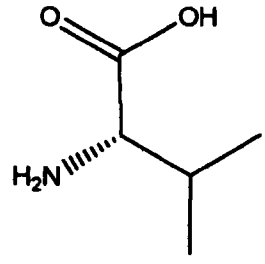

Valine

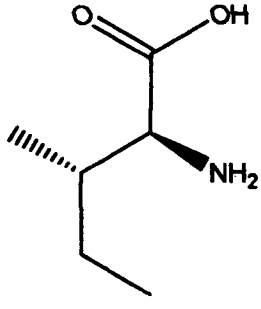

Isoleucine

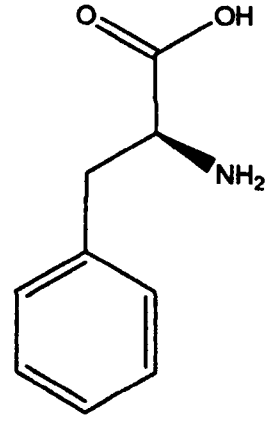

Phenylalanine

Figure 4.29. Structures of amino acids (serine, valine, isoleucine and phenylalanine).

On the UV trace (Figure 4.30 A), the phenylalanine peak went off-scale because at 206 nm, UV is very sensitive to phenylalanine. The serine, valine and isoleucine peaks are very small because they are weakly absorbing at this wavelength. Valine was not included in the mixture for the LC-RID analysis because it could not have been resolved from the serine peak (Figure 4.30 B).

No calibration study was carried out for the UV detector. The calibration plots for the FID and refractive index detector are shown in Figures 4.31 and

4.32 respectively. Table 4.9 shows the regression equations and limits of detections for the amino acids.

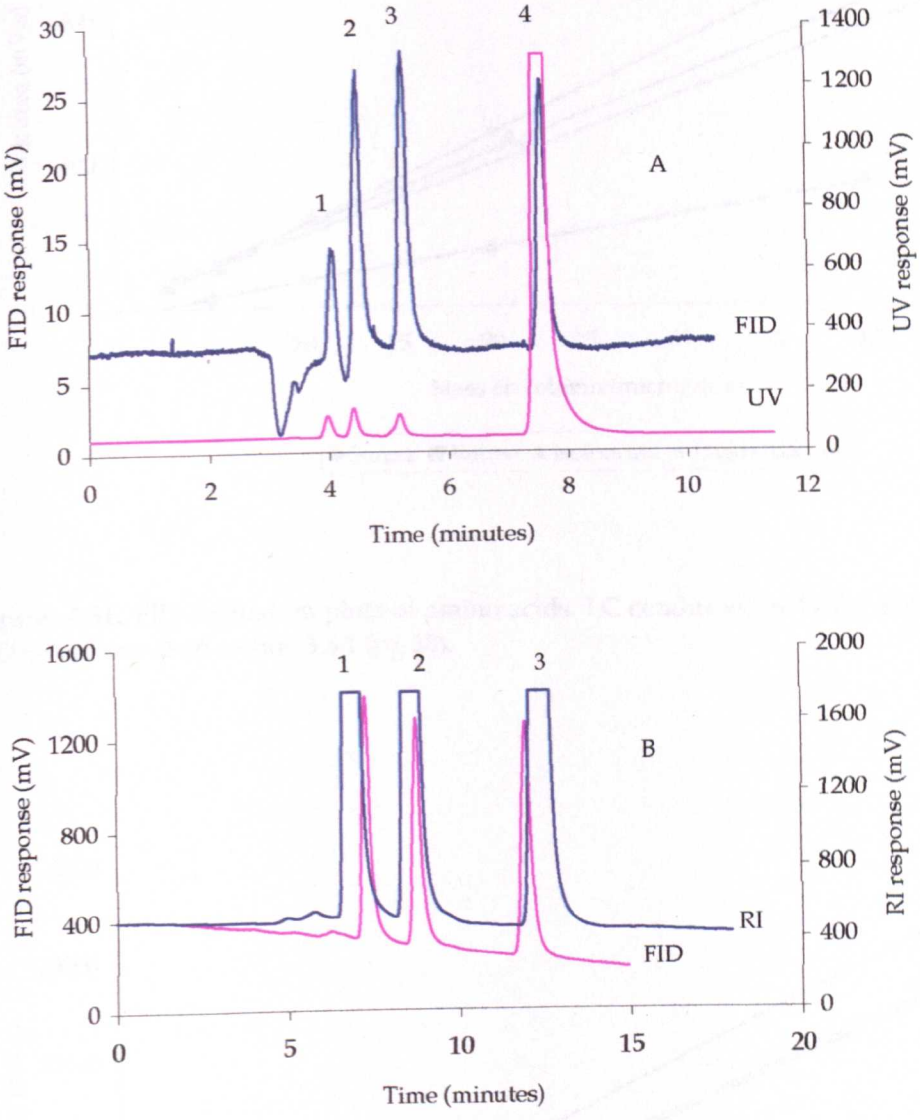

Figure 4.30. Chromatograms of amino acids. Xterra RP 8, 3.5 µm, 4.6 x 150 mm. Oven temperature, 50 °C. Eluent (water adjusted to pH 3 with sulfuric acid) flow, 0.7 mL/min. Detection: UV at 206 nm, FID and RID. Optimum FID conditions as in section 3.3.1 (pg 58). Peak identity in A: 1 = serine, 2 = valine, 3 = isoleucine and 4 = phenylalanine. Peak identity in B: 1 = serine, 2 = isoleucine and 3 = phenylalanine.

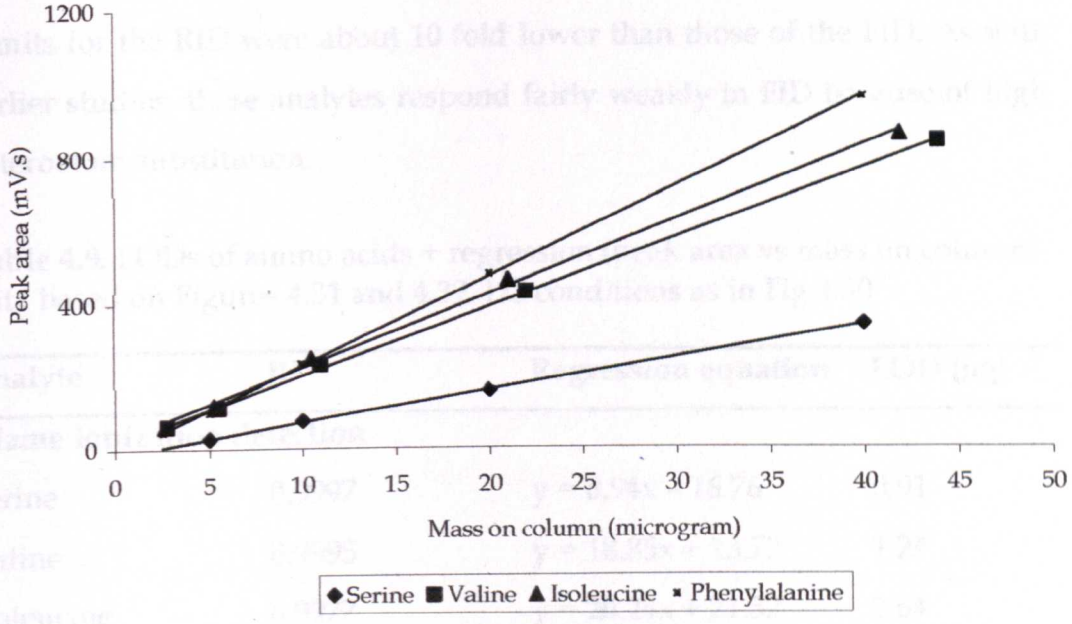

Figure 4.31. FID calibration plots of amino acids. LC conditions as in Fig 4.30. Optimum FID conditions as in section 3.3.1 (pg 58).

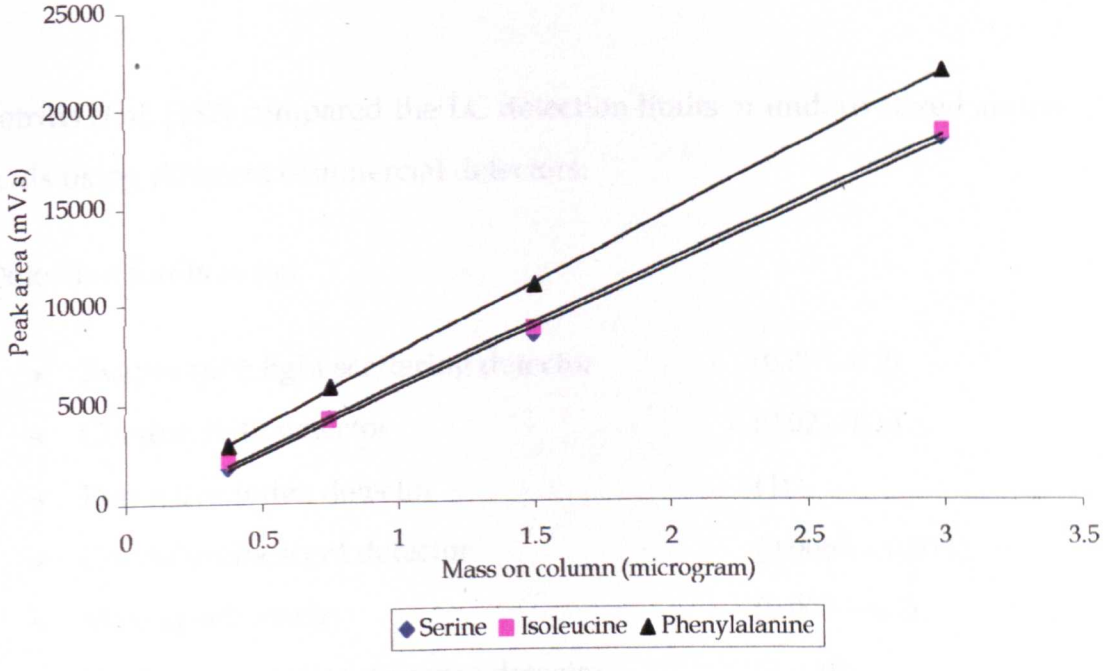

Figure 4.32. RID calibration plots of amino acids. LC conditions as in Fig 4.30.

Detection limits were calculated for the FID and RI detectors (Table 4.9). Limits for the RID were about 10 fold lower than those of the FID. As with earlier studies, these analytes respond fairly weakly in FID because of high heteroatom substitution.

Table 4.9. LODs of amino acids + regression (peak area vs mass on column) data based on Figures 4.31 and 4.32. LC conditions as in Fig 4.30

Analyte	R^2	Regression equation	LOD (µg)
Flame ionization detection			
Serine	0.9997	y = 8.94x – 16.76	0.91
Valine	0.9995	y = 18.85x + 13.72	1.24
Isoleucine	0.9977	y = 20.24x + 21.52	2.64
Phenylalanine	0.9997	y = 24.46x – 14.74	0.91
RI detection			
Serine	0.9986	y = 6280.80x -670.52	0.16
Isoleucine	0.9986	y = 6335.30x – 481.72	0.16
Phenylalanine	0.9999	y = 7182.70x + 270.09	0.04

Petritis *et al.* [132] compared the LC detection limits of underivatized amino acids using different commercial detectors:

Detection limits in µg:

- Evaporative light scattering detector (0.02 – 0.2)
- Conductivity detector (0.02 – 0.5)
- Refractive index detector (1)
- Chemiluminescent detector (0.0066 – 0.014)
- Mass spectrometry (0.004 – 0.1)
- Nuclear magnetic resonance detector (2 – 10)

However, detection limits for amino acids by GC after derivatization are even lower. Silva *et al.* [133] and Nojal *et al.* [134] analyzed derivatized amino acids by GC-FID and reported detection limits of 0.001 - 0.0023 μg and 0.0029 - 0.0090 μg respectively.

4.7 Sugars

In the food industries, colour and aroma are formed by high-temperature roasting of sugar-containing food. However, during this process of roasting, potentially harmful substances, such as acrylamide, are produced [135].

However, these compounds are not volatile and do not possess a chromophore making them difficult to be detected by gas chromatography-flame ionization detection (GC-FID) or high performance liquid chromatography-UV respectively. Determinations by these techniques require derivatization [136].

Derivatization is undesirable in many aspects; it is time-consuming and samples could be lost before analysis. Therefore the analysis of sugars, without derivatization, was carried out by liquid chromatography-flame ionization detection (LC-FID) and liquid chromatography-refractive index detection (LC-RID) under the following conditions: PL HiPlex 8 μm H column; oven temperature, 50 °C and eluent (water adjusted to pH 3 with sulfuric acid) flow, 0.3 mL/min. Figure 4.33 shows the result of the separation of typical sugars. All the analytes eluted in less than 24 minutes. The peaks were not baseline resolved; mannitol and sorbitol even co-eluted. But for the purpose of validating the method for linearity, the analytes were injected individually; Figures 4.34 and 4.35 are the calibration plots for the FID and RI detectors respectively, and linear responses were obtained in each case.

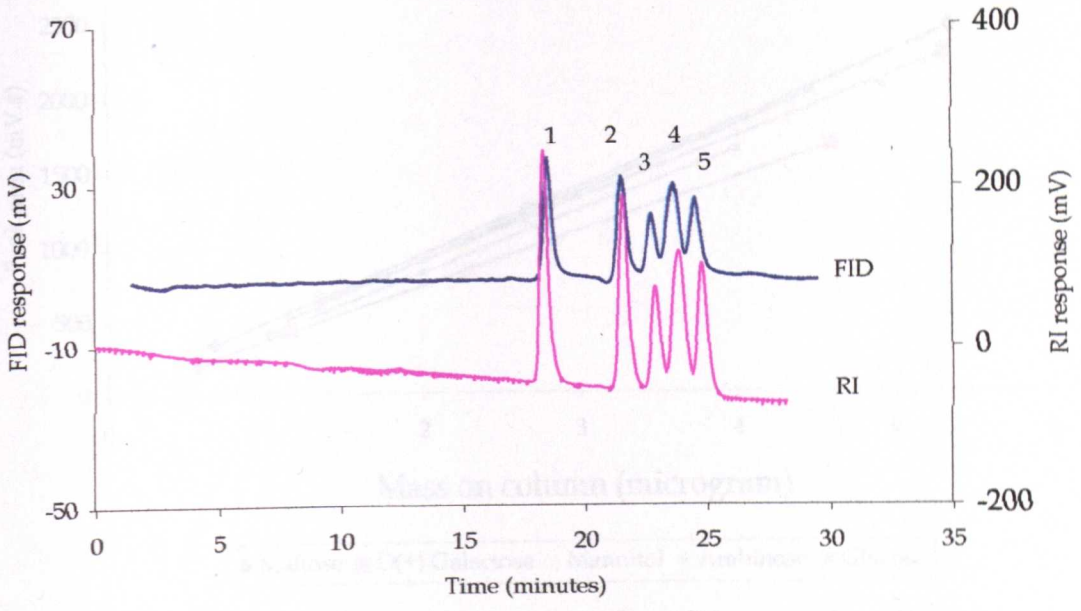

Figure 4.33. Chromatograms of sugars. PL HiPlex 8 µm H column (300 x 7.7 mm). Oven temperature, 50 °C. Eluent (0.00075 M sulfuric acid) flow, 0.3 mL/min. Detectors: FID and RID. Optimum FID conditions as in section 3.3.1 (pg 58). Peak identity: 1 = maltose; 2 = D (+)-galactose; 3 = glucose; 4 = mannitol + sorbitol and 5 = arabinose.

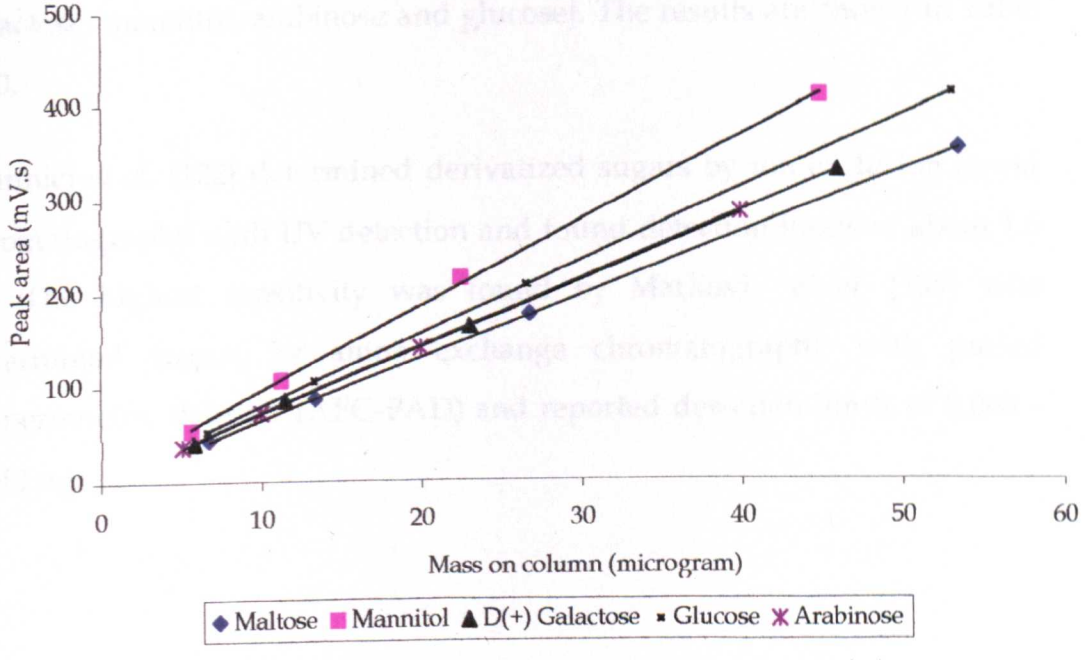

Figure 4.34. Calibration plots of sugars. LC conditions as in Fig 4.33. Optimum FID conditions as in section 3.3.1 (pg 58).

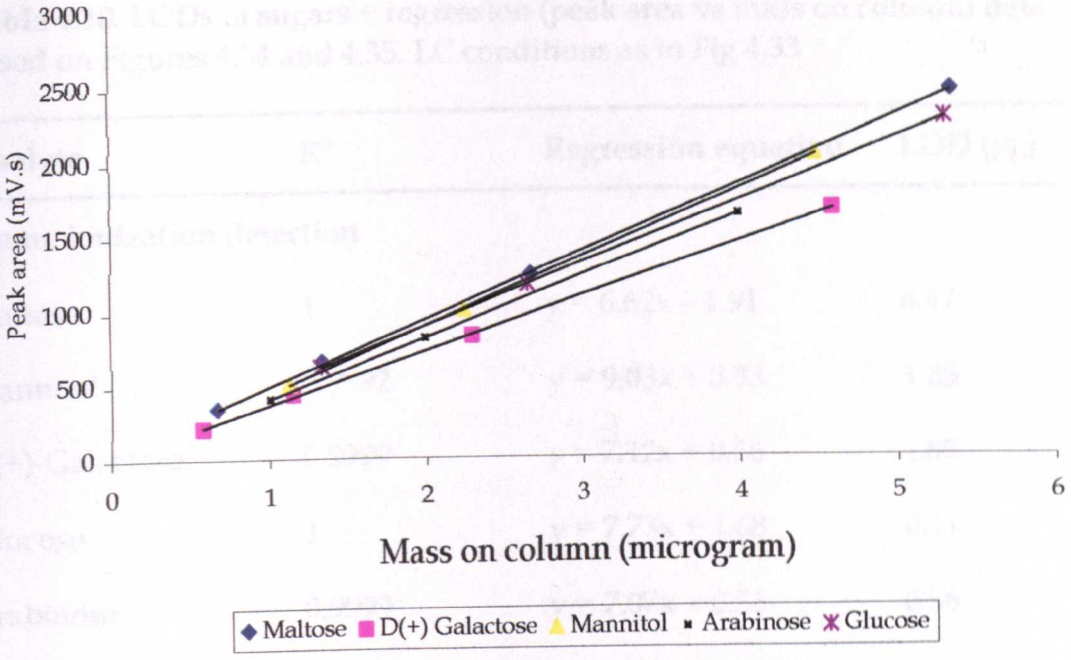

Figure 4.35. Calibration plots of sugars. RI detection. LC conditions as in Fig 4.33.

The calculated RI detection limits were lower than those of the FID; about 4 fold lower for maltose and about 10 fold lower for the other analytes [D(+)-galactose, mannitol, arabinose and glucose]. The results are shown in Table 4.10.

Chinnici *et al.* [122] determined derivatized sugars by ion exclusion liquid chromatography with UV detection and found detection limits of about 1.5 µg. The highest sensitivity was found by Markovi *et al.* [135] who determined sugars by anion exchange chromatography with pulsed amperometric detector (AEC-PAD) and reported detection limits of 0.008 – 0.044 µg.

Table 4.10. LODs of sugars + regression (peak area vs mass on column) data based on Figures 4.34 and 4.35. LC conditions as in Fig 4.33

Analyte	R^2	Regression equation	LOD (µg)
Flame ionization detection			
Maltose	1	y = 6.62x - 1.91	0.47
Mannitol	0.9992	y = 9.03x + 5.43	1.85
D(+)-Galactose	0.9999	y = 7.12x + 0.56	1.85
Glucose	1	y = 7.73x + 1.68	0.41
Arabinose	0.9999	y = 7.07x + 0.56	0.56
RI detection			
Maltose	0.9998	y = 445.55x - 53.79	0.10
Mannitol	0.9997	y = 358.15x + 16.34	0.11
D(+)-Galactose	0.9999	y = 449.28x + 4.51	0.06
Glucose	1	y = 406.85x - 7.59	0.01
Arabinose	1	y = 411.17x - 78.84	0.05

4.8 An overview

a Comparing GC-FID and LC-FID

The LC-FID peaks of the alcohols were less efficient compared to those of the GC-FID probably due to band broadening. The major contributors to band broadening include the packed column, the spray chamber and the wide aerosol path which was a Varian standard metal tube (6 cm, length; 2 mm, internal diameter). Besides, the standard jet (0.450 mm, internal diameter) for packed column in GC-FID was replaced with a ceramic jet of 2 mm internal diameter in this set up.

The carbon-count capability of the FID was seen in both modes (GC and LC); an increase in sensitivity with an increase in carbon number. For example, the sensitivity trend for the alcohols was: methanol < ethanol < propanol < butanol and that of the aldehydes was: formaldehyde < acetaldehyde < propionaldehyde (Table 4.11).

The GC-FID detection limits for the alcohols were about 10 times lower than those of the LC-FID. This can be explained in terms of the phase of the analyte in the flame and sample losses. The FID responds to analytes in the gas phase; the inlet in the GC-FID might be more efficient in transforming the analytes to the gas phase than the nebulization process in the LC-FID. Also, the nebulization exhibits inevitable sample losses as it is designed to remove coarse particles.

b *Heteroatom (oxygen)-containing compounds and sensitivity*

Normally, the sensitivity of the FID depends on the carbon-to-heteroatom (oxygen, chlorine, nitrogen etc) ratio; compounds of high ratios give high FID response and vice versa. Some examples of compounds, their carbon-heteroatom ratios and sensitivities are given in Table 4.11. Compounds of low sensitivities due to low ratios include the amino acids (serine, valine, isoleucine, phenylalanine), the sugars (maltose, mannitol, D (+)-galactose, glucose, arabinose) and the aliphatic acids (citric, malic, acetic and succinic). The reduction in sensitivity could be explained in terms of the difficulty of these compounds to undergo one or more of the stages (cracking, oxidation and finally chemi-oxidation) in the mechanism of detection [111, 137 - 140].

Table 4.11. Summary of carbon-to-heteroatom ratios in analytes and their FID sensitivities

Analyte	Sensitivity	Analyte	Sensitivity	Analyte	Sensitivity
Methanol (C:O)	42.58	*2-Phethanol (8C:O)	117.39	*Benzylamine (7C:N)	640.60
Ethanol (2C:O)	70.29	*3-Phpropanol (9c:o) (9C:O)	134.25	*Aniline (6C:N)	275.51
Propanol (3C:O)	115.11	*4-OHbenzamide (7C:2O:N)	22.71	*Pyridine (6C:N)	124.74
Butanol (4C:O)	152.16	Formaldehyde (C:O)	9.92	4-OHbenzoic acid (7C:3O)	28.27
*Benzyl alcohol (7C:O)	35.37	Acetaldehyde (2C:O)	78.60	Benzoic acid (7C:2O)	31.60
*m-Cresol (7C:O)	41.95	Propionalehyde (3C:O)	854.95	Benzaldehyde aicd (7C:O)	279.36
Cyclohexanol (6C:O)	102.44	Citric acid (6C:7O)	13.53		
2-Hexanone (4C:O)	104.39				

* Aromatic

C:O:N = Carbon:oxygen:nitroagen; OH, hydroxyl; Ph, phenyl

Table 4.11. (Continued)

Analyte	Sensitivity	Analyte	Sensitivity	Analyte	Sensitivity
*o-Methyl-acetophenone (7C:O)	86.74	Phenylalanine (9C:2O:N)	24.46	Acetic acid (C:2O)	5.46
*Propiophenone (8C:O)	61.69	Maltose (11C:11O)	6.62	Succcinic acid (4C:4O)	14.45
2-Heptanone (5C:O)	134.45	Mannitol (6C:6O)	9.03		
*Butyrophenone (9C:O)	33.12	D (+)-Galactose (6C:6O)	7.12		
Serine (3C:3O:N)	8.94	Glucose (6C:6O)	7.73		
Valine (3C:2O:N)	18.85	Arabinose (5C:5O)	7.07		
Isoleucine (4C:2O:N)	20.24	Malic acid (4C:5O)	7.52		

* Aromatic
C:O:N = Carbon:oxygen:nitroagen

c Aromatic compounds and sensitivity

Table 4.11 shows that the aromatic compounds (o-methyl-acetophenone, propiophenone, butyrophenone, 4-hydroxybenzamide, 4-hydroxybenzoic acid, benzoic acid) gave low responses compared to the aliphatic compounds. Again, this can be explained in terms of the difficulty of these compounds to undergo the stages in the mechanism of the FID [111, 137 - 140].

d Volatility and sensitivity

Another factor which may contribute to the low responses of the compounds being discussed in 'b' and 'c' is volatility. As the boiling point increases, the compound becomes increasingly difficult to evaporate, and the part reaching the detector becomes smaller, and so does the FID signal produced [137].

e Limits of detection

In this work, a linear dynamic range (LDR) of two orders of magnitude and detection limits (DL) ranging from 0.5 µg to 4 µg have been reported for the solid analytes. However, a LDR of four orders of magnitude and DLs ranging from 0.0002 µg to 0.005 µg for an eluent-jet interface had been reported previously [58]. Hooijschuur *et al.* [58] also reported that eluent-jet interface gave a LDR of one order of magnitude higher than the nebulization interface. For other aerosol-based detectors, Gamache *et al.* [15] reported DLs of 0.1 to 0.15 µg and 0.005 t0 0.02 µg respectively for ELSD and CAD.

However, Yang *et al.* [89] reported lower DLs for non-volatile analytes such as amino acids using a direct liquid introduction interface; 0.0003 to 0.003 µg. This wide difference in DLs between the aerosol-based detectors and the

direct liquid introduction interface could be explained in terms of loss of analytes during the aerosol-formation process (nebulization) in the former detectors.

f Universality

It can also be concluded that the FID is not a universal detector because compounds of different functional groups gave different responses. For example, an injection of 8 µg each of propanol, propionaldehyde and propiophenone gave approximate responses of 115 mV.s, 854 mV.s and 445 mV.s respectively.

CHAPTER FIVE

Conclusions

The development of the LC-FID method was carried out in two modes; FIA and LC modes.

The FID operating parameters were optimized in the FIA mode and the optimum conditions were: hydrogen, 157 mL/min; air, 650 mL/min and nitrogen, 230–250 mL/min. The most critical parameter was the nebulization; eluent flow rate, collector and spray chamber diameters were not so critical in the operation of the FID.

On the aspect of linearity, detector responses for volatile analytes (methanol, propanol, hexane and dichloromethane) were linear and ran through the origin whereas the responses for non-volatile analytes [ethylene glycol, poly (ethylene glycol), 4-hydroxybenzoic acid, 4-hydroxybenzamide, resorcinol, decyl alcohol and glycerol] were only linear (but with an accompanying reduction in sensitivity) when the anions in H_2SO_4, HNO_3, HCl, Na_2SO_4, $(NH_4)_2SO_4$ were added to the carrier water; the presence of protons and cations were not necessary for the linearization effect.

In the LC mode, compounds of different functional groups were separated using the optimum operating parameters of the FID. The results showed that the FID is not a universal detector; responses were markedly different for different compounds.

The LC-FID could not match the sensitivity of the GC-FID by 10 fold for volatile analytes. The GC separation also showed higher efficiency and shorter run times.

The detection limits of isolated chromophore, involatile analytes such as m-cresol, benzyl alcohol, 2-phenyl ethanol, 3-phenyl propanol, o-methylacetophenone and propiophenone, were comparable for both LC-FID and LC-UV.

Surprisingly, the LC-FID detection limits were, approximately 1 - 100 fold, poorer than those of the LC-RID.

The nebulized LC-FID method is capable of analyzing volatile, non-volatile and non UV-absorbing analytes. It has been demonstrated to give linear (R^2 about 0.999) responses for all test analytes [alcohols, carbonyl compounds (aldehydes and ketones), organic acids, amines, amino acids and sugars].

Future work

Attempts were made to analyse compounds such as cinnamic acid and cinnamaldehyde but did not give good results because they are insoluble in water. In order to enhance the solubility of these compounds in water, methanol was added to the sample and the separation was repeated. However, only a very broad methanol peak was seen; the peaks of the analytes were not observed.

Besides, the FID detection limits for analytes having low carbon-to-heteroatom ratios were unexpectedly higher than those of RID. These two shortcomings have suggested a future work of optimizing the system in order to make the LC-FID technique more versatile. One possible way of improving the sensitivity is to miniaturize the system, including the nebulizer and the spray chamber.

REFERENCES

[1] M.C. McMaster, LC/MS, John Wiley & Sons, New Jersey, 2005, pg 71.

[2] A. Montaser, Inductively coupled plasma mass spectrometry, Wiley-VCH, New York, 1998, pg 7-8.

[3] D.C. Harris, Quantitative Chemical Analysis, 6th ed., W.H. Freeman & Company, New York, 2003, pg 623.

[4] D. Parriott, A Practical Guide to HPLC Detection, Academic Press Inc, Harcourt Brace Jovanovich, San Diego, California, 1993, pg 50.

[5] V.R. Meyer, Practical High-Performance Liquid Chromatography, 4th ed., John Wiley & Sons, Chicester, 2004, pg 88, 92.

[6] T. Toyo'oka, Modern Derivatization Methods for Separation Sciences, John Wiley & Sons, Chicester, 1999, Pg 65, 103, 125.

[7] Q. Qu, X. Jang, C. Wang, G. Yang, X. Hu, X. Lu, Y. Liu, S. Li, C. Yan, Anal. Chim. Acta 572 (2006) 212.

[8] D.C. Harris, Exploring chemical analysis, 3rd edition, W.H. Freeman & Company, New York, 2005, pg 511.

[9] R.M. Smith, Gas and Liquid Phase Chromatography in Analytical Chemistry John Wiley & Sons, Chicester, 1988, pg 244.

[10] D.A. Skoog, F.J. Holler, T.A. Nieman, Principles of Instrumental Analysis, 5th ed., Harcourt Brace College Publishers, London, 1998 Pg 361.

[11] A. Hanning, J. Roeraade, Anal. Chem. 60 (1997) 8, 1496.

[12] RI detector http://www.meadowshplc.com/pdfs/2410_waters.pdf accessed 12/7/2007.

[13] C.M. Montero, M.C.R. Dodero, D.A.G. Sanchez, C.G. Barroso, Chromatographia 59 (2004) 15.

[14] E. Paredes, S.E. Maestre, S. Prats, J.L. Todoli, Anal. Chem. 78 (2006) 6774.

[15] P.H. Gamache, R.S. McCarthy, S.M. Freeto, D.J. Asa, M.J. Woodcock, K. Laws, R.O Cole, LC GC, N. Am. 16 (2005) 6, 345.

[16] S.D. Woodruff, E.S. Yeung, Anal. Chem. 54 (1982) 2124.

[17] D.J. Bornhop, N.J. Dovichi, Anal. Chem. 58 (1986) 506.

[18] ELSD http://www.cyberlipid.org/elsd/elsd0001.htm accessed 12/7/2007

[19] S. Néron, F. EI Amrani, J. Potus, J. Nicolas, J. Chromatogr. A 1047 (2004) 77.

[20] S. M. Pons, A. I. C. Bargalló, M. C. L. Sabater, J Chromatogr. A 823 (1998) 475.

[21] A. Hazotte, D. Libong, P. Chaminade, J. Chromatogr. A 1140 (2007) 131.

[22] B. Marcato, G. Cecchin, J. Chromatogr. A 730 (1996) 83.

[23] Y. Wei, M. Ding, J. Chromatogr. A 904 (2000) 113.

[24] E. Bravi, G. Perretti, L. Montanari, J. Chromatogr. A 1134 (2006) 210.

[25] C.F. Torres, L. Vázquez, F.J. Señoráns, G. Reglero, J. Chromatogr A 1078 (2005) 28.

[26] H. Bünger, L. Kaufner, U. Pison, J. Chromatogr. A 870 (2000) 363.

[27] A. Stolyhwo, H. Colin, G. Guiochon, Anal. Chem. 57 (1985) 1342.

[28] T. Kimura, K. Nakagawa, Y. Saito, K. Yamagishi, M. Suzuki, K. Yamaki, H. Shinmoto, T. Miyazawa, J. Agric. Food Chem. 52 (2004) 1415.

[29] K. Nakagawa, T. Umeda, O. Higuchi, T. Tsuzuki, T. Suzuki, T. Miyazawa, J. Agric. Chem. 54 (2006) 2479.

[30] C. Elfakir, P. Chaimbault, M. Dreux, J. Chromatogr. A 829 (1998) 193.

[31] J.A. Koropchak, C.L. Heenan, L.B. Allen, J. Chromatogr. A 736 (1996) 11.

[32] R.W. Dixon, Anal. Chem. 74 (2002) 2930.

[33] F.P. DiSanzo, S.P. Herron, B. Chawla, D. Holloway, Anal. Chem. 65 (1993) 3359.

[34] J.S. Amaral, S.C. Cunha, M.R. Alves, J.A. Pereira, R.M. Seabra, B.P. Oliveira, J. Agric. Food Chem. 52 (2004) 7969.

[35] R. Trones, T. Andersen, I. Hunnes, T. Greibrokk, J. Chromatogr. A 814 (1998) 55.

[36] S. Héron, A. Tchapla, J. Chromatogr. A 848 (1999) 95.

[37] J.M. Charlesworth, Anal. Chem. 50 (1978) 11, 1414.

[38] L.B. Allen, J.A. Koropchak, Anal. Chem. 65 (1993) 841.

[39] L.G. Angelini, E. Campeol, S. Tozzi, K.G. Gilbert, D.T. Cooke, P. John, Biotechnol. Prog. 19 (2003) 1792.

[40] D.J. Miller, S.B. Hawthorne, Anal. Chem. 69 (1997) 623.

[41] D.M. Padlo, E.L. Kugler, J. Am. Chem. Soc. 10 (1996) 5, 1031.

[42] P. van der meeren, J. Vanderleelen, L. Baert, Anal. Chem. 64 (1992) 1056.

[43] CAD http://www.md-scientific.dk/instruments/corona.html accessed 12/7/2007.

[44] R. Gallagher, 'Evaluation of charged aerosol Detection for use as relative or absolute purity indicator and its application in Protein-ligand binding Studies' poster at HPLC 2005 conference, Stockholm, Sweden. Retrieved October 11, 2006 from http://www.separationsnow.com.

[45] J.E.J. Dalley, R.S. Greenaway, Z. Ulanowski, E. Hesse, P.H. Kaye, Aero. Sci. 36 (2005) 1194.

[46] H.Z. Alisoy, G.T. Alisoy, S.E. Hamamci, M. Koseoglu, J. Phys. D: Appl. Phys. 37 (2004) 1459.

[47] B.R. Graskow, Design and development of a fast aerosol size spectrometer, PhD dissertation (2001) Department of Engineering, Trinity College, University of Cambridge, pg 40.

[48] A. Mizuno, IEEE Transaction on dielectrics and electrical insulations, 7 (2000) 5, 615 – 624.

[49] T. Go´recki, F. Lynen, R. Szucs, P. Sandra, Anal. Chem. 78 (2006) 3186.

[50] R.L. Grob, E.F. Barry, Modern Practice of Gas Chromatography, 4th ed., Wiley, John Wiley & Sons, New Jersey, 2004 pg 298 - 305.

[51] J.V. Hinshaw, LC GC N. Am. 21 (2003) 268.

[52] C. Mühlen, W. Khummueng, C.A. Zini, E.B. Caramão, P.J. Marriott, J. Sep. Sci. 29 (2006) 1909.

[53] T. Holm, J. Chromatogr. A 842 (1999) 221.

[54] T. Holm, J. Chromatogr. A 782 (1997) 81.

[55] T. Holm, J.Ø. Madsen, Anal. Chem. 68 (1996) 3607.

[56] C.A. Bruckner, S.T. Ecker, R.E. Synovec, Anal. Chem. 69 (1997) 3465.

[57] P. Marquet, G. Lachatre, J. Chromatogr. B 733 (1999) 93.

[58] E.W.J. Hooijschuur, C.E. Kientz, U.A.Th. Brinkman, J. High Resol. Chromatogr. 23 (2000) 309.

[59] Ch. E. Kientz, J Chromatogr. 550 (1991) 461.

[60] K. Aitzetmüller, J Chromatogr. Sci. 13 (1975) 454.

[61] D. Guillarme, S. Heinisch, J.L. Rocca, J. Chromatogr. A 1052 (2004) 39.

[62] K. Šlais, M. Krejčí, J. Chromatogr. 91 (1974) 181.

[63] H. Veening, P.P. Tock, J.C. Kraak & H. Poppe, J. Chromatogr. 352 (1986) 345.

[64] J.H. van Dijk, J. Chromatogr. Sci. 10 (1972) 31.

[65] J.B. Dixon, Chimia 38 (1984) 82

[66] C.D. Pearson, S.G Gharfeh, J. Chromatogr. 329 (1985) 142.

[67] C.D. Pearson, S.G Gharfeh, Anal. Chem. 58 (1986) 307.

[68] D.J. Malcolme-Lawes, P. Moss, J. Chromatogr. 482 (1989) 53.

[69] D. Guillarme, S. Heinisch, J.Y. Gauvrit, P. Lanteri, J.L. Rocca, J. Chromatogr. A 1078 (2005) 22.

[70] T.M. Brewer, J. Castro, R.K. Marcus, Spectrochimica Acta Part B 61 (2006) 134.

[71] M.T. Combs, M. Ashraf-Khorassani, L.T. Taylor, J. Chromatogr. A 785 (1997) 85.

[72] T. Yarita, R. Nakajima, K. Shimada, S. Kinugasa, M. Shibukawa, Anal. Chem. 21 (2005) 1001.

[73] T.S. Kephart, P.K. Dasgupta, Talanta 56 (2002) 977.

[74] I.D. Wilson, J. Chromatographia 52 (2000) S28.

[75] R.M. Smith, O. Chienthavorn, I.P. Wilson, B. Wright, Anal. Commun. 35 (1998) 1213.

[76] G.V.P. San, J. Sep. Sci. 29 (2006) 1822.

[77] D.J. Miller, S.B. Hawthorne, Anal. Chem. 69 (1997) 623.

[78] R.M. Smith, R.J. Burgess, J. Chromatogr. A 785 (1997) 49.

[79] T. Greibrokk, T. Anderson, J. Sep. Sci. 24 (2001) 899.

[80] A.M. Edge, S. Shillingford, C. Smith, R. Payne, I.D. Wilson, J. Chromatogr. A 1132 (2006) 206.

[81] R.M. Smith, Anal. Bioanal. Chem. 385 (2006) 419.

[82] J. Tiihonen, E.-L. Peuha, M. Latva-Kokko, S. Silander, E. Paatero, Sep. & Purif. Tech. 44 (2005) 166.

[83] D. Guillarme, S. Heinisch, J.L. Rocca, J. Chromatogr. A 1052 (2004) 39.

[84] W.W.W. Quigley, S.T. Ecker, P.G. Vahey, R.E. Synovec, Talanta 50 (1999) 569.

[85] C.E. Kientz, A.G. Hulst, Ad L. De Jong, E.R.J. Wils, Anal. Chem. 68 (1996) 675.

[86] J. Finell, J. Tanner, H. Vettenranta, K. Hartonen, M.L. Riekkola, 11th International Symposium on Supercritical Fluid Chromatography, Extraction and Processing, Pittsburgh, August 2004, poster B-09.

[87] N. Wu, Q. Tang, J.A. Lippert, M.L. Lee, J. Microcol. Sep. 13 (2001) 41.

[88] A. Ingelse, H. Janssen, C.A. Cramers, J. High Res. Chromatogr. 21 (1998) 613.

[89] Y. Yang, T. Kondo, T.J. Kennedy, J. Chromatogr. Sci. 43 (2005) 518.

[90] E.D. Conte, E.F. Barry, J. Microchem. 48 (1993) 365.

[91] T. Yarita, R. Nakajima, S. Otsuka, T. Ihara, A. Takatsu, M. Shibukawa, J. Chromatogr. A 976 (2002) 387.

[92] Y. Yang, A.D. Jones, J.A. Mathis, M.A. Francis, J. Chromatogr. A 942 (2002) 231.

[93] J.-L. Todoli, V. Harnandis, A. Canals, J.-M. Mermet, JAAS 14 (1999) 1289.

[94] B. Almagro, A.M. Gañá-Calvo, M. Hidalgo, A. Canals, JAAS 21 (2006) 770.

[95] S.E. Maestre, J.L. Todoli, J.M. Mermet, Anal. Bioanal. Chem. 379 (2004) 888.

[96] M. Grotti, C. Lagomarsino, R. Frache, Spectrochim. Acta Part B 59 (2004) 1001.

[97] Zs. Stefánka, G. Koellensperger, G. Stingeder, S. Hann, JAAS 21 (2006) 86.

[98] R.T. Gettar, P. Smichowski, R.N. Garavaglia, S. Farías, D.A. Batistoni, Spectrochim. Acta Part B 60 (2005) 567.

[99] S.C. Westphal, A. Montaser, Spectrochim. Acta Part B 61 (2006) 705.

[100] B. Almagro, A.M. Gañá-Calvo, M. Hidalgo, A. Canals, JAAS 21 (2006) 770.

[101] J.L. Todolí, J.M. Mermet, TrAC 24 (2005) 107.

[102] B. Michalke, Electrophoresis 26 (2005) 1584.

[103] H. Matusiewicz, M. Śtachciński, M. Hidalgo, A. Canals, JAAS 22 (2007) 1174.

[104] J.W. Olesik, J.A. Kinzer, S.V. Olesik, Anal. Chem. 67 (1995) 1.

[105] K.A. Taylor, B.L. Sharp, D.J. Lewis, H.M. Crews, JAAS 13 (1998) 1095.

[106] J.R. Bone, R.M. Smith, PhD Thesis (2002) Chemistry Department, Loughborough University.

[107] Rapid Applications Bulletin Publication No. 210MCN029E CETAC Technologies Inc.

[108] A. Woller, H. Garraud, J. Boisson, A.M. Dorthe, P. Fodor, O.F.X. Donard, JAAS 13 (1998) 141.

[109] J.V. Hinshaw, LC GC N. Am. 21 (3003) 3, 268.

[110] M.O. Fogwill, K.B. Thurbide, J. Chromatogr. A 1139 (2007) 199.

[111] M. Kállai, J. Balla, Chromatographia, 56 (2002) 357.

[112] J.D. Lee, 5th ed., Concise Inorganic Chemistry, London, Chapman & Hall, 1964, 237.

[113] Y. Liu, N. Grinberg, K.C. Thompson, R.M. Wenslow, U.D. Neue, D. Morrison, T.H. Walter, J.E. O'Gara, K.D. Wyndham, Anal. Chim. Acta 554 (2005) 144.

[114] T.H. Walter, P. Iraneta, M. Capparella, J. Chromatogr. A 1075 (2005) 1-2, 177.

[115] M.E. Montgomery, J.M.A. Green, M.J. Wirth, Anal. Chem. 64 (1992) 1170.

[116] Z. Li, S.C. Rutan, S. Dong, Anal. Chem. 68 (1996) 124.

[117] N. Nagae, T. Enami, S. Doshi, LC-GC N. Am. 20 (2002) 964.

[118] A. Stafiej, K. Pyrzynska, A. Ranz, E. Lankmayr, J. Biochem. Biophys. Methods 69 (2006) 15.

[119] M.B. Colket, D.W. Naegeli, F.L. Dryer, I. Glassman, Env. Sci. & Tech. 8 (1974) 1, 43.

[120] I. Mato, S. Suarez-Luque, J.F. Huidobro, Food Res. Internat. 18 (2005) 1175.

[121] M. Wei, C. Chang, J. Jen, Chromatographia 54 (2001) 601.

[122] F. Chinnici, U. Spinabelli, C. Riponi, A. Amati, J. Food Comp. & Anal. 18 (2005) 121.

[123] N.H. Davies, M.R. Euerby, D.V. McCalley, J. Chromatogr. A 1138 (2007) 65.

[124] E. Formal, P. Borman, C. Luscombe, Anal. Chim. Acta 570 (2006) 267.

[125] F. Gritti, G. Guiochon, Anal. Chem. 77 (2005) 1020.

[126] F. Gritti, G. Guiochon, J. Chromatogr. A 1095 (2005) 27.

[127] D.V. McCalley, J. Chromatogr. A 987 (2003) 17.

[128] D.V. McCalley, Anal. Chem. 75 (2003) 3404.

[129] D.V. McCalley, Anal. Chem. 78 (2006) 2532.

[130] S.M.C. Buckenmaier, D.V. McCalley, M.R. Euerby, Anal. Chem. 74 (2002) 4672.

[131] T. Soga, D.N. Heiger, Anal. Chem. 72 (2000) 1236.

[132] K. Petritis, C. Elfakir, M. Dreux, J. Chromatogr. A 961 (2002) 9.

[133] B.M. Silva, S. Casal, P.B. Andrade, R.M. Scabra, M.B. Oliveira, M.A. Ferreira, Anal. Sci. 19 (2003) 1285.

[134] M.J. Nojal, J.L. Bernal, M.L. Toribio, J.C. Diego, A. Ruiz, J. Chromatogr. A 1047 (2004) 1, 137.

[135] M. Murkovi, K. Derler, J. Biochem. Biophys. Methods 69 (2006) 25.

[136] C. Guignard, L. Jouve, M. B. Bogeat-Triboulot, E. Dreyer, J. Chromatogr. A 1085 (2005) 137.

[137] M. Kállai, Z. Veres, J. Balla, Chromatographia, 54 (2001) 511.

[138] W.A Dientz, J Gas Chromatogr. 5 (1967) 68.

[139] Andrew D. Jorgensen, Anal. Chem. 62 (1990) 683.

[140] H.Y. Tong, F.W. Karasek, Anal. Chem. 56 (1984) 2124.

APPENDICES

Appendix A: Calibration data for chapter three

Mass denotes mass injected in µg and area denotes peak area in mV.s

a. Volatile analytes

Methanol		Propanol		Hexane		Dichloromethane	
Mass	Area	Mass	Area	Mass	Area	Mass	Area
18.50	68.77	21.40	177.15	80.00	435.19	46.80	767.28
9.25	34.89	10.70	85.41	40.00	217.59	23.40	383.64
4.63	17.33	5.35	43.11	20.00	116.72	11.70	181.88
2.31	10.82	2.68	22.84	10.00	58.89	5.85	90.37
1.16	7.08	1.34	13.00	5.00	29.44	2.93	45.19
0.58	5.30	0.67	8.15				
0.29	3.90	0.33	5.00				
0.14	3.74	0.17	4.26				
0.07	3.42	0.08	3.62				

b. Non-volatile analytes

Ethylene glycol		Poly (ethylene glycol)		Resorcinol	
Mass	Area	Mass	Area	Mass	Area
22.20	39.54	16.30	40.74	18.00	50.69
11.10	23.65	8.15	27.87	9.00	30.11
5.55	11.22	4.08	18.34	4.50	17.25
2.78	5.16	2.04	10.69	2.25	9.56

4-ydroxybenzoic acid		4-hydroxybenzamide	
Mass	Area	Mass	Area
13.20	57.56	13.00	49.65
6.60	39.48	6.50	35.18
3.30	24.63	3.25	24.58
1.65	15.26	1.63	16.04

Mass	Area	
	Maltose	**Valine**
160.00	160.00	518.52
80.00	80.00	269.26
40.00	40.00	129.63
20.00	20.00	64.81
10.00	10.00	42.41
5.00	5.00	31.20
2.50	2.50	21.10
1.25	1.25	15.05

Decyl alcohol			
Mass	**Area**		
	Water	**Sample in acid**	**Eluent + acid**
36.00	110.48	85.44	97.88
18.00	68.97	42.72	45.97
9.00	34.49	19.36	22.99
4.50	17.02	8.68	11.49
2.25	7.47	4.34	5.75
Glycerol			
0.91	62.24	294.06	7.75
1.81	90.89	428.15	15.50
3.63	168.26	672.82	31.00
7.25	263.55	1163.56	62.00
14.50	379.58		
29.00	594.85		
58.00	883.53		

Appendix B: Calibration data for chapter four

a. GC-FID of alcohols

Methanol		Ethanol		Propanol		Butanol	
Mass	Area	Mass	Area	Mass	Area	Mass	Area
1.47	30.99	1.65	42.01	1.48	43.00	1.72	57.60
0.73	15.65	0.83	21.01	0.74	21.95	0.86	28.87
0.37	7.76	0.41	10.60	0.37	11.34	0.43	14.72
0.18	3.55	0.21	4.86	0.18	5.15	0.22	6.47
0.09	1.64	0.10	2.24	0.09	2.42	0.11	3.17

Cyclohexanol		Benzyl alcohol		m-Cresol	
Mass	Area	Mass	Area	Mass	Area
1.00	42.35	1.91	88.54	1.60	75.00
0.50	21.21	0.96	44.34	0.80	37.09
0.25	10.86	0.48	20.92	0.40	18.46
0.13	5.17	0.24	8.76	0.20	8.25
0.06	2.39	0.12	3.61	0.10	3.55

b. LC-FID of alcohols

Methanol		Ethanol		Propanol		Butanol	
Mass	Area	Mass	Area	Mass	Area	Mass	Area
26.60	1136.52	15.00	1057.85	14.00	1620.78	14.00	2137.41
13.30	542.35	7.50	611.63	7.00	844.19	7.00	1107.72
6.65	280.63	3.75	296.18	3.50	423.82	3.50	556.29
3.33	141.48	1.88	153.51	1.75	211.70	1.75	276.91
1.66	67.67	0.94	59.62	0.88	120.36	0.88	154.34
0.83	34.06	0.47	39.85	0.44	63.51	0.44	74.89

Cyclohexanol		Benzyl alcohol		m-Cresol	
31.60	3275.54	85.60	3031.05	29.40	1236.33
15.80	1759.11	42.80	1576.41	14.70	655.73
7.90	903.32	21.40	776.05	7.35	342.72
3.95	504.01	10.70	390.06	3.68	161.78
1.98	241.33	5.35	191.33	1.84	77.70
0.99	127.55	2.68	124.50	0.92	40.47

c. LC-UV of alcohols

Benzyl alcohol		m-Cresol	
Mass	Area	Mass	Area
85.60	2045.45	29.40	6003.33
42.80	1331.54	14.70	3264.52
21.40	805.30	7.35	1627.27
10.70	468.27	3.68	789.92
5.35	251.64	1.84	377.98
2.68	132.08	0.92	186.33

d. LC-FID data of benzyl alcohol and substituted aryl alcohol

Benzyl alcohol		2-Phenyl ethanol		3-Phenyl propanol	
Mass	Area	Mass	Area	Mass	Area
1.34	116.72	3.69	169.73	1.66	120.62
2.68	267.35	7.38	329.89	3.32	310.67
5.35	484.47	14.76	685.68	6.63	630.18
10.70	977.71			13.26	1287.24

e. LC-UV data benzyl alcohol and substituted aryl alcohol

Benzyl alcohol		2-Phenyl ethanol		3-Phenyl propanol	
Mass	Area	Mass	Area	Mass	Area
1.34	122.96	1.85	169.90	1.66	181.83
2.68	281.98	3.69	373.97	3.32	414.33
5.35	614.02	7.38	786.92	6.63	880.84
10.70	1307.61	14.76	1682.75	13.26	1741.71

f. LC-FID of aldehydes

Formaldehyde		Acetaldehyde		Propionaldehyde	
Mass	Area	Mass	Area	Mass	Area
42.60	416.93	21.40	1570.66	8.56	6747.75
21.30	204.91	10.70	753.89	4.28	2959.80
10.65	100.55	5.35	291.92	2.14	1149.38
5.33	46.69	2.68	112.02	1.07	402.19

g. LC-FID of ketones

2-Hexanone		o-Methyl-acetophenone		Propiophenone	
Mass	Area	Mass	Area	Mass	Area
8.54	785.89	10.54	837.04	10.74	609.44
4.27	330.75	5.27	390.27	5.37	296.88
2.14	119.61	2.64	148.76	2.69	107.83

2-Heptanone		Butyrophenone	
8.44	989.43	83.20	2598.03
4.22	451.73	41.60	1170.94
2.11	130.93	20.80	543.62

h. LC-UVof ketones

o-Methy-acetophenone		Propiophenone		Butyrophenone	
Mass	Area	Mass	Area	Mass	Area
10.54	5104.78	10.74	5863.91	83.20	14710.60
5.27	2307.97	5.37	2675.19	41.60	6465.27
2.64	966.27	2.69	1130.47	20.80	2625.06

i. LC-FID data

4-OHBenzamide		4-OHBenzoic acid		Benzoic acid		Benzaldehyde	
Mass	Area	Mass	Area	Mass	Area	Mass	Area
40.00	917.93	40.00	1087.68	40.00	1209.29	14.40	3989.10
20.00	443.89	20.00	618.68	20.00	492.63	7.20	2104.93
10.00	215.73	10.00	234.27	10.00	183.55	3.60	966.14
5.00	120.11	5.00	121.10	5.00	88.86	1.80	544.27
2.50	70.77	2.50	44.42	2.50	39.52	0.90	203.52

j. LC-FID of aliphatic organic acids

Citric acid		Malic acid		Acetic acid		Succinic acid	
Mass	Area	Mass	Area	Mass	Area	Mass	Area
82.80	1158.24	101.60	735.99	196.60	1049.34	159.60	2317.86
41.40	615.46	50.80	342.43	98.30	517.41	79.80	1152.29
20.70	313.40	25.40	165.58	49.15	242.39	39.90	590.92

k. LC-RID of aliphatic organic acids

Citric acid		Malic acid		Acetic acid		Succinic acid	
Mass	Area	Mass	Area	Mass	Area	Mass	Area
0.98	47407.41	0.51	22212.53	0.80	17353.73	0.41	19967.83
0.49	23703.71	0.25	11342.77	0.40	8701.64	0.21	9952.40
0.25	10973.30	0.13	5534.41	0.20	4325.17	0.10	4400.11
0.12	4510.11	0.06	2070.29	0.10	1672.22	0.05	1768.58

l. LC-FID data

Pyridine		Aniline		Benzylamine	
Mass	Area	Mass	Area	Mass	Area
7.40	1913.29	28.00	2996.49	14.00	8557.84
3.70	873.61	14.00	1400.76	7.00	4187.86
1.85	356.94	7.00	489.98	3.50	1737.04
0.93	144.87	3.50	339.28	1.75	781.08

m. LC-UV of amines

Benzylamine		Phenylethylamine	
Mass	Area	Mass	Area
60.00	2024.68	83.40	4450.67
30.00	857.99	41.70	2020.83
15.00	292.53	20.85	656.12

n. LC-FID of amino acids

Serine		Valine		Isoleucine		Phenylalanine	
Mass	Area	Mass	Area	Mass	Area	Mass	Area
40.00	342.21	44.00	840.34	42.00	860.82	40.00	960.01
20.00	158.59	22.00	430.86	21.00	463.67	20.00	480.82
10.00	74.85	11.00	231.81	10.50	250.50	10.00	235.28
5.00	28.13	5.50	111.56	5.25	118.25	5.00	98.55
2.50	7.86	2.75	61.17	2.63	61.20	2.50	47.00

o. LC-RID of amino acids

Serine		Isoleucine		Phenylalanine	
Mass	Area	Mass	Area	Mass	Area
3.00	18326.43	3.00	18681.75	3.00	21849.40
1.50	8337.97	1.50	8690.40	1.50	10933.47
0.75	4195.59	0.75	4158.52	0.75	5769.85
0.38	1787.26	0.38	2178.35	0.38	2930.15

p. LC-FID of sugars

Maltose		Mannitol		D (+) galactose	
Mass	Area	Mass	Area	Mass	Area
53.60	353.08	45.00	409.02	46.00	328.55
26.80	176.03	22.50	215.28	23.00	163.12
13.40	85.65	11.25	105.96	11.50	84.49
6.70	43.23	5.63	53.30	5.75	40.55

Glucose		Arabinose	
53.20	412.39	40.00	283.95
26.60	208.05	20.00	140.33
13.30	105.12	10.00	71.50
6.65	52.06	5.00	36.60

q. LC-RID of sugars

Maltose		Mannitol		D (+) galactose	
Mass	Area	Mass	Area	Mass	Area
5.36	2445.91	4.50	2028.77	4.60	1666.26
2.68	1234.00	2.25	1007.91	2.30	829.49
1.34	664.66	1.13	514.94	1.15	442.77
0.67	348.384			0.575	215.832

Glucose		Arabinose	
5.32	2268.20	4.00	1635.21
2.66	1166.64	2.00	820.68
1.33	629.61	1.00	414.86

Appendix C: First year report

Analysis of Bioactive Compounds in *Fallopia japonica*

CHAPTER ONE

Introduction

Biologically-active constituents of plants have served as sources of inspiration for generations of medicinal and organic chemists. In addition to the biologically active plant-derived secondary metabolites which have found direct medicinal application as drug entities, many other bioactive plant compounds have been proven useful as 'leads' or model compounds (templates) for drug synthesis or semisyntheses. This research work (Analysis of Bioactive Compounds in *Fallopia japonica*) got its direct inspiration from the preceding facts [1].

1.1 Background to the Study

1.1.1 Negative Attributes of the Plant

Fallopia japonica is the most invasive plant in Britain. For this reason the Wildlife Act 1990 makes it an offence to plant *Fallopia japonica* "or otherwise cause it to grow in the wild". It is now being listed as an injurious weed under the Weeds Act 1957 [3-5].

Specific problems caused by *Fallopia japonica* are [2 – 6]:

- Damage to paving and tarmac areas,
- Damage to flood defence structures,
- Damage to archaeological sites,
- Reduction of biodiversity through out-shading native vegetation,
- Restriction of access to riverbanks for anglers, bank inspection and amenity use,
- Reduction in land values,

- Increased risk of flooding through dead stems washed into river and stream channels,
- Increased risk of soil erosion and bank instability following removal of established stands in riparian areas,
- Accumulation of litter in well established stands, and
- Aesthetically displeasing.

1.1.2 Cost of Control

The recent British Government Review of Non-native Species Policy gives an estimate of the costs to control *Fallopia japonica* countrywide of £1.56 billion which, although unfeasible, gives an indication of the extent of the problem and the high costs associated with control were it is to be attempted. Swansea is one of the worst affected areas [4] with the following consequencies:

- £140,000 for planning and treatment of established populations over the last 6 years
- Using quoted figures of £1 per square meter for spraying and £8 for landscaping estimates for completely treating the current infestation in Swansea cost around £9.5 million
- At the current rate of treatment (2 ha/yr), the current infestation will take 50 years to treat without accounting for its rapid spread (more than 2 ha/yr)
- The cost of removal from development sites is very large – one 30m x 30m site cost developers an extra £52, 785 to deal with the *Fallopia japonica* on the site [4].

1.1.3 Medical Attributes of *Fallopia japonica*

A variety of constituents have been isolated from *Fallopia japonica.* The chemical components are classed as anthraquinones, dianthrones, stilbenes, anthocynins, flavonoids, anthraglycosides, polyphenols, essential oil,

organic acids, chromene, chromone glycosides and vitamins [8] in which anthraquinone derivatives including emodin, aloe-emodin, rhein, physcion, chrysophanol and their glycosides are the accepted important active components. The matrix chemical structure of these hydroxyanthraquinones are similar (Fig. 1.4) and substituents R1 and R2 are shown in Table 1.1.

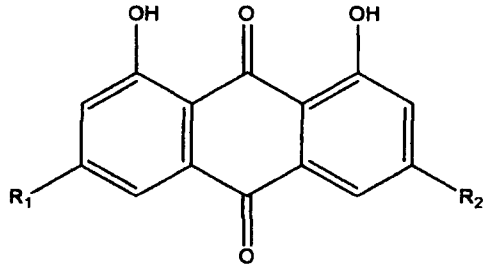

Fig. 1.4: Matrix chemical structure of hydroxyanthraquinones

Table 1.1: Substituents

Compound	*R1*	**R2**
Aloe-emodin	H	CH_2OH
Rhein	H	COOH
Emodin	OH	CH_3
Chrysophanol	H	CH_3
Physcion	OCH_3	CH_3

Fallopia japonica contain compounds called stilbenes and anthraquinones. Stilbenes are aromatic hydrocarbons having the general formula $C_{14}H_{12}$. They include resveratrol, piceid and polydatin [8]. Antioxidants are used to preserve foods by retarding discoloration, rancidity, or deterioration due to

auto-oxidation. However, synthetic antioxidants have been reported to be carcinogenic [9], hence several attempts to replace synthetic antioxidants with natural antioxidants have been developed. The antioxidant properties (Table 1.2) of anthraquinones were studied by Yen *et al.* [10].

Table 1.2: Properties of anthraquinones

Anthraquinone	*Reducing power*	*Chelating ability on iron(II)*	*Scavenging effect on OH radicals*
Anthrone	Yes	No	Yes
Alizarine	Yes	No	No
Aloe-emodin	No	No	Yes
Rhein	No	No	No
Emodin	No	No	Yes
Chrysophanol	No	No	No

These results suggest that the antioxidant mechanism for both emodin and aloe-emodin, possibly depends on scavenging hydroxyl radicals. The strong activity shown by anthrone could be due to its reducing power and the scavenging effects on hydroxyl radicals. The pro-oxidant activity exhibited by chrysophanol might be due to the enhanced production of free radicals [10, 11].

Physiological and biochemical processes in the human body may produce oxygen-centered free radicals and other reactive oxygen species (e.g., superoxide radicals, hydroxyl radicals, and hydrogen peroxide) as by-products. Over-production of such free radicals can cause oxidative damage to biomolecules (e.g. lipids, proteins, DNA), eventually leading to many chronic diseases, such as atherosclerosis, cancer, diabetes, aging, and other degenerative diseases in human [12-13].

Plants (fruits, vegetables, medicinal herbs, etc) may contain a wide variety of free radical scavenging molecules, such as phenolic compounds (e.g. phenolic acids, flavonoids, quinones, coumarines, lignans, stilbenes, tannins), nitrogen compounds (alkanoids, amines, betalains) vitamins, terpenoids (including carotenoids), and some other endogenous metabolites, which are rich in antioxidant activity [14 -16]. Epidemiological studies have shown that many of these antioxidant compounds possess anti-inflammatory, antiatherosclerotic, antitumor, antimutagenic, anticarcinogenic, antibacterial, or antiviral activies to a greater or lesser extent [8, 17]. The chemi-preventive properties of the anthraquinones are summarized in Table 1.3.

Natural antioxidants have been identified with reduced risks of cancer, cardiovascular disease, diabetes, and other diseases associated with ageing [18-20]. The search for potent natural antioxidants, especially from plant sources, as nutritional supplements, health food, and/or phytomedicine has become an important research issue at a world-wide level.

Table 1.3: Chemopreventive properties of anthraquinones

Source	*Activity*	**References**
Resveratrol	• Inhibits the growth of several bacteria and fungi	[21]
	• Exhibits cancer chemopreventive activity by acting as an antioxidant, antimutagen and anti-inflammatory agent	[22] [23]
	• Inhibits protein-tyrosine kinase, which catalyses the phosphorylation of tyrosine	
	• Inhibits lipoxygenate products which are enzymes found in leukocytes in the heart, brain, lung and spleen	[24-25]
Piceid	• Inhibits the deposition of triglycerides and cholesterol in the liver of mice	[26]
Resveratrol and piceid	• Reduce the elevation of aspartate transaminase and alanine transaminase by inhibiting lipid peroxidation in the livers of rats	[27]
Polydatin	• Inhibits platelet aggregation after treatment with clonidine, an antihypertensive drug	[28-29]
Emodin	• Inhibits the motor activity of a parasitic Schistosoma species. It has antineoplastic and antimutagenic activities	[30]
P.cuspidatum	• Promotes healing of burns by enhancing immune system and cardiac functions	[31]

Table 1.3: (Continued)

Source	*Activity*	*References*
Naphthoquinones and anthraquinones	• Inhibited mutagenicity induced by 2-amino-3-methylimidazo[4,5-f]quinoline in Salmonella typhimurium	[32]
Polygonum hypoleucum Ohwi	• Inhibits tumor cell proliferation	[33]
Emodin	• It showed antiprotozoal activity against both Trypanasoma species and P. falciparum	[34]
Anthraquinones	• Showed in vitro antiplasmodial activity	[35]
Emodin and water extracts of Polygonum cuspidatum	• Markedly decreased the mutagenicity of 1-nitropyrene (1-NP)	[36]
Emodin and the crude extracts of Rheum palmatum, Polygonum cuspidatum	• Decreased the mutagenicity of benzo[a] pyrene(B[a]P), 2-amino-3-methyl imidazo[4,5-f]quinoline and 3-amino-1-methyl-5H-pyrido[4,3-b]indole	[37]
Anthraquinones and flavonoids	• Exhibited antioxidant properties against 1,1-diphenyl-2-picrylhydrazyl (DPPH) and superoxide radical	[38]

1.2 Aims and Objectives

The project was set out to provide answers to the following research questions:

- Does distribution affect the chemical constituents of *Fallopia japonica*?
- Are there differences in the chemical constituents among different species (such as *F. japonica var. japonica, F. japonica var. compacta, F. sacchalinensis and F. bohemica)*?

A β-cyclodextrin modified capillary electrophoresis method will be used for the analysis in order to achieve the aims and objectives of this work as represented by the research questions. Prior to analysis by this technique, extraction will be carried out with a solvent combination of H_2SO_4, CH_2Cl_2 and CH_3OH using reflux.

CHAPTER TWO

Literature Review

2.1 Analysis Procedures for Anthraquinones

Because of the medical attributes of the anthraquinones, different methods have been developed for their determination. Table 2.1 is a summary of few of such methods.

Table 2.1. Methods for the analysis of anthraquinones

Technique/method	Reference (s)
CD-MEKC. Phosphate buffer (pH, 10.4), 20 mM sodium dodecyl sulphate, 20 mM sodium cholate and 10 mM beta-cyclodextrin. Voltage, 20 kV.	[39, 40]
MEKC. 15 mM sodium tetraborate/15mM sodium dihydrogenphosphate buffer (pH, 8.6), 30 mM sodium deoxycholate, 17 vol. % acetonitrile. Voltage, 28 kV.	[41, 42]
CE: 30mM sodium borate (pH =10.56) and acetonitrile (9:1). Voltage, 20 kV. HPLC: gradient elution with 20 mM KH_2PO_4:0.05% orthoorthoorthophosphoric acid (pH=2.91) methanol	[43]
CD-CZE. 0.03 M borate sulphate (Ph, 10.5), 0.005 M alpha cyclodextrin, 10% acetonitrile. Voltage, 20 kV	[44]
CD-CZE. 0.1 M borate buffer (pH, 9), 0.05 M hydroxypropyl-gamma-cyclodextrin, 10% acetonitrile. Voltage, 20 kV.	[45]
MEEKC	[46]
CEC	[47]
HPLC	[48, 49]

CHAPTER THREE

Experimental

3.1 Chemicals and Reagents

Rhein, emodin and heptakis, (2,6-di-o-methyl)-beta-cyclodextrin were bought from Sigma, UK. Chrysophanic acid was supplied by Aldrich, UK. Fisher Scientific Company, UK supplied HPLC grade methanol and dichloromethane. Fisons Scientific Equipment (UK) supplied Potassium dihydrogen orthophosphate and di-sodium tetraborate. Fused silica capillary (75 µm id, 375 µm o.d) was bought from Composite Metal Services LTD) (UK).

3.2 Equipment

Capillary electrophoresis separations were carried out with a P/ACE 2050 System (BECKMAN) equipped with UV detector (photodiode). Capillary tubing of the following dimension was used: 75 µm with an effective length of 50 cm and a total length of 57 cm. Operations and data collections were enabled with an IBM 433/DX microcomputer with Beckman System Gold personal chromatograph software.

3.3 Sample Preparation

The method employed was developed by Li *et al.* [50]. 1g of powdered *Fallopia japonica* rhizome was hydrolysed with 1M tetraoxosulphate (VI) acid in 20 mL dichloromethane for 35 minutes. Reflux was stopped, extraction solution neutralised and 60 mL of methanol added. Reflux was resumed and continued for 2 hours. The extract was evaporated to dryness with a rotary evaporator. Residue was dissolved in 70% methanol to make the final extract. Portions for injections were made by diluting the final crude extract in 70% methanol (1:4).

3.4 Methodology

New capillary was treated using a rinse-cycle of 1 M sodium hydroxide for 30 minutes, 70% methanol for 30 minutes and water for 10 minutes. Prior to an injection, the capillary was always flushed with the buffer for at least 30 minutes.

The crude methanolic extract was divided into four aliquots. One aliquot was injected directly. The other three aliquots were spiked respectively with the reference compounds; 150 µg/mL of emodin, chrysophanol and rhein. All the four separations were carried out under the same optimized conditions: 20 mM potassium dihydrogen orthophosphate, 20 mM tetraborate (pH = 10.4), 3 mM (2,6-di-o-methyl)-beta-cyclodextrin and an applied voltage of 15 kV. Detection was made at a wavelength of 254 nm.

CHAPTER 4

Results and Discussion

4.1 Identification of Peaks

The methanolic extract of the *Fallopia japonica* was divided into four aliquots. The four aliquots of the extract were analyzed; the control portion (without spiking) and the other three aliquots which were spiked respectively with emodin, chrysophanol and rhein. The resulting electropherograms are shown in Figures 4.1 - 4.4; 4.1 for the control, 4.2, 4.3 and 4.4 for the aliquots spiked respectively with emodin, chrysophano and rhein respectively. A comparison of the Figure 4.1 with Figures 4.2, 4.3 and 4.4 showed that only emodin was present in the extract; its peak increased without shouldering (Figure 4.2)

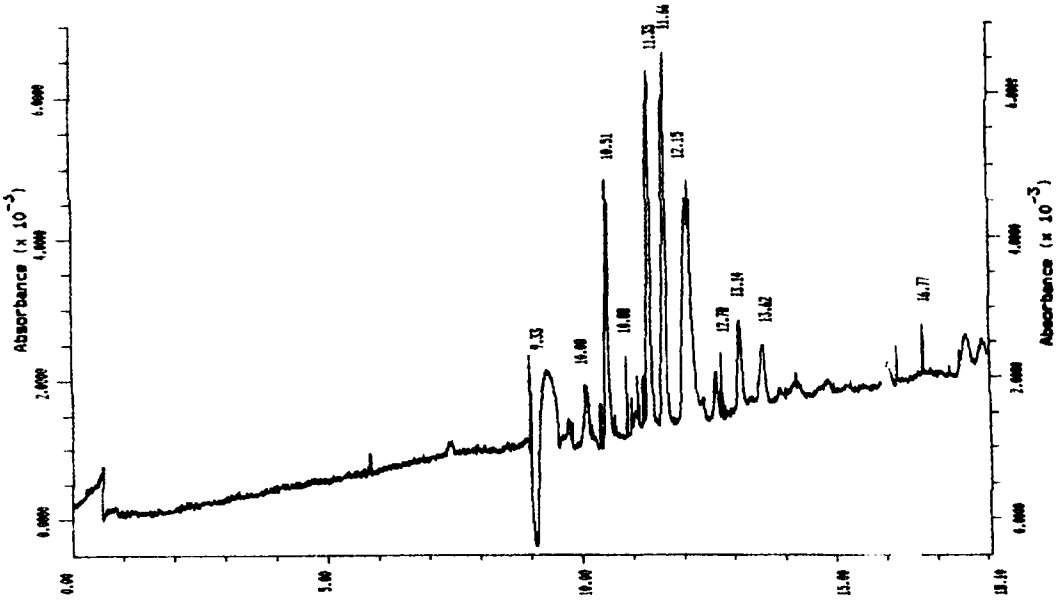

Fig. 4.1: Crude extract. Optimized conditions: 20 mM potassium dihydrogen orthophosphate 20mM tetraborate, 3 mM (2,6-di-O-methyl)-beta-cyclodextrin, pH=10.4, capillary length 57 cm (50 cm to detector) x 75 micrometer id. Applied voltage, 15kV, wavelength, 254 nm.

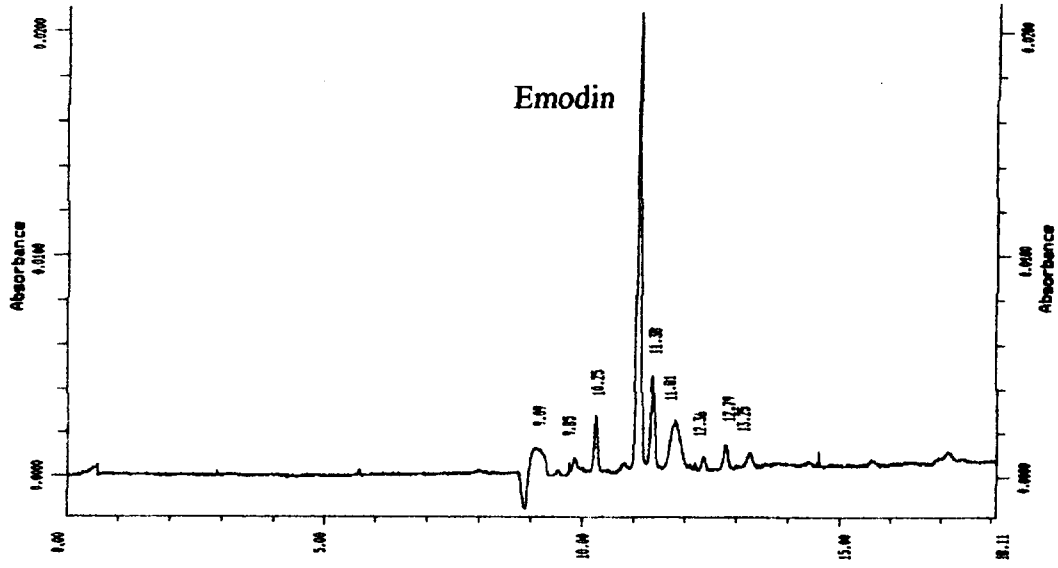

Fig. 4.2: Sample spiked with 150 µg/mL of emodin. Emodin identified at 11.13 minutes. See Figure 4.1 for experimental conditions.

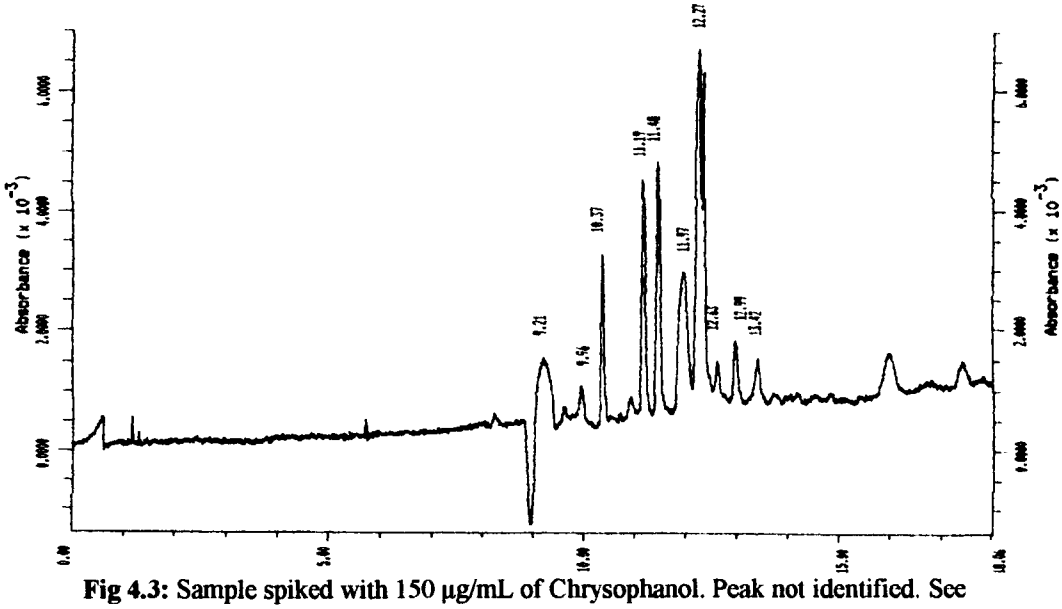

Fig 4.3: Sample spiked with 150 µg/mL of Chrysophanol. Peak not identified. See Figure 4.1 for experimental conditions.

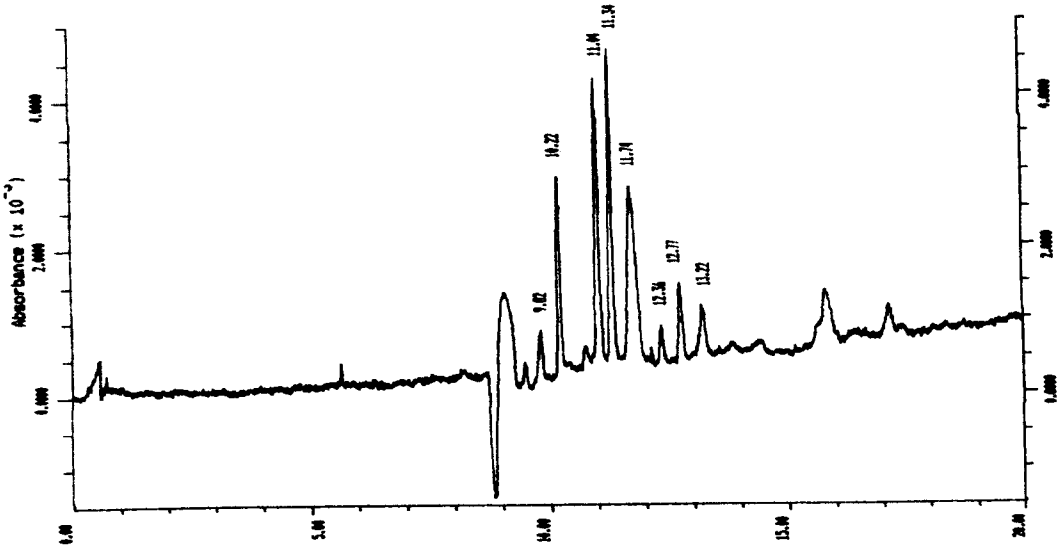

Fig 4.4: Sample spiked with 150 µg/mL of rhein. Peak not identified. See Figure 4.1 for experimental conditions.

CHAPTER FIVE

Conclusion and Termination of the Project

In the qualitative analysis of the crude extract of *Fallopia japonica,* only emodin was identified; chrysophanol and rhein were not identified. Precision tests (intra- and inter-day) showed that the method was not repeatable and reproducible. The lack of precision was probably caused by a batch-to-batch variability in buffer preparation, poor temperature control in the system and fluctuations in the applied voltage.

The project was set out to examine a capillary electrophoresis method for the speciation of anthraquinones in *Fallopia japonica.* This would have involved the identification of these bioactive compounds, quantification and a comparative study of the quantities across species, origin and seasons. Unfortunately, the project was discontinued for several reasons. The species of interest were not available. The other reasons were instrumental that resulted in non-repeatable and non-reproducible electropherograms; the most probable problems were changes in the surface chemistry of the capillary after few injections, poor thermostating system and fluctuations in the applied voltage.

References

[1] A.D. Kinghorn, M.F. Balandrin, Human Medicinal Agents from Plant, ACS Symposium series 534, Washington (1993).

[2] http://ex.ac.uk/knotweed.htmL accessed 22/12/04.

[3] http://www.co.clark.wa.us/weed/documents/knotweed.pdf accessed 12/12/2004.

[4] www.cornwall.gov.uk/environment/knotweed accessed 31/7/2005.

[5] www.ex.ac.uk/knotweed accessed 31/7/2005.

[6] www.cabi.org/BIOSCIENCE/japanese-knotweed-alliance.htm accessed 31/7/2005.

[7] http://www.cornwall.gov.uk/environment/knotweed accessed 22/12/04.

[8] W.J. Zheng, S.F. Wang, X.G. Chen, Z.D. Hu, Biomed. Chromatogr. 18 (2004) 3, 167.

[9] G.-C. Yen, P.-D. Duh, D.-Y. Chuang, Food Chem. 70 (2000) 437.

[10] G.-C. Yen, P.-D. Duh, D.-Y. Chuang, Food Chem. 70 (2000) 437.

[11] T.Z. Czaky, Introduction to general pharmacol., Appleton Century-Crofts, 2nd Ed. New York, 1997.

[12] B. Halliwell, Lancet 344 (1994) 721.

[13] E. Niki, Food factors for Cancer Prevention, Springer 431 (1997) 55.

[14] R.A. Larson, Phytochem. 27 (1988) 4, 969.

[15] F. Shahidi, M. Naczk (1995) In: Y. Cai, Q. Luo, M. Sun, H. Corke, Life Science 74 (2004) 2157.

[16] Y.S. Velioglu, G. Mazza, G. Cao, L. Oomah, J. Agric. & Food Chem. 46 (1998) 10, 4113.

[17] A. Sala, M.D. Recio, R.M. Giner, S. Manez, H. Tournier, G. Schinella, J.L. Rios, J. Pharm. & Pharmacol. 54 (2002) 3, 365.

[18] M.G.L. Hertog et al. In: Y. Cai, Q. Luo, M. Sun, H. Corke, Life Science 7 (2004) 2157.

[19] J.W. Mclarty (1997) In: Y. Cai, Q. Luo, M. Sun, H. Corke, Life Sciences 74 (2004) 2157.

[20] J. Sun, Y.F. Chu, X.Z. Wu, R.H. Liu, J. Agric. & Food Chem. 50 (2002) 25, 7449.

[21] M. Kubo, Y. Kimura, H. Shin, T. Haneda, T. Tani, K. Namba, Shoyakugaku Zasshi 31 (1981) 1, 58.

[22] M. Jang, L. Cai, and G.O. Udeani, Science 275 (1997) 218.

[23] G.S. Jayatilake, H. Jayasuriya, E.S. Lee, N.M. Koonchanok, R.L. Geahlen, C.L. Ashendel, J.L. McLaughlin, C.J. Chang, J. Nat. Prod. 56 (1993) 10, 1805.

[24] Y. Kimura, H. Okuda, M. Kubo, J. Ethnopharmacol 45 (1995) 2, 131.

[25] A.L. Lehninger, D.L. Nelson, M.M. Cox, Principles of Biochemistry, 4th ed., Plagrave Macmillan, New York, 2004.

[26] H. Arichi, Y. Kimura, H. Okuda, K. Baba, M. Kozawa, S. Arichi, Chem. Pharm. Bull. 30 (1982) 5, 1766.

[27] Y. Kimura, M. Kozawa, K. Baba, K. Hata, Planta Med. 48 (1983) 3,164.

[28] C.W Shan, Effects of Polydatin on platelet aggregation of rabbits, Acta. Pharm. Sin. 23 (1988) 5, 394.

[29] S.F. Luo, C.L. Yu, P.W. Zhang, Acta Pharmacol. Sin. 11 (1990) 2, 147.

[30] M. Anantaphruti, M. Terada, A.I. Ishii, H. Kino, M. Sano, M. Kuroyanagi, S. Fukushima, J. JPN. Parasitol. 31 (1982) 4, 321.

[31] Z.H. Luo, C.H. Cheng, H. Shao, S. Wai, Ko Tsa Chih 9 (1993) 1, 56.

[32] R. Edenharder, C. Speth, M. Decker, K. L. Platt, Z Lebensm Unters Forsch A 207 (1998) 464.

[33] Y.-C. Kuo, C.-M. Sun, J.-C. Ou, W.-J. Tsai, Life Science 61 (1997) 23, 2335.

[34] Z.H. Mbwambo, S. Apers, M.J. Moshi, M.C. Kapingu, S.V. Miert, M. Claeys, R. Brun, P. Cos, L. Pieters, Planta Medica, 70 (2004) 8, 706.

[35] N. Nandkumar, J.A.O. Ojewole, Methods and Findings in Experimental and Clinical Pharmacology 24 (2002) 7, 397.

[36] H.Y. Su, S.H. Cherng, C.C. Chen, H. Lee, Mutation Research-Fundamental and Molecule Mechanisms of Mutagenesis, 329 (1995) 2, 205.

[37] H. Lee, S.J. Tsai, Food and Chem. Toxicology, 29 (1991) 11, 765.

[38] X.F. Zhang, P.T. Thuong, W. Jin, N.D. Su, D.E. Sok, S.S.B. Kang Archives of Pharmacol Research 21 (2005) 321.

[39] X. Shang, Z. Yuan, Anal. Chim. Acta 456 (2002) 2, 18.

[40] X. Shang, Z. Yuan, Bioorg. & Med. Chem. Letter 13 (2003) 4, 17.

[41] C. Kuo, S.W. Sun, Anal. Chim. Acta 482 (2003) 1, 47.

[42] C.-H. Kuo, S.-W. Sun, Anal. Chim. Acta 482 (2003)1, 47.

[43] W.-C. Weng, S.-J. Sheu, J. High Resol. Chromatogr. 23 (2000) 143.

[44] J. Koyama, I. Morita, K. Kawanishi, K. Tagahara, N. Kobayashi, Chem. & Pharm. Bull. 51 (2003) 4, 418.

[45] J. Koyama, I. Morita, K. Tagahara, J. Bakari, M. Aqil, Chem. &Pharm. Bull. 50 (2002) 8, 1103.

[46] S.-W. Sun, P.-C. Yeh, J. Pharm. & Biom. Anal. 36 (2005) 995.

[47] L.S.Yan, Z.H. Wang, G.A. Luo, Y.M. Wang, Chem. J. Chinese Universities-Chinese 25 (2004) 5, 827.

[48] C. -L. Liu, P. -L Zhu, M.-C. Liu, J. Chromatogr. A 857 (1999) 1-2, 167.

[49] Y.S. Han, B. Hofte, R.V. Heijden, R. Verpoote, Phytochem. Anal. 14 (2003) 298.

[50] F. Li, Q.-E Cao, Z. Ding, Chromatographia 59 (2004) 11-12, 753.

Appendix D: Professional development courses attended

Course	Date
HPLC method development (3 M Healthcare)	Oct. 10, 2004
Plagiarism, citation and managing your references	Nov. 10, 2004
Powerpoint for clerical/secretarial staff	Dec. 16, 2004
Teaching skills	
• Part A	April 26, 2005
• Part B	May 3, 2005
• Part C: Supervising practical activities	June 8, 2005
Factor Analysis	April 19, 2005
Measures of analysis of variance (ANOVA)-part A and B	13 and 20 April, 2005
Discriminant Analysis	April 12, 2005
Excel (parts A and B)	17 and 31 March, 2005
Overview of regression	March 22, 2005
Hypothesis testing	March 8, 2005
SPSS (parts A and B)	28 February and 7 March, 2005
Analytical Chemistry Forum (organized by RSC)	July 18-20, 2005
HPLC/LC-MS/SPE Seminars, Sheffield	April 27, 2005
Types of data and experimental design	March 7, 2007
Getting articles published	March 6, 2007
Introduction to the job of lecturer for postgraduates and research assistants	April 17, 2007
Viva-what happens	March 3, 2007
Designing and producing conference posters	March 13, 2007
What is Literature Review	June 19, 2007
Report Writing	May 22, 2007
ARF conference, Glasgow	16 - 18 July, 2007